FINAL REPORT

Optimizing Selection Pressures and Pest Management to Maximize Cultivation Yield (OSPREY)

Award #DE-EE0008902 to the New Mexico Consortium

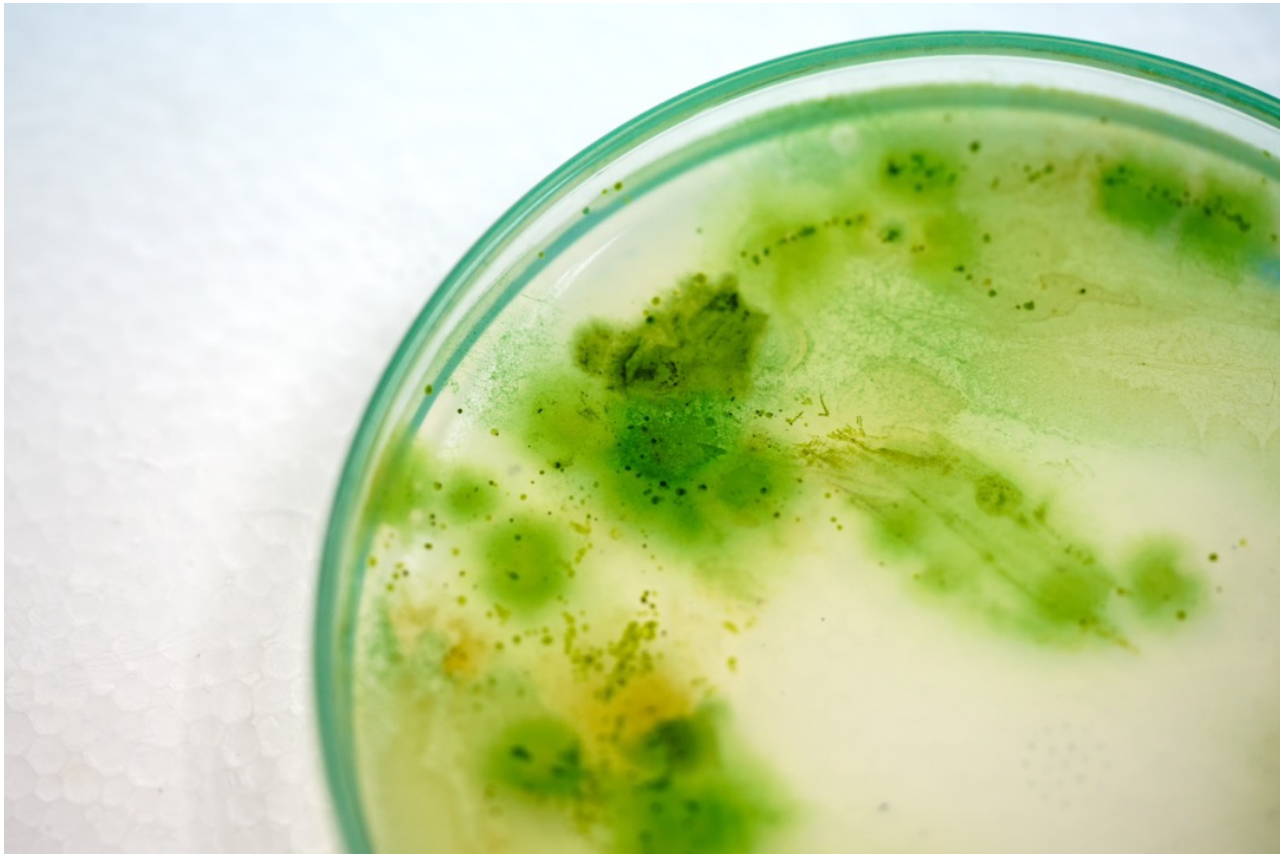

Acknowledgement: This material is based upon work supported by the U.S. Department of Energy's Office of Energy Efficiency and Renewable Energy (EERE) under the Bioenergy Technologies Office (BETO) Award Number DE-EE0008902.

Table of Contents

1. Rationale and Background

This project was proposed in response to AOI 1, Cultivation Intensification Processes for Algae, within the FY19 Bioenergy Technologies Office Multi-Topic Funding Opportunity Announcement (FOA Number: DE-FOA-0002029). The work was designed to address a critical industry need to improve annualized productivity, stability, and quality of algal production strains for biofuels and bioproducts. The overall project goals were to generate process innovations rooted in established outdoor systems for strain selection, improvement, maintenance, and cultivation as well as pest detection and tracking. Planned advances included a 50% improvement in harvest yield based on AFDW (g m^2 d^{-1}), 50% improvement in robustness based on stability metrics (e.g., high-productivity cultivation days, pond uptime), and 20% improvement in conversion yield. Individually, each of our planned process improvements (e.g., pest tracking) had the potential to increase productivity. However, to realize increases in yield at the system level, improvements to one unit's process must be balanced against potential effects on other processes. For example, changes to strains, cultivation, and pest management developed in isolation may hurt other unit operations. Therefore, a critical success factor of the project was the integration of the pipeline components, achieved through iterative field-to- (short term) lab testing. In addition, through sustainability models, we evaluated how improvements would alter industry scenarios.

Our project's technical components, (1) Balancing Indoor and Outdoor Selection Pressures, (2) Optimization of Pest Management, and (3) Improvement of Field Strain Performance, Resiliency, and Composition are built on a *single foundation*: the year-round cultivation of a *Nannochloropsis* strain in 3 outdoor systems **(Fig. 1-1)**. We used a field-adapted (since 2017) strain collected from Qualitas ponds in Imperial, TX to seed ponds in California (University of California San Diego, UCSD), New Mexico (New Mexico State University, NMSU) and Hawaii (Cyanotech) field sites. We envisioned that the unique environmental selection

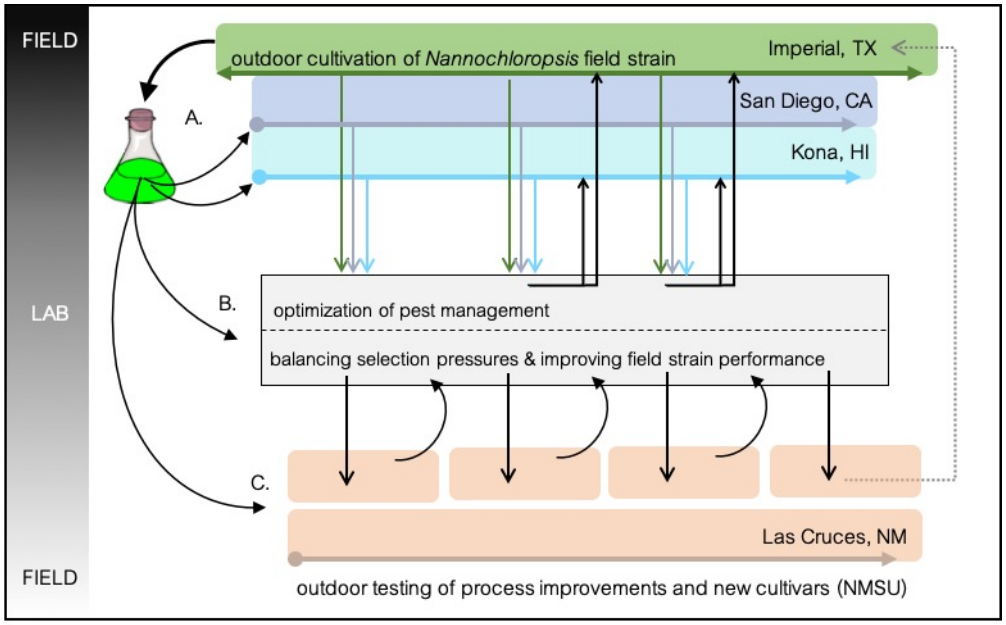

Fig. 1-1. Project overview illustrating the iterative nature of the project approach, rooted in the outdoor cultivation of a *Nannochloropsis* strain that has been in outdoor culture since 2017. Field-scale testing occurred at the scale of at least 300L and lab scale testing occurred at scales from 5 to 500mL.

pressures of each outdoor system would allow us to develop robust cultivars and will facilitate process innovations with broad geographic applicability. We also established the field adapted *Nannochloropsis* strain in three laboratories at NMSU, Los Alamos National Laboratory (LANL), and UCSD. Throughout the project, we tracked trait evolution across the field and lab sites, developed novel pest tracking tools, and improved the field strain through non-GM methods. As pest tracking tools came online, they were validated and deployed at field sites. In addition, we tested improved strains and process innovations (e.g., in field mutagenesis) at the NMSU testbed. Finally, assessed improvements through techno-economic and sustainability modeling based on open raceway architectures, leveraging existing models and including fuel and co-product production pathways.

2. Long Term Outdoor Cultivation

2.1 Isolation of the Industrial Strain

A field adapted strain of *Nannochloropsis* was obtained from Qualitas Health, Inc. on March 13, 2020. At the time of collection, the strain had been cultured outdoors in Imperial, TX for more than five years. To generate clonal isolates from the field population and help remove associated bacteria, we used fluorescence activated cell sorting (FACS) with a BD Influx flow cytometer to sort single *Nannochloropsis* cells into individual wells of standard flat bottom 96-well plates. Wells were filled with three types of media: (1) OSPREY field medium, (2) sterile filtered OSPREY medium, (3) and the commercial medium 16NFL previously used at Sapphire Energy, Inc. The OSPREY medium recipe is similar to 16NFL used at Sapphire Energy and in other studies (Lee et al., 2018; Mandal and Corcoran, 2022). This medium contains nitrogen (N), phosphorus (P), trace metals, and iron (Fe), but no vitamins. Approximately 15 plates of sorts were collected. Outgrowth of the sorts that allowed for unaided visualization of viable wells took approximately two weeks. Approximately 50% of all wells (~250 isolates) with sterile OSPREY medium and 20% of all wells (~100 isolates) with sterile 16NFL medium yielded algal growth. All media control wells with sterile OSPREY and 16NFL media remained clean. All unsterilized media control wells showed considerable non-target (algae and bacteria) growth; none of these wells were used for further outgrowth or analysis.

Twenty-four clonal isolates from a distribution of the 96-well outgrowth plates were selected to move forward. These clonal isolates went through DNA

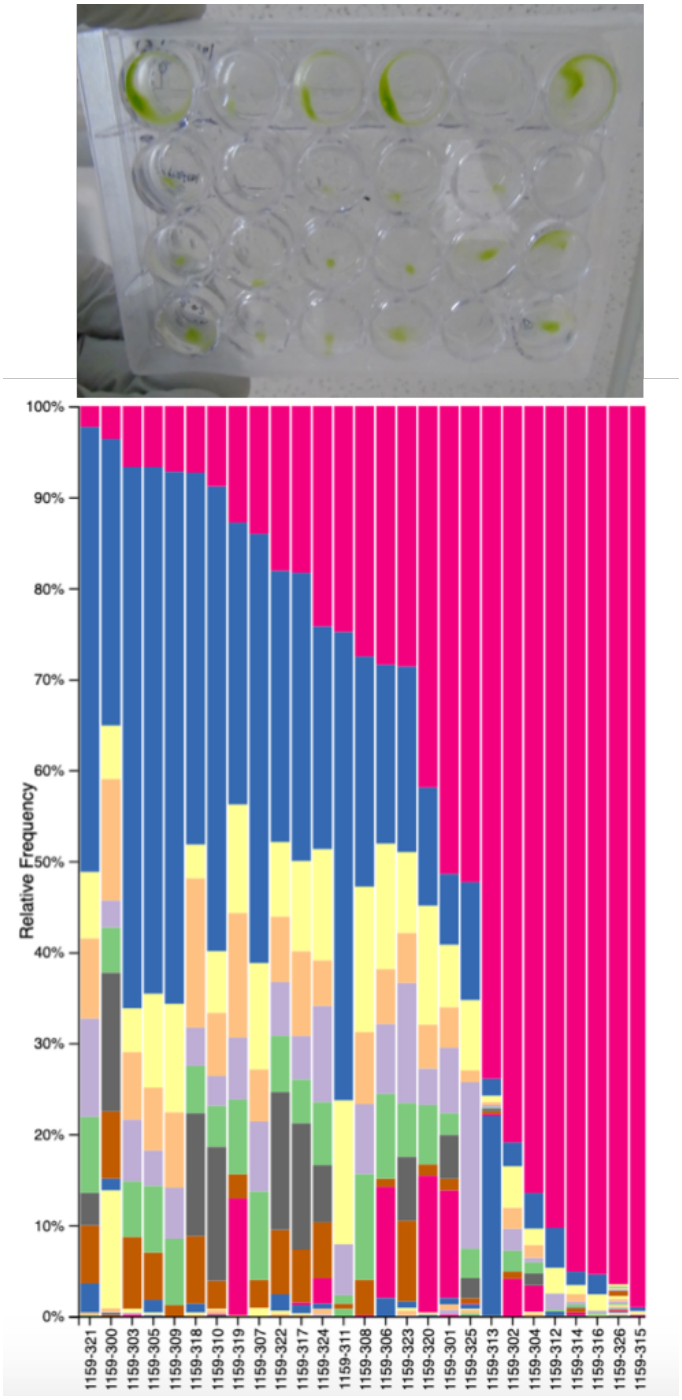

Fig. 2-1. Results from 16S sequencing of the original QT001 strain. The hot pink color dominant in bars towards the right-hand side of the plot is the chloroplast-encoded 16S rRNA gene of *Nannochloropsis*.

purification using a ZymoResearch Fungal/Bacteria kit to collect a DNA template that was used for PCR genotyping analysis. Both 18S and the LANL developed CcsA (from the DOE-PEAK project STS, Starkenburg and Corcoran, DE-EE0008122) primers for PCR amplification and sequencing were used to confirm isolate identity. The clonal isolate that had the fewest associated bacteria, identified via 16S sequencing, containing 98.7% *Nannochloropsis oceanica* chloroplast abundance, was chosen as the project baseline strain (subsequently referred to as QT001) **(Fig. 2-1)**. The bacteria initially identified to be associated with the clonal isolate included two Bacteroidetes taxa (including a *Balneola* sp.) and one Proteobacterium. However, we isolated *Salinibacter* (Rhodothermales, formerly Bacteriodetes), not found in the original QIIME run, from this strain. Interestingly, in late 2023 (3+ years into the project), we conducted another QIIME run and found additional bacteria **(Table 2-1)**. The xenic QT001 strain was distributed to project partners in July 2020. Multiple copies of the strain were also cryopreserved for future comparison to evolved strains. The genome of this isolate was sequenced and made publicly available (Sanchez et al., 2022).

Fig. 2-2. Scaling cultures from the lab (top) to ponds (bottom, from left to right: UCSD, Cyanotech and NMSU).

2.2 Establishment of Outdoor Cultures at Each of Three Additional Field Sites

Cultures were established at field sites at UCSD (San Diego, CA; 32.885575, -117.230162), NMSU (Las Cruces, NM; 32.279262, -106.771913) and Cyanotech (Kailua-Kona, HI; 19.734593, -156.053035) between 09/01/20 and 11/12/20. To inoculate ponds, cultures were scaled from ~10 mL to 20 L carboys in the laboratory, multiple carboys were used to inoculate a pond, and scaling in the field continued until three or four replicate ponds of *Nannochloropsis* were established **(Fig. 2-2)**. UCSD and NMSU scaled the QT001 strain in OSPREY medium through field cultivation, whereas Cyanotech site scaled the QT001 culture in a different medium than the OSPREY medium and transitioned the culture over to the

Table 2-1. Bacteria associated with original QT001 isolate.

Genus	Relative Abundance
Balneola	.0015
Pseudomonas	.00067
Rickettsiales	.00067
Delftia	.00061
Magnetospira	.00046
Leptospiraceae	.00036
Escherichia-Shigella	.00030
Ekhidna	.00030

target medium in the field. OSPREY medium was made with local tap water from each of the sites and commercial grade salts. Sources of N and P were sent from Qualitas Health to UCSD and NMSU. Due to shipping restrictions, Cyanotech purchased N and P stocks that conformed to Qualitas specifications. By November 12, 2020, all three field sites were cultivating QT001 in at least three ponds per site. Qualitas Health maintained the initial population in its cultivation ponds. Initial pond targets for pH and density were shifted in December 2020 to accommodate industry practices. Operating parameters were similar across sites, although pond design varied slightly **(Table 2-2)**. According to what has already been described for shallow aquaculture ponds, vertical water movement is not as effective as horizontal water movement for pond mixing (Hargreaves, 2003). Regarding the flow velocity, ~1 ft/sec is the most common flow velocity used for biomass production (Oswald and Golueke, 1960), however lower velocities such as 0.49 ft/sec has also been reported effective for *Nannochloropsis oceanica* cultivation in pilot-scale raceways ponds (Cunha et al., 2020). Flow velocity was tested and showed that 0.49 ft/sec is well suited for UCSD ponds (higher velocities were too turbulent, risking water splashing). At both NMSU and UCSD, fluorescein sodium salt was used to conduct video-recorded dye-tracing. At both sites, mixing was rapid, and no dead zones were detected. For ongoing cultivation, pH was adjusted to keep it below 8 by using CO_2 on demand supplied to ponds. Each growth cycle was defined by an initial and a final biomass target used according to previous studies (Millán-Oropeza and Fernández-Linares, 2017; Mohan et al., 2021; Narala et al., 2016). Ponds were harvested and cultures diluted with fresh medium once the target biomass concentration was reached. Harvesting was done by draining ponds to a desired depth based on the final and initial biomass targets. Depending on the location, harvested cultures were sent to an evaporation pond or bleached and discarded subsequently.

Table 2-2. Characteristics of ponds used across the different field sites. Due to the lack of data provided by Qualitas Health for the final report, Qualitas ponds are not included here.

	Kailua-Kona (HI)	Las Cruces (NM)	San Diego (CA)
Material	Plastic	Fiberglass	Plexiglas (painted white)
Area (m^2)	1.195	1.987	0.7961
Volume (L)	200.6	260	150
Depth (cm)	17	20	19
Flow rate (cm/s)	30	15	15
Paddle wheels	horizontal	horizontal	vertical
Start Date	11/12/20	9/1/20	10/17/20

During the cultivation campaigns, samples were collected Monday through Friday for metrics of biomass and pond health apart from winter and holiday periods where sites shifted to Monday, Wednesday, and Friday sample and data collection to accommodate slow winter growth or lack of personnel. Site-wide metrics included optical density at 750 nm (OD_{750}) and ash free dry weight (collected pre- and post-harvest). Additional metrics collected at NMSU were chlorophyll fluorescence with an excitation wavelength of 430 nm and emission wavelength at 685 nm. Additional metrics collected at Cyanotech and NMSU were metrics of photosynthetic health (Fo, Fm, and Fv/Fm). Site wide parameters of pH, temperature, and depth were recorded

during sample collection. At NMSU and UCSD salinity was recorded during sample collection apart from UCSD using a refractometer in the lab when the handheld probe was not working properly. Cyanotech did not have an option to collect salinity readings in the field and used a refractometer for the duration of the project. Samples were collected three times a week to archive for metagenomic and genetic analysis for Task 4. OD_{750} (and chlorophyll fluorescence at NMSU) was measured using a microtiter plate reader (SpectraMax M2, Molecular Devices, USA) in Las Cruces, NM; a cuvette modular fluorometer/spectrophotometer (Turner Trilogy, Turner Designs, USA) in San Diego, CA; and a cuvette UV/Vis spectrophotometer (UV-1600PC, VWR, USA) in Kailua-Kona, HI. A one-to-one dilution was used for OD_{750} measurements to ensure the linear range of the analytical method. A one to twenty dilution was used for chlorophyll measurements to ensure the linear range of the analytical methods. Ash-free dry weight (AFDW) was measured pre- and post-harvest following procedures described in (Van Wychen and Laurens, 2016) for the three sites. To aid in rinsing salts from the media all sites used 40 mL deionized water to rinse the volume of algae filtered. AFDW-based productivity (aerial productivity in g m^2 d^{-1}) was calculated as:

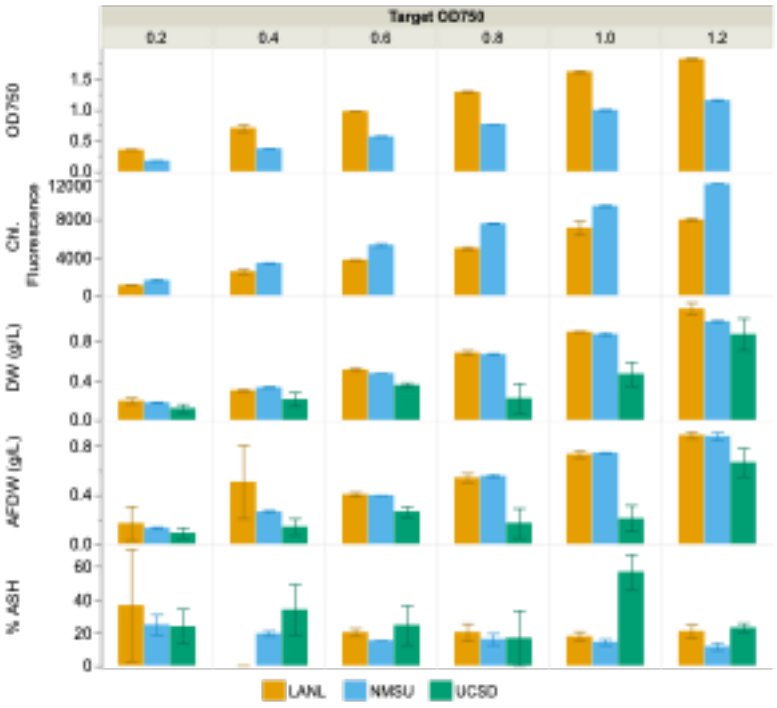

Fig. 2-3. OD, chlorophyll fluorescence, dry weight, ash-free dry weight, and % ash measured at LANL, NMSU and UCSD during the first harmonization.

$$\frac{(AFDWpre - AFDWpost) * V}{A * t}$$

where $AFDW_{pre}$ and $AFDW_{post}$ are the ash free dry weights at the end and at the beginning of growth cycle (g L^{-1}) respectively, V is the pond volume (L), A is the pond area (m^2), and t is the duration of the growth cycle (days). Fo, Fm, Fv/Fm were measured using a MINI-PAM (Walz Version 2.00) in Las Cruces, NM and in Kailua-Kona, HI. Pond parameters were recorded using a YSI 1030 in Las Cruces, NM; a Cole-Parmer PC100 pH/Conductivity Meter in San Diego, CA and in Kailua-Kona, HI. Every six weeks, field cultivation samples were streaked in duplicate onto selective agar plates (OSPREY media 18 ppt) to mitigate against loss of evolved field strains. Fortunately, there was no complete loss of cultures in the field from invaders, pond management, or environmental factors.

2.3 Harmonization of Analytical Techniques

To prepare for multiple sites collecting metrics of biomass and pond health from outdoor and indoor cultivation systems, a method harmonization across laboratories was completed. At three points in 2020 and 2021, one *Nannochloropsis* sample was diluted across a gradient of OD_{750} into six samples and distributed among sites (Cyanotech, LANL, NMSU, and UCSD) for independent analysis. Work instructions were agreed upon prior to analysis and samples were analyzed blind. Due to shipping restrictions for Hawaii, the initial dilution series sent to Cyanotech was not permitted into the state.

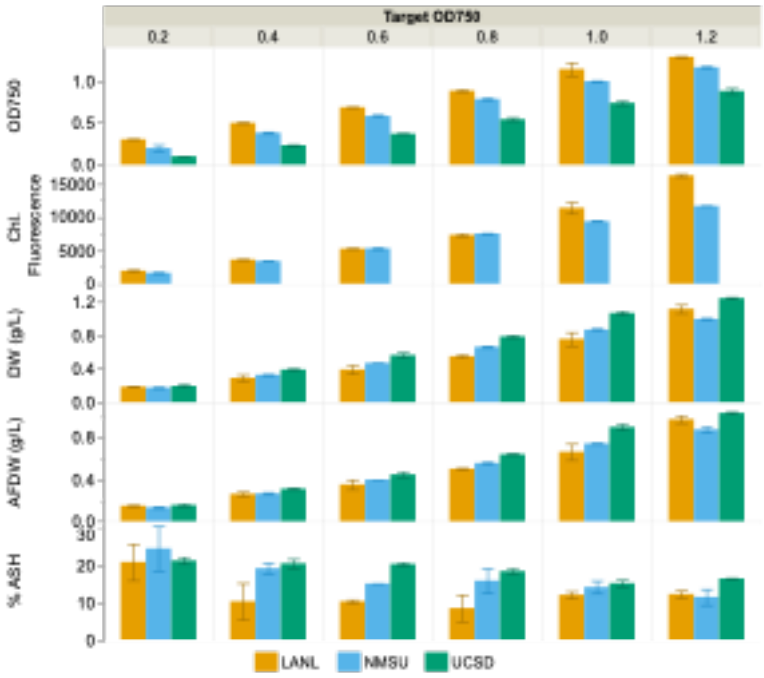

Fig. 2-4. OD, chlorophyll fluorescence, dry weight, ash-free dry weight, and % ash measured at LANL, NMSU and UCSD during the second harmonization.

Initial results **(Fig. 2-3)** acquired in February 2020 alignment between NMSU and LANL but under-quantification at UCSD for dry weight. Ash free dry weight did not align across sites, as UCSD under-quantified and LANL overquantified compared to NMSU. Differences observed in dry weight and ash free dry weight were attributed to inconsistent volumes filtered, low rinse volumes, and different filters being used between sites. OD_{750} and chlorophyll fluorescence varied across sites, as would be expected given different plate readers. In addition, LANL was missing an adapter that should be used for top reads of the Spectramax M2 at LANL. UCSD did not have a reliable plate reader available during this time and did not complete OD_{750} and chlorophyll fluorescence readings.

The second dilution series was generated in June of 2020 and sent to UCSD and LANL to repeat analysis, ensuring all supplies being used were the same and instruments were calibrated and being used as designed. Results from the second dilution series showed alignment between LANL, NMSU, and UCSD **(Fig. 2-4)**.

The third harmonization done in January 2021, focusing on Cyanotech, showed alignment in both dry weight and ash free dry weight between Cyanotech and NMSU **(Fig. 2-5)**. NMSU had higher variation in % ash compared to Cyanotech. OD_{750} and Chlorophyll fluorescence readings were significantly different from each other, but PAM (F, Fm, and Fv/Fm) values were in line across sites. Cyanotech generated the dilution series using a plate reader that reads significantly higher than the NMSU plate reader; because of this all NMSU plate reader values are significantly lower than Cyanotech. The greater ash content at NMSU was attributed to Cyanotech rinsing with 40mL of water, vs the 20mL project standard.

At the end of the harmonization, results across labs were within range of one another **(Fig. 2-5)**. Ash free dry weight, specifically, varied across labs by 0.002 to 0.121 g/L. Based on these results, all field sites moved forward with collecting DW g/L, AFDW g/L, % ash, and OD_{750} (used in conjunction with AFDW g/L to estimate growth for harvest purposes). Cyanotech and NMSU additionally collected PAM for overall pond health, and NMSU used chlorophyll fluorescence as an additional metric. LANL moved forward using OD_{750} and chlorophyll fluorescence to compare cultures in laboratory experiments. Lessons learned were based on fine tuning processes; we adjusted to rinsing AFDW filters with 40 mL of

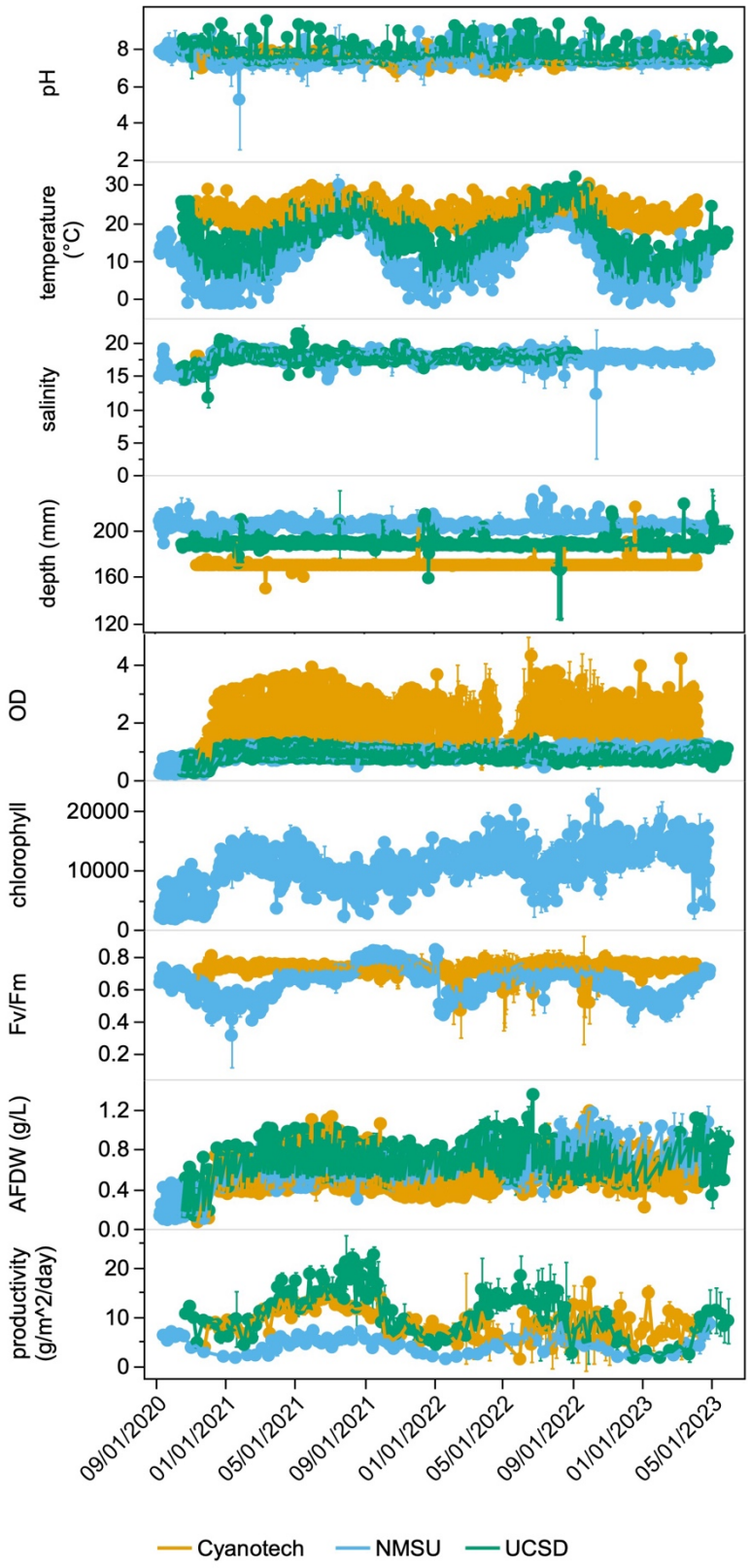

Fig. 2-6. pH, temperature, salinity, depth, optical density, chlorophyll fluorescence, Fv/Fm, AFDW and productivity at Cyanotech, NMSU and UCSD through the cultivation period.

deionized water to accurately remove excess salts from the culture that could contribute to ash values, and instruments need to be checked for calibration and proper use prior to project start.

2.4 Outdoor Cultivation

Outdoor ponds were maintained from November 12, 2020, until April 28, 2023. Measurements of temperature (°C), salinity (ppt), and depth (mm) were taken daily **(Fig. 2-6)**. pH was maintained at 7.4 ± 0.2 with deviations outside that range due to CO_2 solenoid malfunctions, CO2 tanks emptying, or site power issues. Temperature fluctuated with season and location with Cyanotech being the most stable throughout each year, NMSU having the most variable temperatures, and UCSD having more variation than Cyanotech but less than NMSU **(Fig. 2-6)**. Salinity was maintained at 18 ppt with deviations from rain diluting the cultures, and post-harvest media additions being slightly inaccurate due to shifting/unlevel ground causing ponds to move or tilt slightly in one direction and cause volumes to not be as consistent across ponds. If salinity was not available during morning sample collection in the field a refractometer was used to take measurements in the lab. Cyanotech performed all salinity measurements in the lab with a refractometer, NMSU performed weekly checks to compare to the handheld readings with a refractometer, and UCSD used a refractometer when handheld instruments were not working or being replaced. Depths were maintained at targets with exceptions of rain or autofill malfunctions (NMSU). Rain events would have two possible outcomes depending on the severity of the storm. Small rain events would overfill ponds; after these events, ponds were allowed to evaporate on their own to normal operating depths. Larger rain events required decreasing depths of ponds to avoid culture's overflowing onto the ground with added rainwater. If volume increases lasted more than a day, nutrients were added in amounts equivalent to the volume of rainwater added and ponds were drained back to operating depths.

Metrics of biomass showed clear cross-site differences. Productivity was generally greatest at UCSD and lowest at NMSU, with Cyanotech being intermediate. Site differences were driven not only by site-specific climatic drivers, but also factors such as different pond styles, holding volumes, and depths (Echenique-Subiabre et al., 2023). Biomass productivity varied seasonally at UCSD and NMSU. At NMSU, Fv/Fm values followed temperature trends, suggesting an overall health change in the culture during colder months at NMSU. Fv/Fm values were more consistent at Cyanotech, consistent with the relatively stable climate. Differences in productivities were also seen across years, with overall greater productivities at UCSD in the first summer season compared to the second. Finally, there were some site differences seen in the data (e.g., plate reader differences with Cyanotech reporting significantly greater OD750 values than the other sites).

Bleach was used as a crop protection strategy at each site. The frequency and amount of bleach doses varied across sites due to different pest pressures. Cyanotech experienced consistent temperatures and invaders consisted of diatoms, ciliates, flagellates, amoeba, and cyanobacteria. NMSU and UCSD had fluctuating temperatures and observed more invaders

during the warmer months, resulting in bleach doses being increased in either frequency or amount during those times. NMSU also had temperatures with lower lows and higher highs than the other two sites that corresponded with overall higher bleach doses in the summer and overall lower bleach doses in the winter.

2.5 Disturbances to Cultivation

Over the three-year cultivation period (2020-2023), sites periodically experienced several disturbances to cultivation. Some disturbances were similar across sites (e.g., power outages, CO_2 tanks emptying) and resulted in loss of pond control or pH not being maintained at target for short periods of time, typically 1-3 days. While these interruptions in cultivation were brief and easily fixed so not to cause significant damage to cultures, other interruptions were site specific and oftentimes proved more challenging.

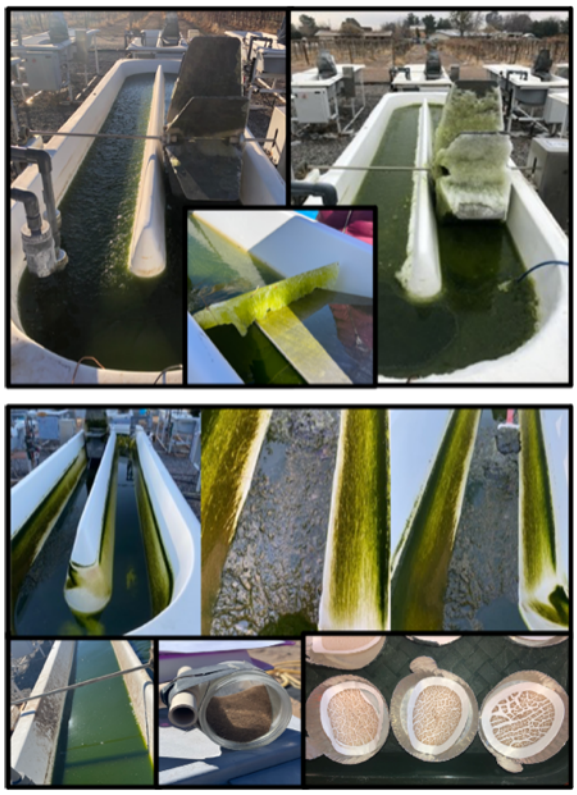

Fig. 2-7. Freezing conditions (top) and sediment accumulation due to high winds (bottom) in NMSU ponds.

NMSU experienced freezing temperatures each winter causing variations of frozen ponds from slushy water columns to frozen paddle wheels and up to 1 inch of ice on the top of the water columns **(Fig. 2-7)**. Winter practices were changed to have paddle wheels turn off at 7pm and on at 9am, and sampling times were shifted to midday. In the spring each year, high winds (gusts up to 55 MPH) resulted in large amounts of sediment in the ponds and significant increases in the amount of ash **(Fig. 2-7)**. To help remedy having so much sediment in the ponds, cultures were allowed to settle, transferred to a holding pond, original ponds were cleaned with bleach, and cultures returned. All ponds were cleaned in the third quarter of each year. In the third quarter of 2022, a large rain event diluted cultures by 13% of the total pond volume and ponds allowed to evaporate down resulting in slow growth for approximately two weeks. The fourth quarter of 2022 had two rain events, one diluting cultures by 3% and causing a power outage resulting in loss of pH control and paddle wheel mixing for three days, and the second diluting cultures by 6% with a layer of ice forming.

UCSD received 0.1 to 1.0 inches of rain a month between July and March of each year. In the fourth quarter of 2020, a rain event over a weekend caused one of the ponds to turn light green with poor growth, resulting in the need to reseed **(Fig. 2-8)**. In the second quarter of 2021, a biofilm was observed on the walls and paddlewheels of the ponds during harvesting. Foam on top of the water column also started to appear during this period and was frequently observed until the fourth quarter of 2022 **(Fig. 2-8)**. In the fourth quarter of 2021 the handheld meter failed, and all salinities were captured with a refractometer for a few days. Also, during this period, several rain events were observed that diluted cultures by 13% and caused one paddle

wheel motor to fail (fixed within 24 hours). A small dip in OD_{750} was observed in the pond with the broken motor. In the first quarter of 2022, CO_2 flow was frequently interrupted between February and March due to a decrease in the CO_2 pressure from the tank to the circuit, this caused high pH peaks throughout these months. In the third quarter of 2022, there was an increase in invaders (amoeba, ciliates, flagellates, and cyanobacteria) and decrease in productivities, resulting in reactive bleach dosing. Recovery in productivity took over a month and samples were sent for sequencing during this period to capture any invaders or changes in community. A couple times during the cultivation period the ponds were observed leaking at the seams where the walls were glued together. Each time the seams were sealed to prevent culture loss. Cyanotech received ~1.5 to 3 inches of rain each month, with greater rainfall amounts during the monsoon season of April through October. Depending on the severity of each rainstorm, cultures were diluted slightly, depths were dropped in preparation of large rain events, nutrients were added to accommodate added rainwater, and ponds were drained back to operating depth. In the fourth quarter of 2020, Cyanotech experienced floating masses of spiral bacteria **(Fig. 2-9)** that were treated with 5 ppm of bleach to resolve. Third quarter of 2021 scope observations started showing diatom presence. This caused an accumulation of diatoms and debris on the paddle wheels and required cleaning paddle wheels frequently (1-2x/week or as it appeared) with a bleach solution to help keep diatoms out of the algae culture. Predatory amoebae were also observed during this period and coincided with low productivity. To help remedy the low productivity, ponds were transferred to a holding pond, original ponds were cleaned with bleach, and cultures were returned. In the first quarter of 2022, ponds experienced two pond crashes from nutrient poisoning caused by pond mismanagement. Following the crashes,

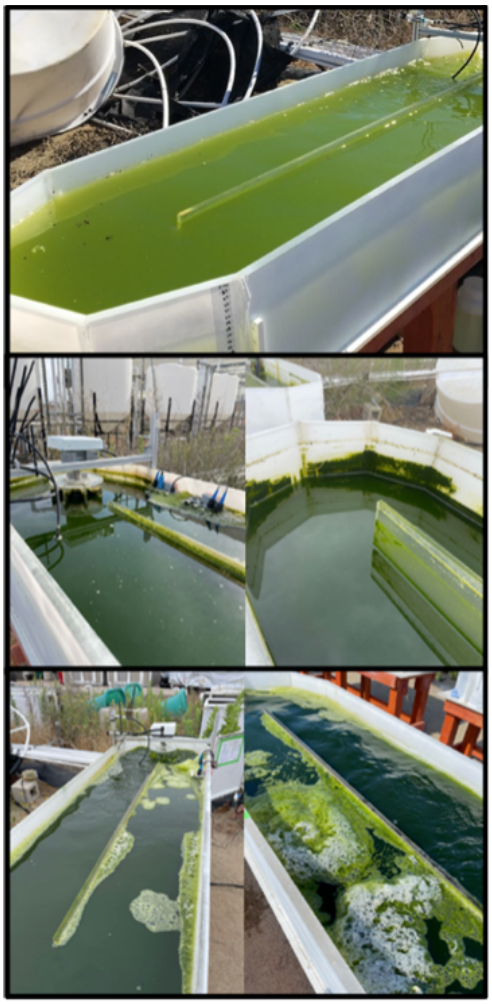

Fig. 2-8. Rain event (top), biofilm accumulation (middle) and foam (bottom) at the UCSD ponds causing poor culture conditions.

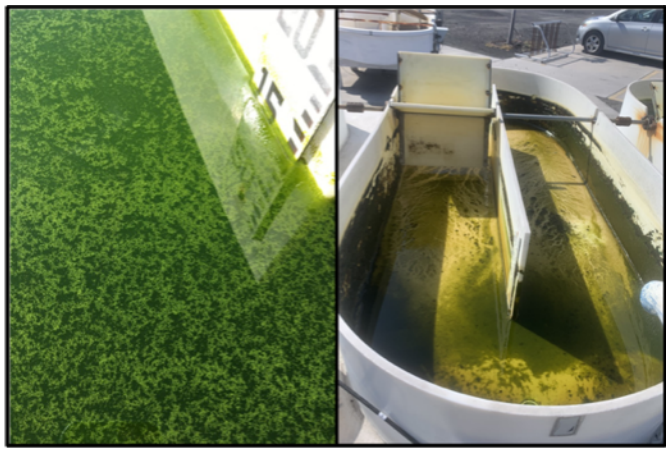

Fig. 2-9. Floating masses of spiral bacteria (left) and biofilm accumulation (right) on the walls of Cyanotech ponds.

the two ponds were reinoculated from the other healthy field culture and practices reviewed and followed moving forward (nutrients added to a pond will only equal the volume taken out during harvest or added based on analytical values reporting low nutrient levels). In the second quarter of 2022, large amounts of ciliates (~35/10 mL large predatory and 60+/10 mL small) and amoeba (~15/10 mL) were observed in the ponds. This resulted in significantly lower productivity for this period and needing to add 50% culture from healthy ponds to bring back better productivity values. These invaders and lack of bleach dosing to control them was not noticed for several months. In the third quarter of 2022, a biofilm was observed **(Fig. 2-9)** on the walls of the ponds and the paddlewheel resulting in ponds being cleaned with bleach. Also, during this period, a freshwater line burst, and ponds were without water for three days seemingly without a significant effect on cultures. In the fourth quarter of 2022, a volcano eruption resulted in heavy cloud cover and fog for four months. Invaders increased during this period, with observations of ciliates, amoeba, cyanobacteria, and diatoms. To reduce invaders, the ponds were cleaned with bleach and bleach doses increased. Also, during this period, a large rain event diluted ponds by 25% resulting in ponds being replenished with nutrients and drained back to operating depth. In the first quarter of 2023, the continued heavy cloud cover from the volcano caused almost daily power outages ranging from minutes to hours with the worst being on 2/20/23 at 16 hours. During this time pH control was lost and a drop in Fv/Fm was observed.

2.6. Hindcasting Productivity Across Field Sites

To support experimental work that tracked trait drift and evolution in field cultivars, we used a modeling approach to understand the relative importance of local drivers on productivity at three of the field sites: Cyanotech, NMSU, and UCSD. We used pond data collected from November 2020 to April 2022 at Kailua-Kona, September 2020 to April 2022 at Las Cruces, and October 2020 to April 2022 at San Diego. Local weather station data was collected throughout the experiments and both data sets were used to hindcast productivities, which were then compared to the observed productivities to quantify model accuracy. Hindcasting comprised of: (1) pond temperature hindcasting and validation; (2) growth hindcasting with published strain parameters for *N. oceanica* (Greene et al., 2021); (3) stochastic site-specific strain parameter fitting; (4) and growth hindcasting with multi-site average strain parameter values. As pond temperature was not recorded for the full duration of the growth experiments at each site, a thermal model (Greene et al., 2021) was used to hindcast pond temperatures with hourly resolution at each site. The model relies on the following weather parameter inputs at hourly intervals: ambient temperature (K), average wind speed (m/s), global horizontal irradiance (W/m^2), and relative humidity (%).

Hindcasted pond temperatures were compared with measured temperatures at three of the four sites with site-specific thermal modeling accuracy quantified **(Fig. 2-10)**. The thermal model displayed an average error of 0.58 ± 1.42°C (0.41% absolute average error) at Kailua-Kona, -0.36 ± 1.53°C (0.49% absolute average error) at Las Cruces, and -0.98 ± 3.58°C (1.07% absolute average error) at San Diego. The higher standard deviation at San Diego was most likely due to unique pond geometry and a vertical submerged paddlewheel which varies from the horizontal elevated paddlewheel used for previous validation studies (Greene et al., 2021).

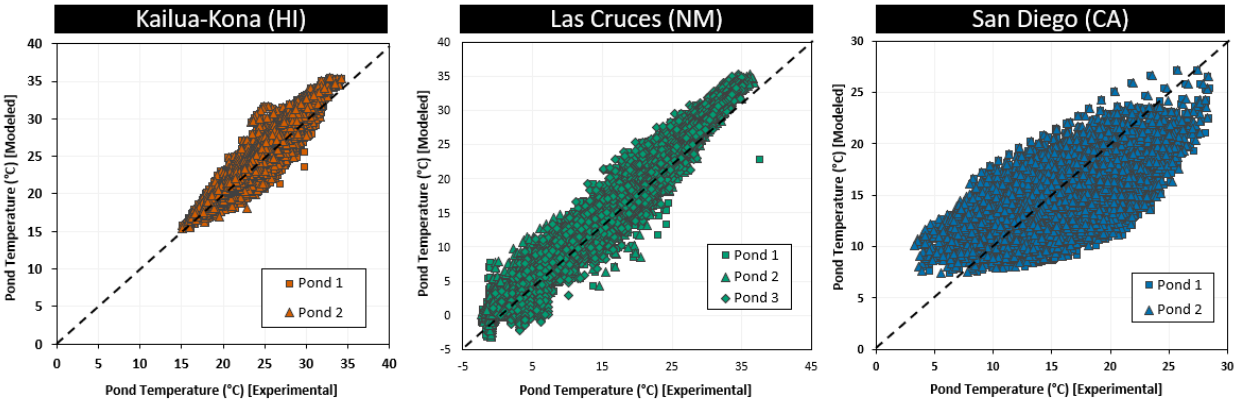

Fig. 2-10. Thermal model accuracy shown for each site by plotting modeled vs. experimentally measured pond temperatures. The dotted black line in each figure represents 100% accuracy between hindcasted and measured pond temperatures. Sample size was 11751 for Kailua-Kona, 22266 for Las Cruces, and 3911 for San Diego.

Previous work has shown the increased impact of evaporative cooling from paddlewheels in mini-ponds due to the thin film of water exposed to ambient air on the paddlewheel surface (Quiroz et al., 2021). The vertical paddlewheel may have influenced pond temperatures by impacting the total amount of evaporative cooling. Overall, the thermal model achieved a high degree of accuracy across the full datasets from each site **(Fig. 2-10)**, laying a robust foundation for the subsequent growth hindcasting effort **(Fig. 2-11)**. Growth hindcasting with strain parameter values from literature resulted in the lowest modeling accuracy **(Fig. 2-11)** of the three exercises. Ponds at Kailua-Kona, and San Diego overperformed the hindcasted predictions whereas ponds at Las Cruces underperformed. Modeled harvest concentrations varied from measured values by -0.21 ± 0.17 g/L at Kailua-Kona, 0.30 ± 0.34 g/L at Las Cruces, and -0.30 ± 0.06 g/L at San Diego.

Greater modeling accuracy was achieved when using site-specific strain parameters. Several of these parameters, such as the dark respiration rate and optimal temperature were adjusted in alignment with the site-specific data and observed productivity trends. However, other parameter adjustments could not be validated with experimental data and warrant further investigation into model functionality and limitations. For example, the large discrepancies in the site-specific saturation light intensity are difficult to explain. The ponds at Kailua-Kona and San Diego overperformed the initial hindcasted predictions **(Fig. H.)**. Light intensity saturation was increased at these sites, boosting the hindcasted productivities closer to the observed values and minimizing error. Conversely, ponds at Las Cruces underperformed the initial hindcasted predictions and saturation light intensity was decreased to minimize modeling error. To match the observed performance, the saturation light intensity at Las Cruces was lowered to nearly half that of the other three sites. A site-to-site difference this large seems unlikely when growing the same strain with the same protocol. These large adjustments to the saturation light intensity may have acted as a mechanism to lower or raise the overall site-specific productivity to compensate for the environmental drivers and pest pressures not captured in the modeling framework. Alternatively, the large site-to-site difference may be influenced by strain

adaptation to environmental conditions. Higher overall ash contents were recorded at Las Cruces potentially causing increased light attenuation in the ponds. It is possible that cultures at this site have adapted over time to prefer lower light intensities.

Site-specific strain parameters were averaged and used to hindcast growth at each of the four sites **(Fig. H.)**. The multi-site averages were used as a middle-ground between the highly variable site-specific values. Hindcasted harvest concentrations varied from measured values by 0.0 ± 0.20 g/L at Kailua-Kona, and -0.29 ± 0.08 g/L at San Diego, indicating lower average differences but higher standard deviations compared to growth hindcasted with strain parameters from literature. This modeling exercise resulted in disproportionate shifts in the hindcasted predictions for Las Cruces yielding unrealistic harvesting concentrations (upwards of 4.5 g/L) and a significant increase in modeling error (1.29 ± 0.89 g/L compared to 0.30 ± 0.34 g/L). While predictions for Las Cruces were dramatically shifted, results for the other three sites fell between those using literature and site-specific values. In general, the disproportionate shift in the predictions for Las Cruces suggests that large adjustments to the saturation light intensity variable are more than just a means of calibrating for consistent underprediction. Instead, the high sensitivity to this variable is being exploited by the model to capture the impacts of additional productivity drivers not captured in the modeling framework. These results emphasize the disconnect between the low productivities observed in Las Cruces and the largely favorable weather conditions, and predicted performance closer to that achieved in San Diego. Further details on the hindcasting effort and the full study have been published (Echenique-Subiabre et al., 2023).

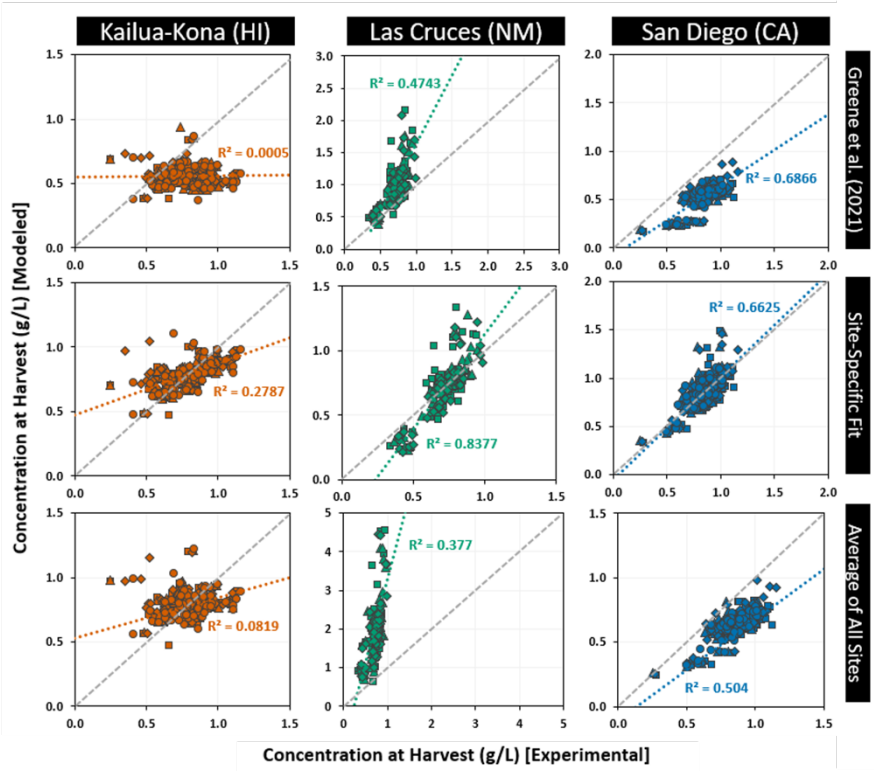

Fig. 2-11. Growth hindcasting using strain parameters obtained from Greene et al. 2021 for N. oceanica [top row], through site-specific stochastic model fitting [middle row], and by taking the average of the site-adjusted strain parameter values [bottom row]. Trendlines in each graph (with the r^2 value displayed) were generated using the multi-pond average concentration at harvest for each site and applying a linear fit. Dotted gray lines in each graph represent a 1:1 agreement between hindcasted and measured values.

2.7 Associated Experiments

Experiments were conducted throughout the project to provide context for possible contributing drivers of productivities across sites, specifically the low productivity at the NMSU site. **Table 2-3** summarizes all experiments completed. Data from these experiments are not published but are available upon request.

Table 2-3. Experiments conducted in the lab to isolate potential drivers of differences in productivity across sites.

Dates	Experiment ID	Description	Summary
2/20/21 – 3/1/21	NMSU-L-015	Nutrient Addition/Omission– Plate experiment using field media components and the NMSU field strain with specific nutrient omissions/additions.	The nutrients tested did not limit growth of the NMSU field culture.
3/30/21 – 4/5/21	NMSU-L-018	Nutrient Source – Flask experiment using original vs new stocks of UAN, 10-34-0 (PO_4), and Fe with the NMSU field strain.	The nutrient stocks tested did not limit growth of the NMSU field culture.
5/17/21 – 6/7/21	NMSU-L-019	Field Dry Components – Plate experiment comparing CA, HI, and NM field salts ($NaHCO_3$, NaCl, KCl, $MgSO_4$, CaCl) in NM tap water and NM liquid nutrients (UAN, 10-34-0, Trace metals, Fe).	The different sources of salts did not affect culture growth.
1/21/22-4/3/22	NMSU-F-030	Sediment – Field experiment aimed to determine the role of sediment accumulation in the growth of the NMSU field strain.	Sediment accumulation alone could not explain cross-site differences in productivity.
11/22/21 – 2/9/22	NMSU-F-032	NMSU Productivity – Evaluation of the role of pond design, depth, and media on productivity at NMSU. Two new ponds of a different design were started using Task 2 OSPREY maintenance pond culture. Also tested 18NFL media and different depths (88mm/260L, 203mm/600L)	Pond depth influenced productivity, but not pond design or media type. There were some differences in running depths across sites, but these were minimal.
11/18/21 – 11/23/21	NMSU-L-033	Testing Growth Limits – Scaling of the cold mutant ponds (Exp 028) was slow, coincident with OSPREY maintained ponds not growing from 11/12 to 11/17. Aim is to bring cultures inside, to more ideal conditions to confirm they grow.	When cultures were brought inside the growth returned to the expected rate. Growth was slow due to environmental conditions.

04/05/22 – 05/09/22	NMSU-F035	Outdoor Common Garden Experiment – Bulk sorted strains from all field sites were scaled up and cultivated at the NMSU field site using NMSU ponds.	There was no trait drift or evolution (for growth rate, stability, and biomass composition) across field sites. These data will be published in a forthcoming manuscript.
05/30/22 – 6/10/22	NMSU-L-047	Nutrient Addition/Omission – Plate experiment using field media components and the NMSU field strain and a clean QTOO1 with specific nutrient omissions/additions.	The nutrients tested did not limit growth of the NMSU field culture or clean strain.
7/5/22 – 7/22/22	NMSU-L-051	Water Source Comparison – Plate experiment aimed to determine if a contaminant in field site water was limiting growth. Used NMSU lab water and field water (filtered and unfiltered).	Water source did not affect culture growth.
3/6/23 – 3/7/23	NMSU-L-068	NO_2 Toxicity – NO_2 concentrations above 20ppm have been observed in NMSU ponds. Plate experiment with field culture and QT001 to quantify the toxicity of NO_2 (0, 20, 40, 80, and 120 ppm) to the strain.	Concentrations greater than 40 ppm were toxic, but concentrations that high have not been observed in the field.

2.8 Pond Geometries

Multiple experiments were done **(Table 2-3)** to understand why NMSU exhibited low productivities compared to what was hindcasted. Suspecting a strong role of pond geometries, we conducted common garden experiments at UCSD. In one experiment, field culture from NMSU was shipped to UCSD to be

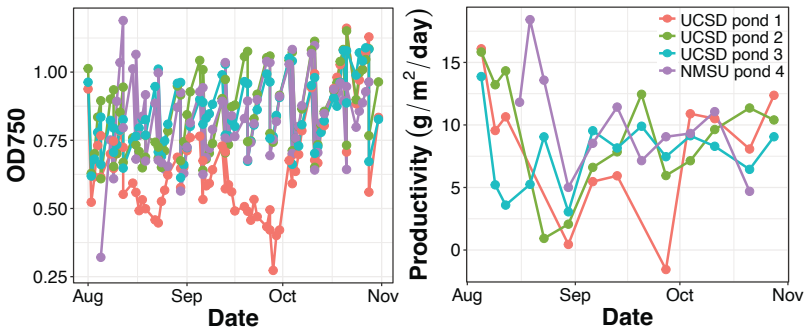

Fig. 2-12. NMSU culture at UCSD on day 0 (top left) and days 2-3 (top right). Plots show OD and productivity data of the ponds at UCSD.

cultivated in UCSD ponds and in another experiment NMSU ponds were shipped to UCSD to cultivate UCSD cultures in NMSU ponds at UCSD. In the first experiment, a new pond was inoculated with NMSU culture in August 2022. This culture performed as well as UCSD ponds during the period of cultivation **(Fig. 2-12)**. Pests for the NMSU culture were minor for the first month with diatoms being detected early on and over the months new invaders were observed. In the second experiment, a pond swap experiment was performed at UCSD to test the effect of pond design in productivity differences observed in NMSU compared to UCSD. This experiment was run from May 2nd to May 30th, 2023, and two replicates per pond design were used **(Fig. 2-13; upper images)**. The same seed culture, the UCSD field-adapted strain, was used to re-start the cultivation experiment in all 4 ponds. We monitored OD and AFDW, and estimated productivities **(Fig. 2-13; bottom graphs)**. Biomass accumulation was limited in NMSU ponds compared to UCSD ponds. Growth rates (g L-1 d-1) were ~50% greater in UCSD ponds compared to NMSU ponds. When aerial productivities were calculated, these differences were magnified (i.e., different holding volumes and surface areas, data not shown). We conclude that pond design accounted for some of the differences in productivity across sites.

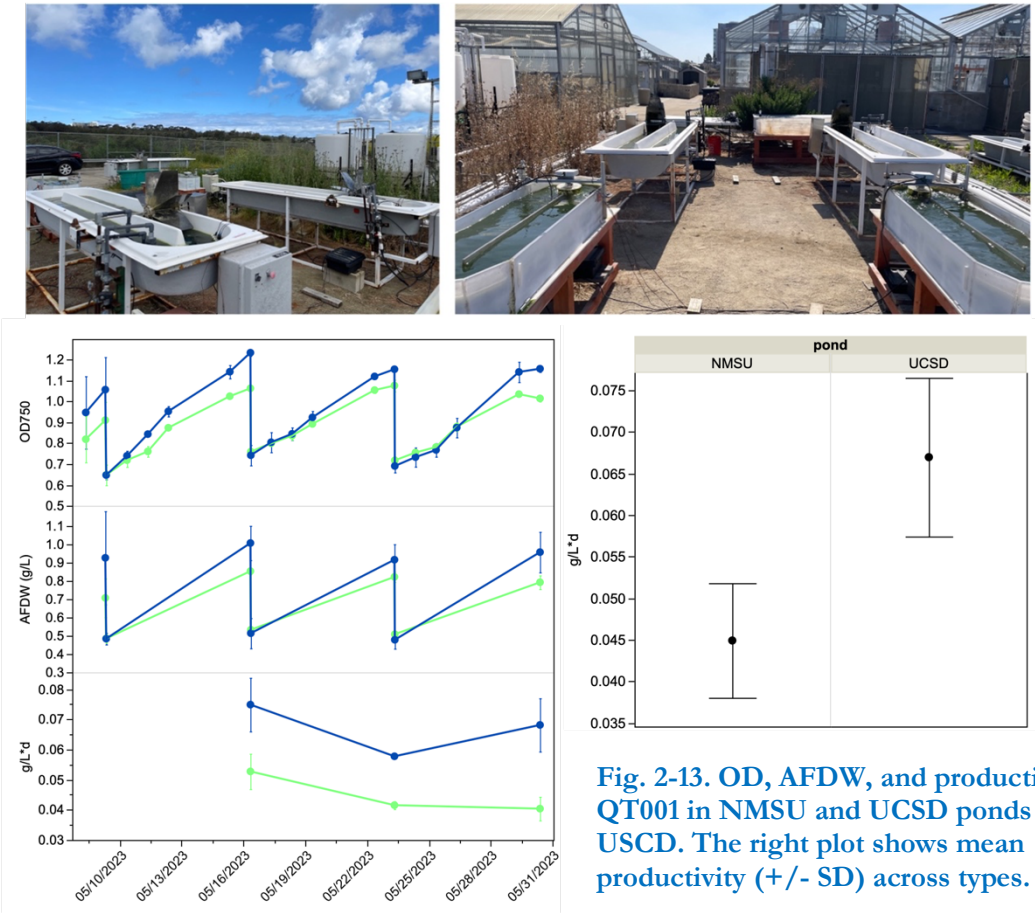

Fig. 2-13. OD, AFDW, and productivity of QT001 in NMSU and UCSD ponds at USCD. The right plot shows mean productivity (+/- SD) across types.

We compared light availability inside ponds over the course of a growth cycle in June 2023, from 6/22 to 6/27 at UCSD site. We used the same cultures and pond set-up from the previous productivity comparison and two replicates per pond design **(Fig. 2-14A-D)**. We performed

measurements of Photosynthetically Active Radiation (PAR) in 3-4 sides of the pond's walls using a Li-193 Spherical Quantum sensor **(Fig. 2-14E-H)**. Measurements were done two times a day: in the morning (at east sun position) and afternoon (at top sun position) at two different depths: bottom (0-6 cm) **(Fig. 2-14G)** and below the surface (8-14 cm; 9-15 cm for UCSD and NMSU ponds respectively) **(Fig. 2-14H)**. Density and chlorophyll-a increased over the experiment, showing that *Nannochloropsis* was actively growing **(Fig. 2-15A-B)**. The increase in chlorophyll-fluorescence was greater in NMSU ponds compared to UCSD ponds **(Fig. 2-15B)** based on the slope differences. Large differences were observed among pond designs **(Fig. 2-15C)**; for example, for UCSD ponds at the bottom values ranged from 1.7 to 25.47 µmol/m2/s while at NMSU ponds, PAR ranged between 0.04 and 0.71 µmol/m2/s, being highly light limited compared to UCSD ponds **(Fig. 2-15D)**. The below surface PAR measurements values were higher as expected; however, PAR values were still higher in UCSD ponds **(Fig. 2-15C)** ranging between 5.17 and 108.1 µmol/m2/s. For NMSU ponds, PAR values ranged from 0.29 to 32.7 µmol/m2/s. Variation in light availability at the individual pond level was related to weather conditions, time of the day (i.e., morning or afternoon measurements) and side (i.e., 1-4). Overall, our results revealed that PAR values were greater in UCSD ponds no matter the depths or side position when comparing to NMSU ponds. Moreover, we hypothesize that the difference in chlorophyll-a concentrations is related to light limitation. We conclude that the combined effect of light availability and pond design in our experimental set-up are key factors promoting algal growth and the main reason why productivity at the UCSD site was greater than that at NMSU.

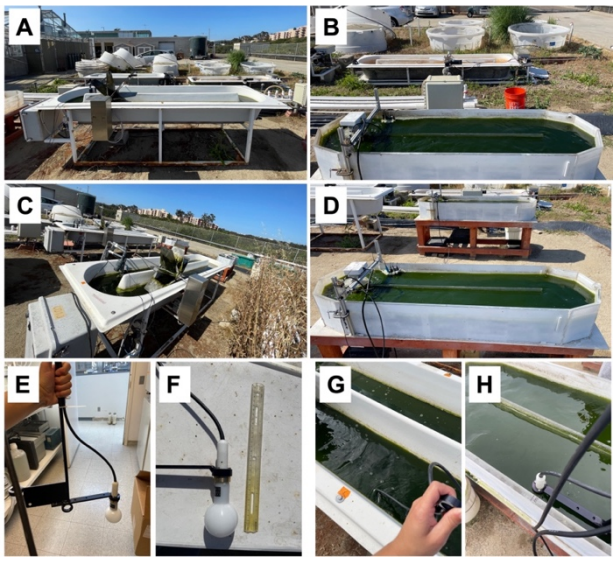

Fig. 2-14. Light measurements at UCSD. NMSU pond designs are show in (A) Minipond 6 and (C) Minipond 5. UCSD pond designs are Minipond 1 (B) and Minipond 3 (D). For PAR measurements, the Li-193 Spherical Quantum sensor was used (E-F) at two different depths: bottom (G) and below surface (H).

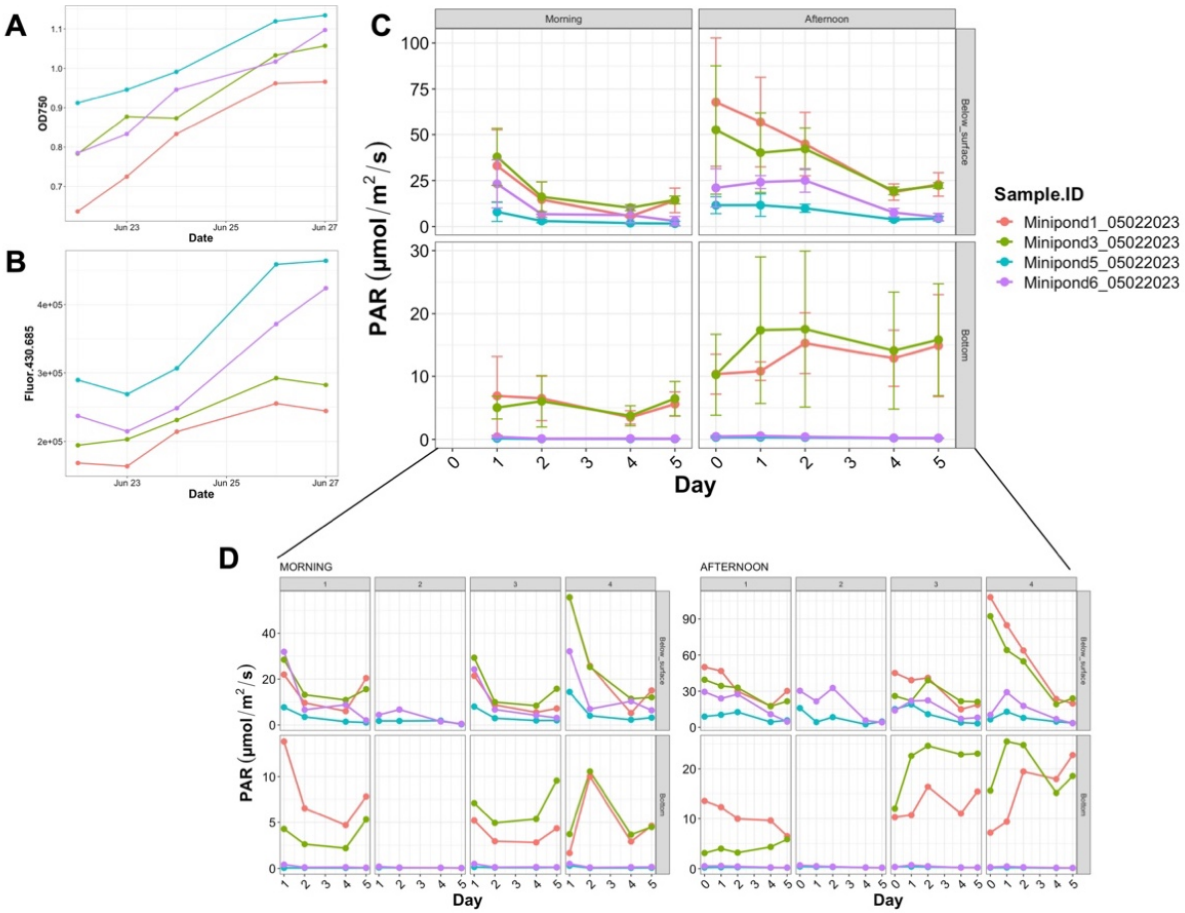

Fig.2-15. Measurements of light at UCSD in NMSU and UCSD ponds. OD750 (A) and chlorophyll-a (B) measurements over the course of the frow out. Average light availability (PAR) (C) measured over 5 days two times a day (morning and afternoon) at the surface and bottom of the ponds. The detail of light availability measurements is shown in (D), in which the numbers are 4 sides of each pond. Side 2 measurements are missing for UCSD ponds since the paddlewheel was located there blocking the access for the Li-193 Spherical Quantum sensor. UCSD ponds are Miniponds 1 & 3 and NMSU ponds are Miniponds 5 & 6. In (C-D) note that y-axis scales differ to visualize PAR differences.

3. Balancing Indoor and Outdoor Selection Pressures

3.1 Background

Outdoor algal production systems experience diel and seasonal variability in environmental conditions, erraticism due to extreme weather or operation failures, and ecological threats from invaders. Yet, to generate strains that will be cultivated outdoors, a lab-to-field pipeline is typically followed, as one can select for or enhance traits of interest (e.g., growth rate, lipid content) (Borowitzka, 2013). Such a pipeline can be successful if candidate strains are quickly moved outdoors to verify performance metrics (Corcoran et al., 2018; White and Ryan, 2015). However, adaptation to the lab commonly leads to failures in the field (Grobbelaar, 2012; Sheehan et al., 1998). As noted in the FOA to which this project responded, developers of algal biofuel technologies are challenged by poor translatability of laboratory-scale research systems and larger-scale or mass-production systems. Here, we proposed that the disconnect between lab and field stems in part from different selection pressures in these environments **(Table 3-1)**. We argued that selection pressures must be rigorously quantified and balanced to maintain productive and stable strains in the field.

Farm conditions select for or enhance desired traits from an industry perspective, including a broader temperature range, tolerance to a variable chemistry in growth media, and cellular investment in defenses against competitors, predators, and parasites (e.g., thicker cell walls, secondary compounds) **(Table 3-1)**. In contrast, laboratory systems do not impose these pressures **(Table 3-1)**; as a result, desired traits are lost. For example, after long-term culture, algal isolates can exhibit lower photosynthetic efficiency, a weaker circadian rhythm, changes in toxicity, a loss of sensitivity to shear, and a loss in grazer resistance (Berge et al., 2012; Borowitzka, 2013; Demott and McKinney, 2015; Lakeman et al., 2009). In cell lines ranging from bacterial to mammalian, it is recognized that passage number (i.e., the number of times a strain has been passaged) contributes strongly to genotypic and phenotypic variation (Cooper, 2014; Liu et al., 2014; Mouriaux et al., 2016). This result has led to practices that discourage serial passage including a formalized concept of maximum passage number (Hughes et al., 2007), which has not yet been indoctrinated within algal biology. However, the general principle is one of the main drivers for the adoption of cryopreservation techniques for algal strains by US and foreign algal culture collections. Field strains are also subject to trait loss. For example, wildtype counterparts commonly display lower productivity than cultivars bred or selected for

Table 3-1. Examples of selection pressures associated with indoor maintenance and outdoor cultivation. Note that positive selection pressures associated with culture maintenance must be imposed by design.

	Indoor Maintenance	Outdoor Cultivation
Positive pressures (increase desired traits)	**NONE**	Variable temperature Presence of pests Commercial-grade medium Natural sunlight
Negative pressures (decrease desired traits)	Constant temperature Lack of pests Permissive media Low, poor quality light	Frequent harvest Chemical treatment

production (Henry and Nevo, 2014; Schröder and Prasse, 2013). Biochemical composition can also shift, necessitating unique cultivation strategies (Ayre et al., 2017; Borowitzka, 2013). In addition, high-intensity cultivation practices, whether in agriculture, aquaculture, or algaculture, induce strong selection pressures on the target cultivar (Dermauw et al., 2013; Hien et al., 2017; Santos and Ramos, 2018; Tomasetto et al., 2017). Indeed, industrial isolates can respond, positively or negatively, to a chemical treatment or harvesting method. However, to our knowledge, there has been no concerted effort made by researchers or producers to quantify the magnitude or time scale of phenotypic trait evolution in field systems. To balance the selection forces associated with strain maintenance in the laboratory with those imposed by high-intensity outdoor cultivation systems **(Table 3-1)**, producers must understand the degree and time scales of trait change in their systems. Such knowledge, coupled with that of strain evolution in the lab, would inform best practices for strain maintenance and cultivation. For example, if desired biomass composition is lost via field cultivation, we can alter cultivation practices to reseed with desired cultivars. Likewise, if laboratory maintenance leads to a loss of desired traits, we can impose constant pressures to maintain or reacquire those traits. More directly, we can use natural selective pressures from our year-round field campaigns to improve strain resiliency.

3.2 Specific Objectives and Strain Maintenance

The specific objectives of this project component were to (1) quantify trait drift and evolution through time across three field sites (Cyanotech, NMSU, and UCSD) and labs (LANL, NMSU and UCSD) and (2) and use resulting knowledge on trait drift and evolution to balance positive and negative selection pressures through changes in cultivation practices. For example, if data demonstrated that field cultivation resulted in loss of a desired trait (e.g., maximum specific growth rate), periodic reseeding could be a modification of cultivation practices in the field. Phenotypic traits of interest were growth rate, stability, and biomass composition. With respect to maintenance practices in the lab, we were interested in determining the effects of different approaches to strain maintenance (e.g., cryopreservation, plate storage, batch cultivar) on trait drift and evolution. We were also interested in quantifying the role of different operators at the different laboratories. In the lab, the initial field-adapted strain was maintained following three different practices: on plates with transfers every three months, in batch culture with transfers every 14 days and in Algem® photobioreactors simulating the outdoor cultivation conditions at an industrial partner (Imperial, TX), with regimes shifting every month. Batch and plate cultivars were maintained at LANL, NMSU, and UCSD, and the photobioreactor cultivar was maintained at LANL only. The LANL lab sourced water from NMSU.

The strains under batch and photobioreactor cultivation were maintained for 73 and 150 harvest cycles, respectively **(Fig. 3-1)**. The NMSU batch-maintained strain did not establish well at the beginning of the cultivation period due to issues in environmental conditions. It recovered after the first four harvest cycles. The batch-maintained cultivars were generally maintained between optical densities of 0.2 to 4, although there were deviations in this range at LANL and NMSU due to health issues and reinoculation. The bioreactor-maintained strains

were kept between optical densities of 0.2 to 1.2 until April 2022. At this point, there was a change in personnel and cultivars reached higher densities. Through time, we noticed macroscopic changes in the batch-maintained cultivars at NMSU and UCSD. Specifically, these cultivars would start to flocculate and would turn to a green-brown color by day 10 of the harvest cycle. The batch-maintained cultivars at UCSD and NMSU were treated with an antibiotic cocktail (ampicillin, chloramphenicol, streptomycin, and tetracycline) in August 2021 that helped improve culture health and decreased bacterial load. Growth rates of the UCSD batch-maintained strains also decreased through time, with the cultivars reaching a lower OD after April 2022. Two events might explain this decrease: new personnel helping to prepare culture media and the re-incidence of bacterial contaminants. Every six months, we characterized trait drift and evolution of the field and lab-maintained cultures through common garden experiments conducted in 300 mL bubble column reactors **(Fig. 3-2)**. Genotyping was also conducted on samples run through the bubble column reactors during these time points. This work is described in the next sections.

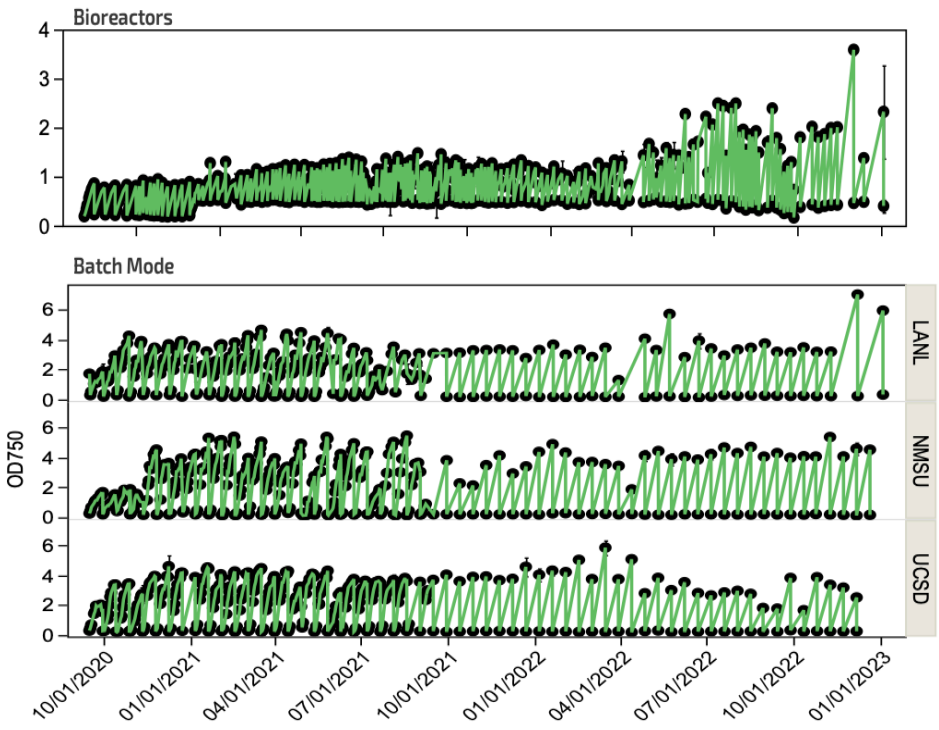

Fig. 3-1. Time series data of OD for batch and Algem-maintained strains. Points show the mean ± SD of three and two replicates for the batch and photobioreactor maintained strains, respectively.

Fig. 3-2. Photo of the bubble column reactors used for the phenotype characterizations.

3.3 Common Garden Experiments to Quantify Growth, Stability, and Biomass Composition

Five common garden experiments were conducted over 27 months of strain maintenance in the lab and field. In each common garden experiment, each cultivar was grown in four replicates for two harvest cycles. Experiments were carried out in batch mode using OSPREY media at ambient temperature. pH was maintained at 8 by CO_2 injection on demand with continuous aeration to ensure mixing and dissolved oxygen degassing. Diurnal lighting provided an irradiance of 200 µE m^{-2} s^{-1}. The optical density of the cultivars was measured daily at 750 nm using a Spectramax M2 (Molecular devices, USA). The Ash Free Dry Weight (AFDW) concentration was determined at the end of each harvest cycle by filtering 50 mL of each cultivar through a 1.2 µm pre-combusted filter (GE Healthcare Life Sciences, China), followed by drying at 100°C for one hour, then combusting at 500°C for four hours. In addition, the maximum photosynthetic efficiency of photosystem II (Fv/Fm) was determined daily using a mini-PAM (Heinz Walz GmbH, Germany) to assess the cell physiological status.

We compared performance of each of the site strains to a resurrected strain cryopreserved at the start of the experiment. This cryopreserved strain was pulled from -80°C storage before each characterization, gradually thawed, and scaled up to the flask stage to be used in common garden experiments. To determine the biochemical composition, the biomass was harvested from each bubble column at the end of each grow-out by centrifugation at 3700 rpm for 20 min (Eppendorf 5920R, Germany), washed twice with distilled water, lyophilized, and used for the analyses. Carbohydrate, lipid, and protein contents were quantified following NREL methods (Van Wychen and Laurens, 2015). Lipids were accounted for as total Fatty Acid Methyl Esters (FAME). FAME contents and profiles were determined by gas chromatography (GLC 461C, NuChek Prep Inc. USA).

With respect to lab-maintained cultivars, the cryopreserved strain displayed the most stable growth across all characterizations **(Fig. 3-3)**. LANL batch- and plate- maintained strains showed consistent growth trends across characterizations. The batch and plate-maintained strains from UCSD and NMSU exhibited greater variability in growth across characterizations compared to the cryopreserved, LANL batch, and Algem maintained strains **(Fig. 3-3)**. In fact, starting at the second characterization after 9 months of maintenance, these plate and batch- maintained strains took longer times to establish and only recovered during the second harvest cycle. With respect to field strains, cultivar growth was variable across characterizations and compared to the cryopreserved strain **(Fig. 3-4)**. In the ponds at field sites, the field strain at UCSD exhibited the best growth whereas the lowest growth was found at the NMSU site. However, in the common garden experiment, NMSU, Cyanotech and UCSD field strains showed similar growth during the second harvest cycle **(Fig. 3-4)**. These results demonstrate a strong role of the environment and little to no role of trait drift and evolution. One can conclude that the initial *Nannochloropsis* strain exhibited high plasticity allowing it to grow under a wide range of environmental conditions. Of note, field cultivars in the first characterization (i.e., after three months of maintenance outdoors) were more in line with the cryopreserved strain than in the other characterizations.

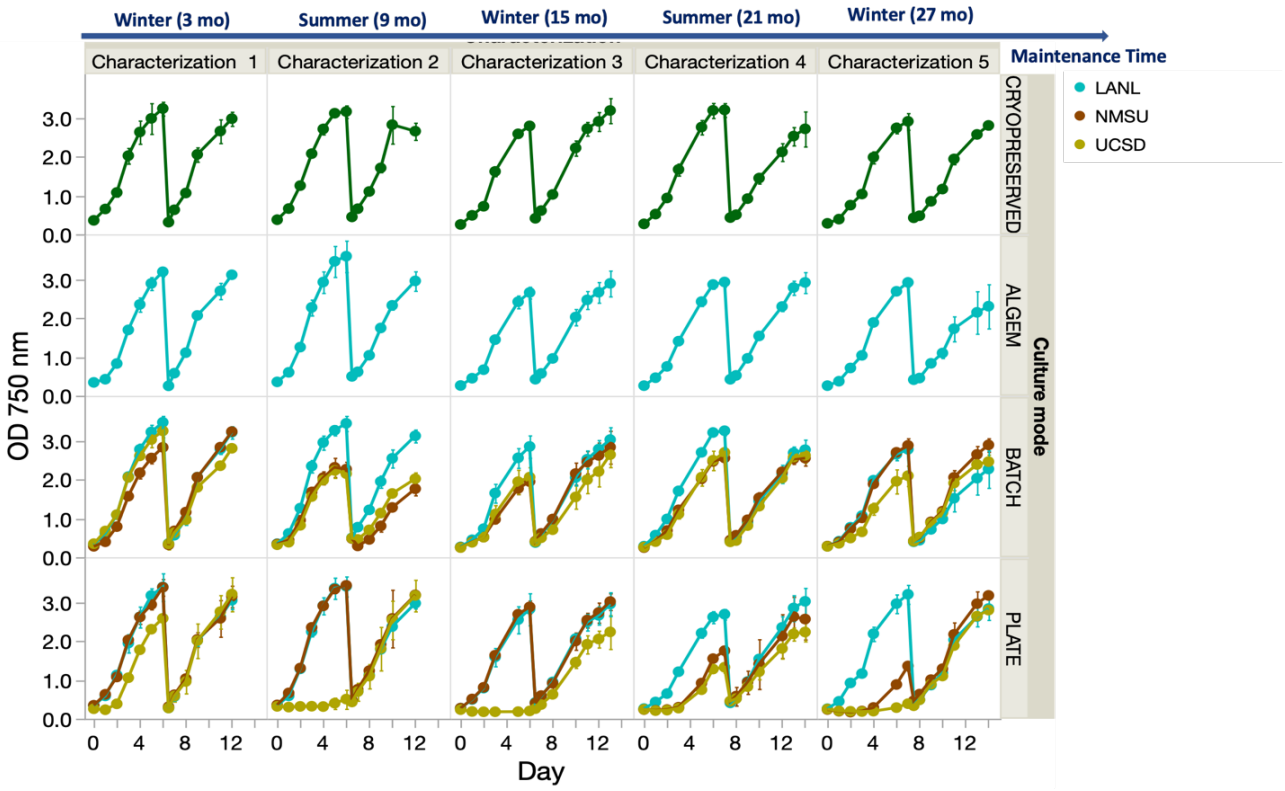

Fig. 3-3. Optical density of each of the lab-maintained cultures in the bubble column experiment. Points represent means (± standard deviation) of four replicate bubble column cultures.

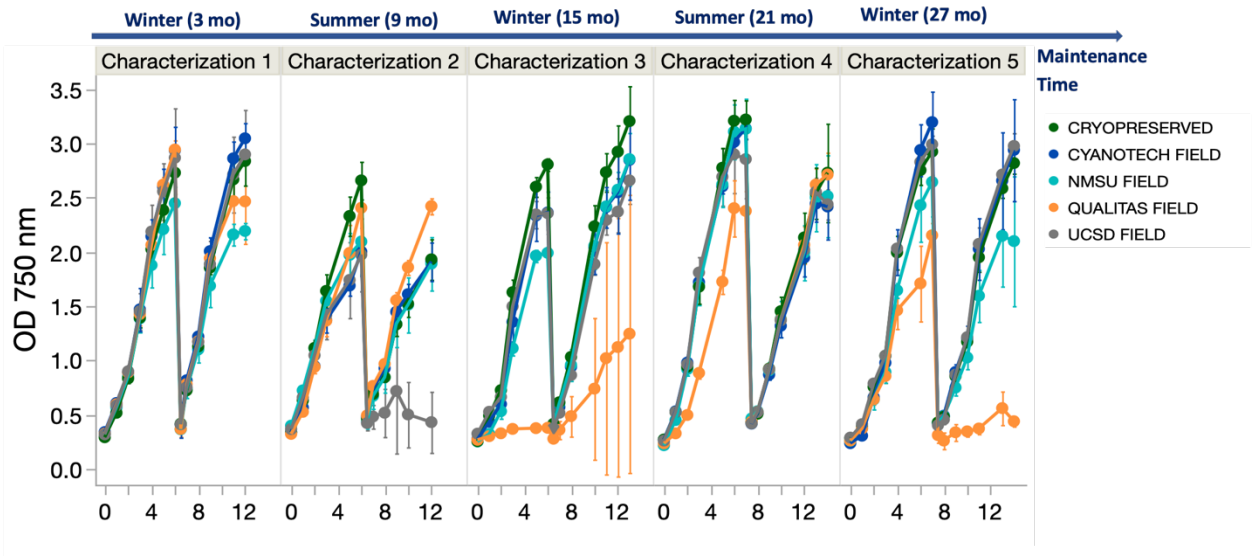

Fig. 3-4. Optical density of each of the lab-maintained cultures in the bubble column experiment. Points represent means (± standard deviation) of four replicate bubble column cultures.

Fig. 3-5. AFDW-based of productivity of lab strains at each harvest cycle for each characterization during the common garden experiments. Points represent means (± standard deviation) of four replicate bubble column cultures.

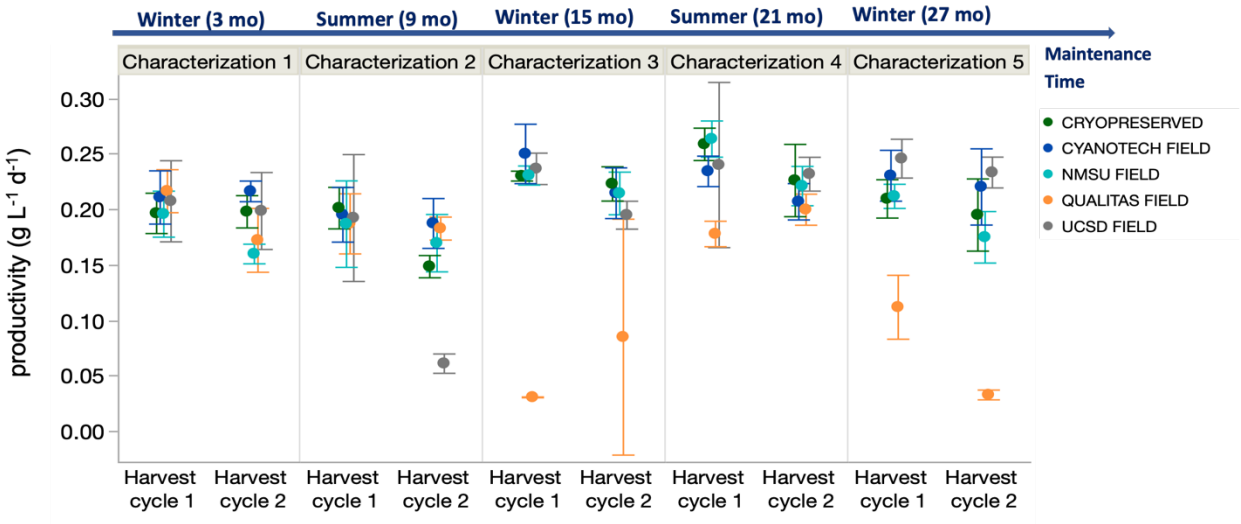

Fig. 3-6. AFDW-based of productivity of the field strains compared to the cryopreserved strain at each harvest cycle for each characterization during the common garden experiments. Points represent means (± standard deviation) of four replicate bubble column cultures.

AFDW-based productivity was calculated for both grow-outs for each characterization. Productivities ranged from 0.04 g L^{-1} d^{-1} to 0.3 g L^{-1} d^{-1} for lab cultivars and from 0.03 g L^{-1} d^{-1} to 0.26 g L^{-1} d^{-1} for field cultivars. The cryopreserved, LANL batch, and Algem-maintained strains were the most productive among lab strains **(Fig. 3-5)**, and the Qualitas strain was the most variable field strain **(Fig. 3-6)**. This variability can be explained by the lack of managing pests that were brought into the lab with the field cultivars. To assess stability, we used the metric of temporal CV, calculated on biomass, growth rates, and productivity during each characterization. This metric showed that cultivars were stable except for the UCSD plate, NMSU plate, UCSD field, and Qualitas field cultivars (data not shown), consistent with variances in productivity **(Fig. 3-6)**.

Biochemical composition evaluated after each harvest during the common garden experiments showed that regardless of lab, field site, or the cultivation mode, the proteins accounted for the major biomass fraction whereas the lipid content ranged from 7% to 12% **(Fig. 3-7, 3-8)**. No consistent trend of the variation of biomass composition across characterizations was observed.
Additionally, strain biochemical composition didn't show a higher total content when using a particular cultivation practice over another. Maintained in batch, plate, or Algem culture, the maximum content was generally ~60% which is within the range of biomass composition reported by NREL methods. Because of a lyophilizer issue, samples of the third characterization were lost. Thus, backup cultivars used to inoculate bubble columns photobioreactors for that

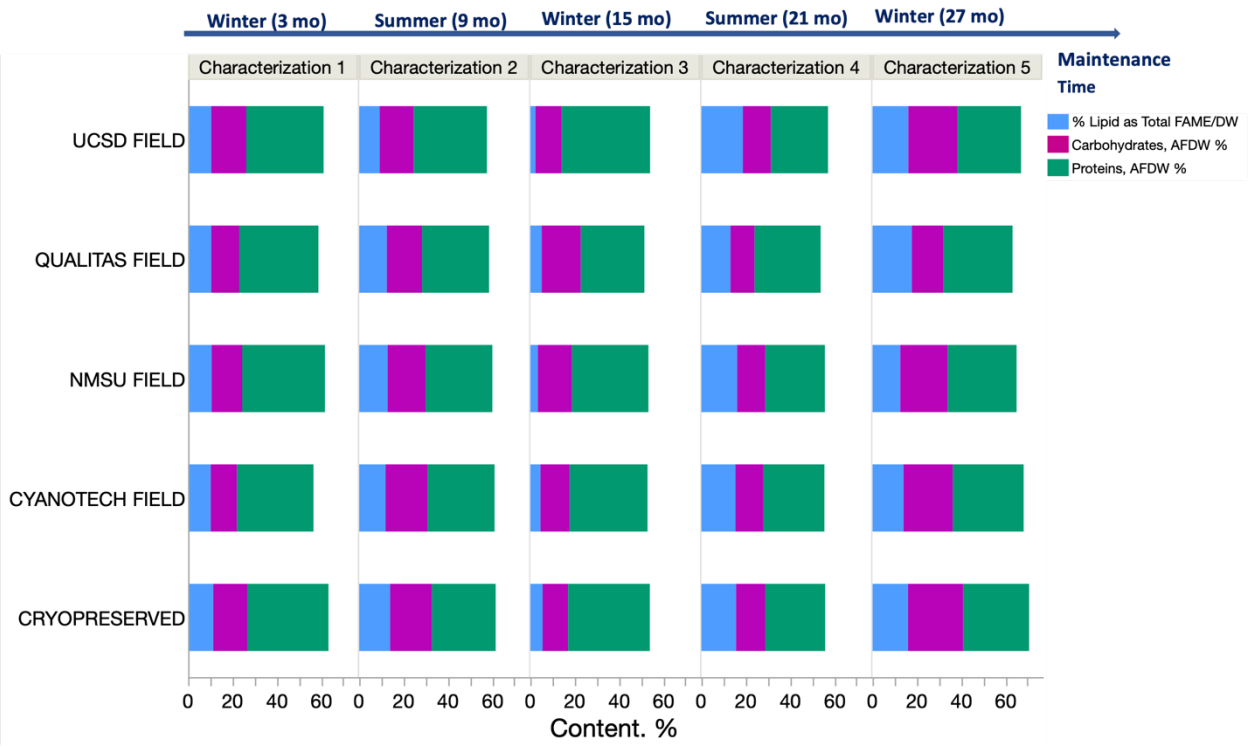

Fig. 3-7. Biomass composition of the field strains compared to the cryopreserved strain at each characterization during the common garden experiments. Average biomass composition is shown, although variability around the mean for each replicate was 1.4 to 7%.

phenotype characterization were used. These data are likely not comparable to date from other characterizations.

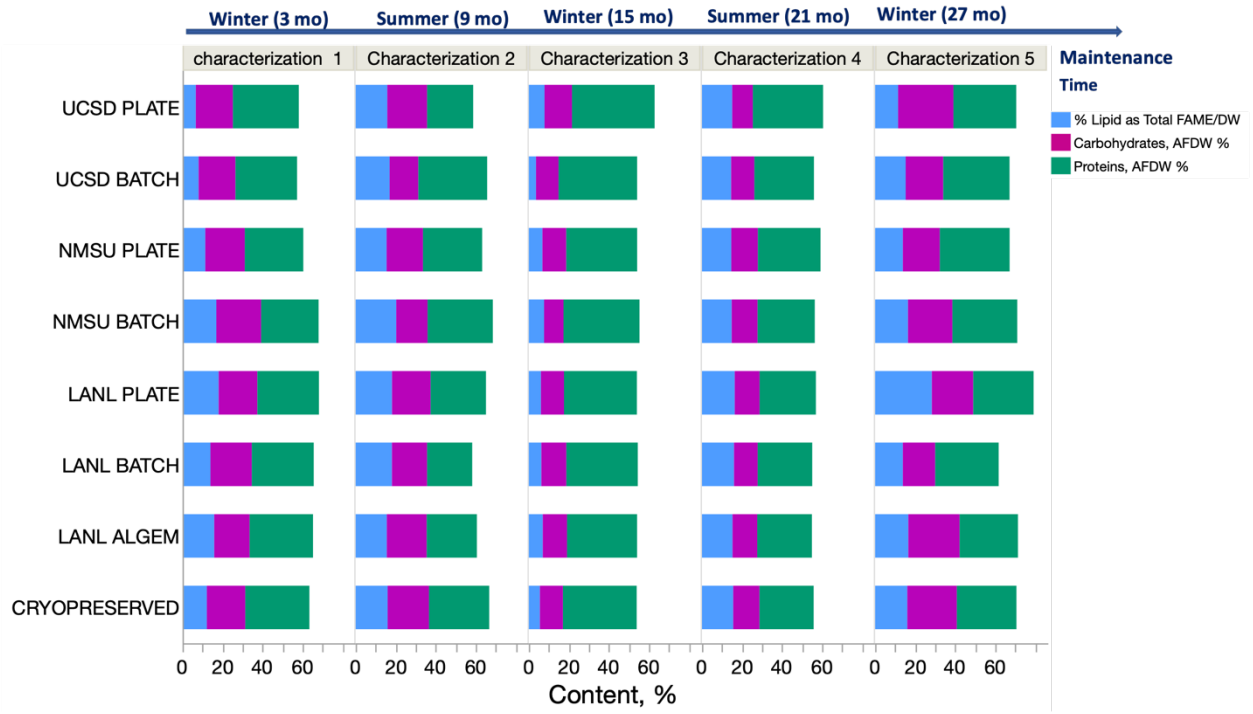

Fig. 3-8. Biomass composition of the field strains compared to the cryopreserved strain at each characterization during the common garden experiments. Average biomass composition is shown, although variability around the mean for each replicate was 1.8 to 8%.

To better visualize phenotypic changes through time, we calculated the deviation in traits (growth rate, productivity, biomass composition) compared to the cryopreserved strain in each common garden experiment. Prior to these comparisons, however, we wished to ensure the traits of each resurrected cryopreserved strain did not change across characterizations. Deviation plots showed that growth rate and productivity of

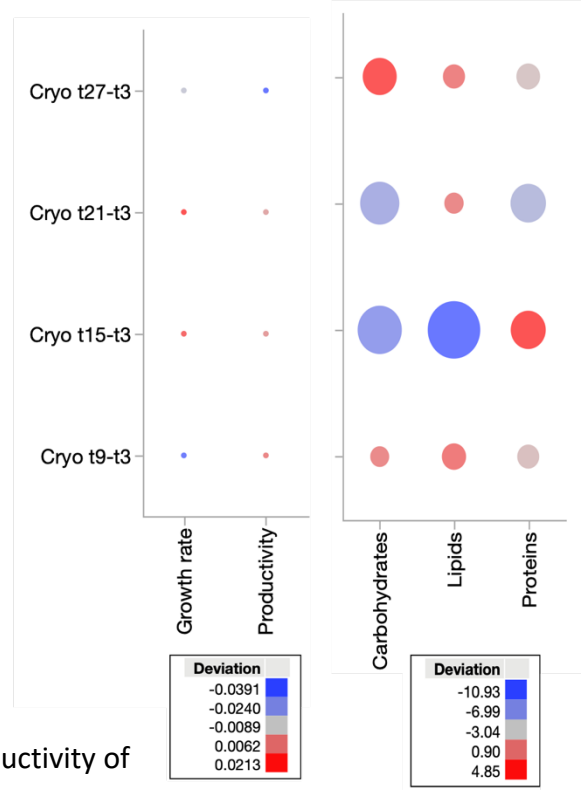

Fig. 3-9. Deviation of growth rate, productivity and % carbohydrates, lipids and proteins compared to the resurrected cryopreserved strain at the first characterization (T3) The size of the bubble indicates the magnitude of deviation, and the color indicates the sign of the deviation. Note the different scale bars for growth and productivity vs. biomass composition.

the cryopreserved strain did not change through time **(Fig. 3-9)**. There was some variability in biomass composition across characterizations, but this variability was generally less than 5% and did not show patterns in sign (i.e., loss, gain) or through time **(Fig. 3-9)**. Biomass composition was the most variable at the third characterization (month 15), due to the lyophilizer issue previously mentioned. Deviation plots of the lab and field-maintained strains relative to the cryopreserved strain at each characterization time point showed there was an increase in variability with time in each cultivar **(Fig. 3-10)**. Field strains tended to underperform compared to the cryopreserved strain, whereas lab strains showed minimal deviation and was in most cases positive except for the UCSD plate-maintained strain. However, there was no clear patterns that would confirm a consistent shift in phenotypes.

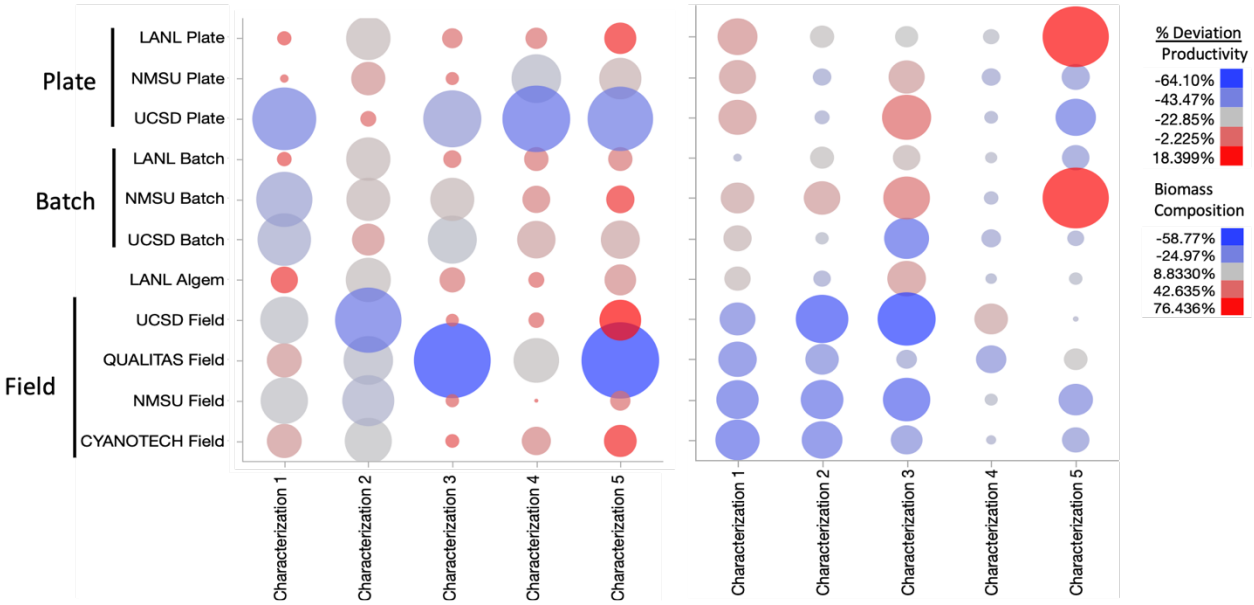

Fig. 3-10. Deviation of productivity (left) and lipid content (right) in each of the strains compared to the cryopreserved strain cultured at each characterization. The size of the bubble indicates the magnitude of deviation, and the color indicates the sign of the deviation.

3.4 Genomic Changes

Whole genome sequencing (WGS) was performed on each cultivar every six months to track genomic changes through time. Genomic libraries were prepared for Illumina sequencing using the Nextera sample preparation kit (Illumina). Barcoded libraries were quantified on an Invitrogen Qubit Fluorometer and submitted for 150 bp paired end sequencing on an Illumina HiSeq 2000. The reads were aligned against the reference strain of QH25 using BWA and default parameters for paired end reads. Mapped reads were converted into a SAM file format for each strain. A file containing uniquely mapped reads was generated from the original SAM file and compressed into a BAM file to perform variant analysis against the cryopreserved strain using DeepVariant (Li and Durbin, 2009; Poplin et al., 2018). Across cultivars, mutations generally increased through time **(Fig 3-11)**. These mutations and their associated allele frequencies were tracked through the 27-month period **(Fig. 3-12)**. Mutations were then identified to be within gene regions and a delta allele frequency was calculated for each

mutation over time. Most mutations identified at three months were relatively stable through time if the initial frequency had reached fixation. Few mutations displayed a net increase in allele frequency across culturing methods (Table 3-2). These mutations were identified in cultivars that are populations of cells, grown up over time allowing the frequencies of the mutations to change. The effect of these mutations is likely neutral since the phenotypes of these cultures largely remained constant through time. A similar pattern of allele frequencies identified in the lab were also seen in the outdoor ponds (Fig. 3-13). Of note, mutations identified in TLP1 were identified across conditions (plate, flask, Algem, and pond) across all sites and displayed a large increase in frequency (Tables 3-2, 3-3). To test the effect of mutations that increased in frequency, clonal isolation and phenotype assays would need to be done to associate the mutations with any phenotype. Interestingly, there were recurrent mutations identified across cultivation type as well as shared between sites.

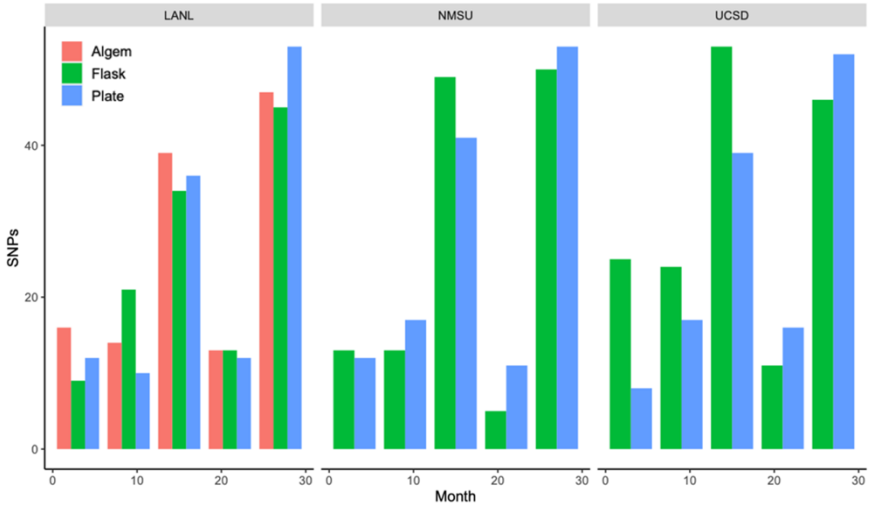

Fig. 3-11 Bar chart showing the number of single nucleotide polymorphisms (SNPs) present in each strain over 27 months at the different labs (left to right). SNPs were filtered based on their presence in the baseline line strain.

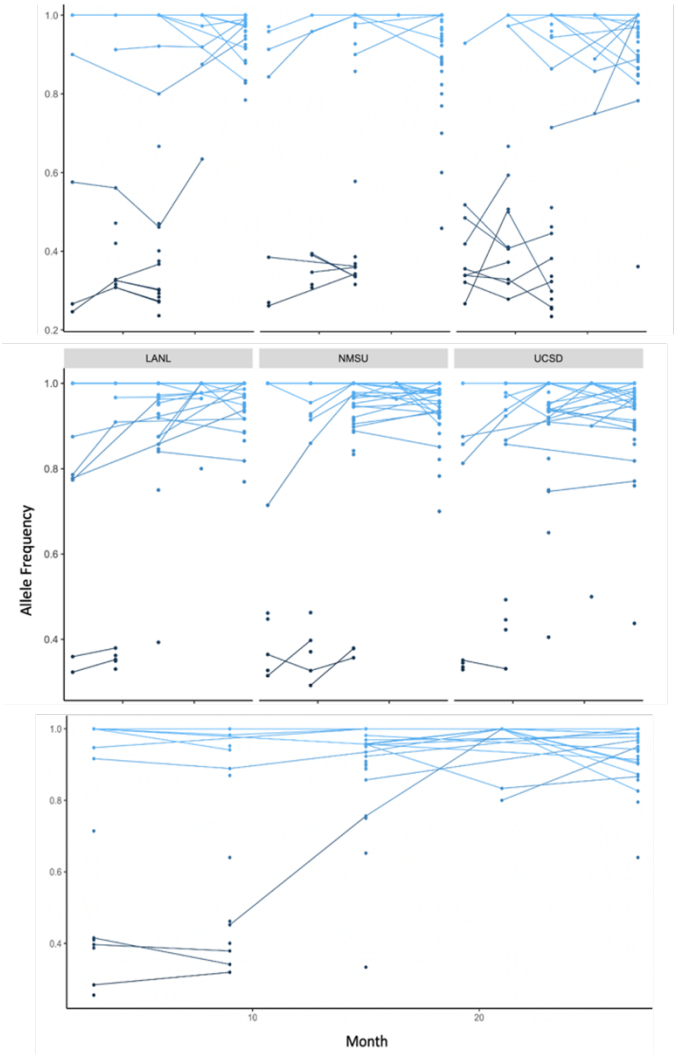

Fig. 3-12. Allele frequencies of single nucleotide polymorphisms (SNPs) identified in flask- (top), plate- (middle), and photobioreactor- (bottom) maintained cultures. Flasks and plates were maintained at LANL, NMSU, and UCSD. Allele frequencies greater than 0.8 are shown in blue.

Table 3-2. Mutations that displayed a net increase in allele frequency across culturing methods. 'I' indicates intergenic, and 'IU' indicates upstream of an intergenic region.

Site	Culture Method	ΔAF (%)	Type	CDS	Ref	Alt
NMSU	Flask	0.18939167	IU	Similar to CaMKMT: Calmodulin-lysine N-methyltransferase	C	G
UCSD	Plate	1.190475	I	Similar to Dhx36: ATP-dependent DNA/RNA helicase DHX36	T	G
LANL	Plate	0.39457083	I	Similar to Dhx36: ATP-dependent DNA/RNA helicase DHX38	A	G
LANL	Plate	0.66550833	I	Similar to Dhx36: ATP-dependent DNA/RNA helicase DHX39	G	A
NMSU	Flask	0.83333333	I	Similar to EMB1025: Pentatricopeptide repeat-containing protein	C	T
LANL	Flask	1.16161667	I	Protein of unknown function (g01819)	T	C
UCSD	Plate	1.5625	I	Protein of unknown function (g01819)	T	C
LANL	Plate	0.5456375	I	Protein of unknown function (g01819)	T	C
LANL	Algem	0.09578333	I	Protein of unknown function (g08222)	A	G
NMSU	Flask	0.1736125	I	Protein of unknown function (g08222)	A	G
UCSD	Flask	0.05290952	I	Protein of unknown function (g08222)	A	G
LANL	Plate	0.11010556	I	Protein of unknown function (g08222)	A	G
UCSD	Plate	0.12345556	I	Protein of unknown function (g08222)	A	G
NMSU	Plate	0.25252778	I	Protein of unknown function (g08222)	A	G
LANL	Algem	0.54220556	I	Protein of unknown function (g08222)	G	A
UCSD	Flask	1.13636667	I	Protein of unknown function (g08222)	G	A
LANL	Flask	0.57108333	I	Protein of unknown function (g08222)	G	A
NMSU	Flask	0.39849583	I	Protein of unknown function (g08222)	G	A
LANL	Flask	0.36810476	I	Protein of unknown function (g08222)	G	A
UCSD	Flask	0.13227619	I	Protein of unknown function (g08222)	G	A
UCSD	Plate	0.63972778	I	Protein of unknown function (g08222)	G	A
NMSU	Plate	0.24470556	I	Protein of unknown function (g08222)	G	A
NMSU	Plate	0.39682778	I	Similar to HAC1: Histone acetyltransferase HAC1	C	G
LANL	Algem	0.2193	I	Similar to HAC1: Histone acetyltransferase HAC2	G	C
UCSD	Flask	0.21128333	IU	Similar to ycsN: Uncharacterized oxidoreductase YcsN	T	C
UCSD	Plate	0.30153333	IU	Ankyrin repeat and zinc finger domain-containing protein 1	G	A
UCSD	Flask	0.56935833	I	Protein of unknown function (g07360)	C	T
LANL	Algem	4.56989167	I	Similar to TLP1: Thaumatin-like protein 1	A	G
LANL	Flask	0.32437778	I	Similar to TLP1: Thaumatin-like protein 2	A	G
LANL	Plate	1.57815	I	Similar to TLP1: Thaumatin-like protein 3	A	G
NMSU	Plate	2.18253333	I	Similar to TLP1: Thaumatin-like protein 4	A	G
UCSD	Plate	0.04735	I	Similar to TLP1: Thaumatin-like protein 5	A	G
NMSU	Plate	0.77972778	I	Similar to TLP1: Thaumatin-like protein 6	A	G

Table 3-3. Mutations that displayed a net increase in allele frequency in ponds.

Coordinate	Site	Pond	ΔAF (%)	Gene
contig_78:253958	Cyanotech	Pond.1	3.28282778	TLP1: Thaumatin-like protein 1
contig_77:65611	Cyanotech	Pond.1	2.55555	Intergenic
contig_5:2139	Cyanotech	Pond.1	0.92593333	Intergenic
contig_94:4109	Cyanotech	Pond.1	0.89408333	Intergenic
contig_52:37100	Cyanotech	Pond.1	0.50505	Intergenic
contig_51:24400	Cyanotech	Pond.1	0.4629625	Intergenic
contig_5:2140	Cyanotech	Pond.1	0.4386	Intergenic
contig_6:562715	Cyanotech	Pond.1	0.41486667	g08222.t1_hypothical protein
contig_94:3655	Cyanotech	Pond.1	0.41451667	Intergenic
contig_38:1663	Cyanotech	Pond.1	0.39682778	Intergenic
contig_94:3476	Cyanotech	Pond.1	0.31241667	Intergenic
contig_94:3654	Cyanotech	Pond.1	0.25366111	Intergenic
contig_117:3467	Cyanotech	Pond.1	0.12365833	Intergenic
contig_77:68451	NMSU	Pond.1	2.94118333	Intergenic
contig_78:253958	NMSU	Pond.1	2.88825833	TLP1: Thaumatin-like protein 1
contig_90:422	NMSU	Pond.1	2.08333333	g00733_Protein of unknown function
contig_51:24400	NMSU	Pond.1	1.20613333	Intergenic
contig_37:1081943	NMSU	Pond.1	1.17556667	p7C12_g04432.t1
contig_65:150705	NMSU	Pond.1	1.08196667	Intergenic
contig_61:116463	NMSU	Pond.1	0.76755	Intergenic
contig_64:516619	NMSU	Pond.1	0.69445	Intergenic
contig_65:150790	NMSU	Pond.1	0.60551667	Intergenic
contig_6:562715	NMSU	Pond.1	0.34994167	g08222.t1_hypothical protein
contig_62:68084	NMSU	Pond.1	0.3367	p7C12_g00050.t1
contig_94:3654	UCSD	Pond.1	3.23066667	Intergenic
contig_64:516619	UCSD	Pond.1	1.66666667	Intergenic
contig_76:20093	UCSD	Pond.1	1.094275	Intergenic
contig_106:34786	UCSD	Pond.1	0.83333333	p7C12_g01679.t1
contig_51:24400	UCSD	Pond.1	0.74074167	Intergenic
contig_94:3655	UCSD	Pond.1	0.684175	Intergenic
contig_25:148216	UCSD	Pond.1	0.46296667	Intergenic
contig_38:1663	UCSD	Pond.1	0.2924	Intergenic

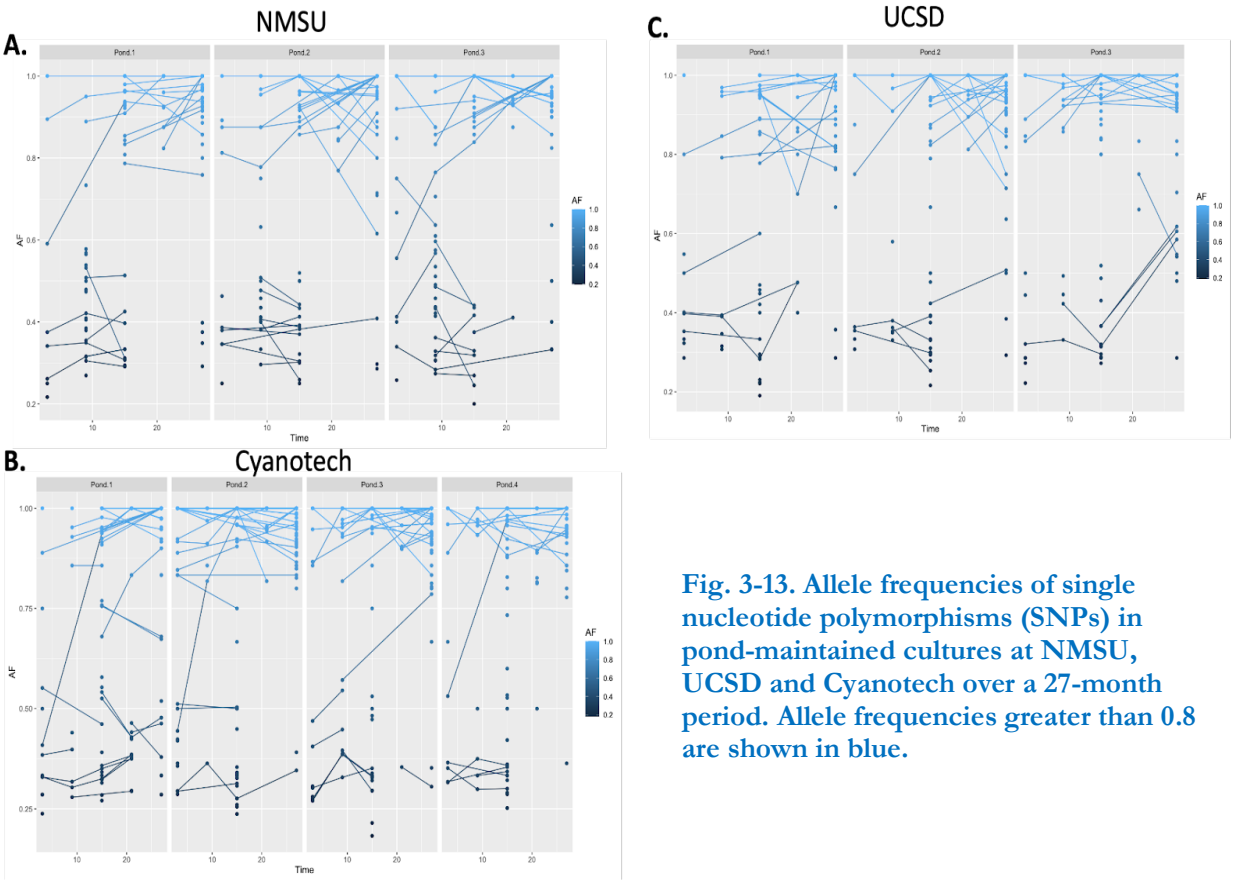

Fig. 3-13. Allele frequencies of single nucleotide polymorphisms (SNPs) in pond-maintained cultures at NMSU, UCSD and Cyanotech over a 27-month period. Allele frequencies greater than 0.8 are shown in blue.

3.5 The Role of the Microbiome

A challenge associated with the use of common garden experiments to study genetic vs. environmental effects in algae is that algae acquire unique microbiomes that can affect phenotypic traits. In our study, it is possible that variability in growth across maintained strains using the same cultivation practices could be explained by differences in microbiomes. To begin to evaluate the role of the microbiomes on growth, stability, and biomass production, we characterized bacterial communities in field- and lab-maintained cultivars, sampled at the six-month intervals. We extracted DNA using a Zymo kit from each cultivar and performed 16S and 18S analysis. Briefly, a 2-step PCR was performed to create an amplicon, targeting the 16S and 18S region respectively. This was followed by a secondary PCR step used to add Illumina specific primers for binding to the flow-cell and adding index sequences to the different samples. We then used the Edge Qime 2 analysis tool to run the 16S and 18S characterization fastq files to determine relative abundance of both prokaryotic and eukaryotic microbial genera. Using the 16S/18S Silva amplicon type for De-multiplexed reads, standard trimming parameters were used to process the raw reads (Trim 5' end Forward & Reverse = 20, truncation Len F & R = 0, SE trim length = 20, SE truncation Len = 0. Sampling depth = 1000 with auto-adjust on, Quality Offset = Phred+33).

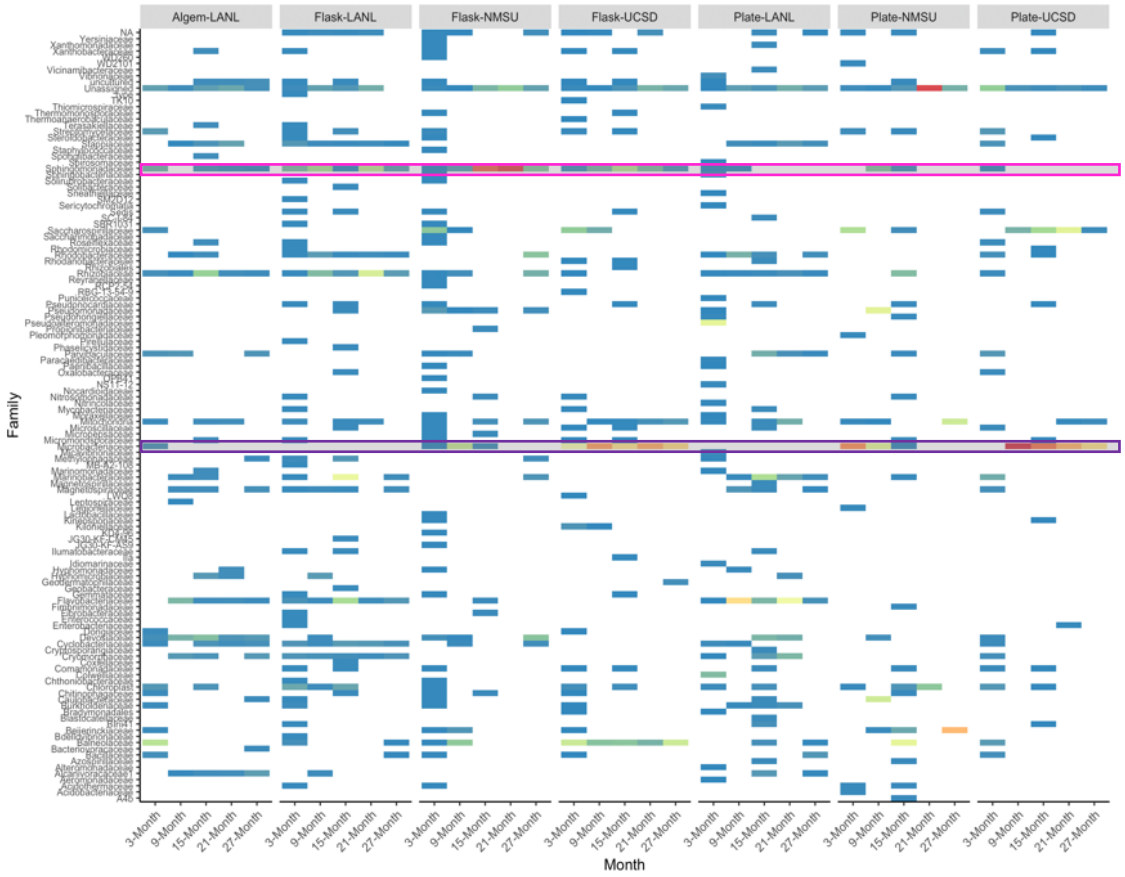

Fig. 3-14. Relative abundance of bacterial families associated with lab-maintained cultivars. Hotter colors indicate a greater relative abundance. Bars highlight high abundance.

With respect to lab cultures, we identified *Microbacteriaceae* as the most abundance microbial family in plate and flask cultivars at UCSD. This microbial family was also found at NMSU to a moderate level **(Fig. 3-14)**, but not identified at LANL (purple bar). Microbacteria are common contaminants of laboratory reagents, which can lead to them being misrepresented in microbiome data. Moreover, Microbacteria have already been described as pathogenic for algal cultures, promoting cell lysis (Ivanova et al., 2014; Lian et al., 2018). It is unclear if this bacterium had a negative effect on the growth of the UCSD plate cultivar. Furthermore, species from the *Devosia* genus was identified at a higher frequency in LANL cultures which have been identified in the plant growth-promoting phytomicrobiome members. These bacterial strains would need to be isolated to determine their effect on growth but would be interesting candidates to test. One family of bacteria, *Sphingomonadaceae* (pink bar), was identified at moderate to high levels in all flask cultivars across sites. To determine eukaryotes within the lab cultivars, we performed 18S analysis and only found one species in cultivars after 21 months of cultivation. Species within the genus *Malassezia* are naturally found on skin surfaces of many animals, including humans, which may have been a contaminate from handling the cultures over time.

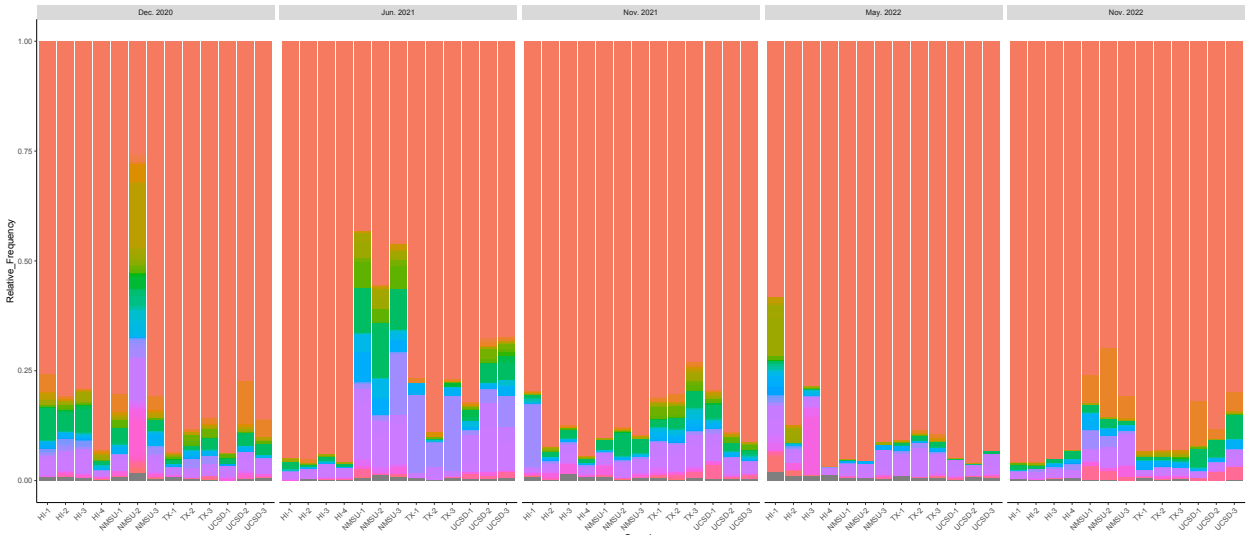

Fig. 3-15. Stacked bar chart displaying relative abundance of bacterial families associated with field-maintained cultivars over time. From left to right are the four HI ponds, three NMSU ponds, three TX ponds, and three UCSD ponds. The salmon color shows the frequency of *N. oceanica*.

With respect to outdoor field cultivars, bacterial abundance varied across sites, ponds (in some cases) and through time **(Fig. 3-15)**. Some families of bacteria were found universally across sites such as *Devosia*, *Flavobacteriaceae*, *Hyphomonadaceae* and *Rhodobacterales* (purple bar) **(Fig. 3-16)**. However, bacterial community composition varied strongly across sites. Although no ponds officially crashed, there were ponds that contained members from the *Bdellovibrionales* family that contain *Bdellovibrio*-and-like-organisms (BALOs), a group of well-described predatory bacteria that contain FD111. This family of bacteria was found in two ponds at NMSU, one pond at Qualitas and one pond at UCSD. Decreased productivity at UCSD was coincident with the presence of the *Bdellovibrionales* family (pink bar) **(Fig. 3-16)**. However, there did not seem to be an effect at the NMSU site, suggesting that there may be many different potentially virulent strains within this family. There was no evidence of this family at Cyanotech, which displayed a consistent level of productivity over time. Overall, NMSU ponds displayed the highest level of diversity at the first two time points; this diversity decreased with time **(Fig. 3-15, Fig. 3-17).** Pieluo's evenness (an index that measures diversity along with species richness) identified NMSU ponds at three and nine months to have the highest diversity **(Fig. 3-15)**. Lastly, UCSD ponds displayed the greatest increase in productivity, particularly at the last characterization. The family *Pseduoaltermonadae* was found to have high abundance in these ponds, especially during the later time points (green bar). This family contains a variety of species that are known to produce an array of low and high molecular weight compounds with antimicrobial, anti-fouling, algicidal and various pharmaceutically relevant activities. Overall, our data can help extrapolate general trends and associations through time, but further work will be needed to uncover the links between pond productivity and particular taxa. As our microbiome and productivity data will be made publicly available, this will be one starting point for such work.

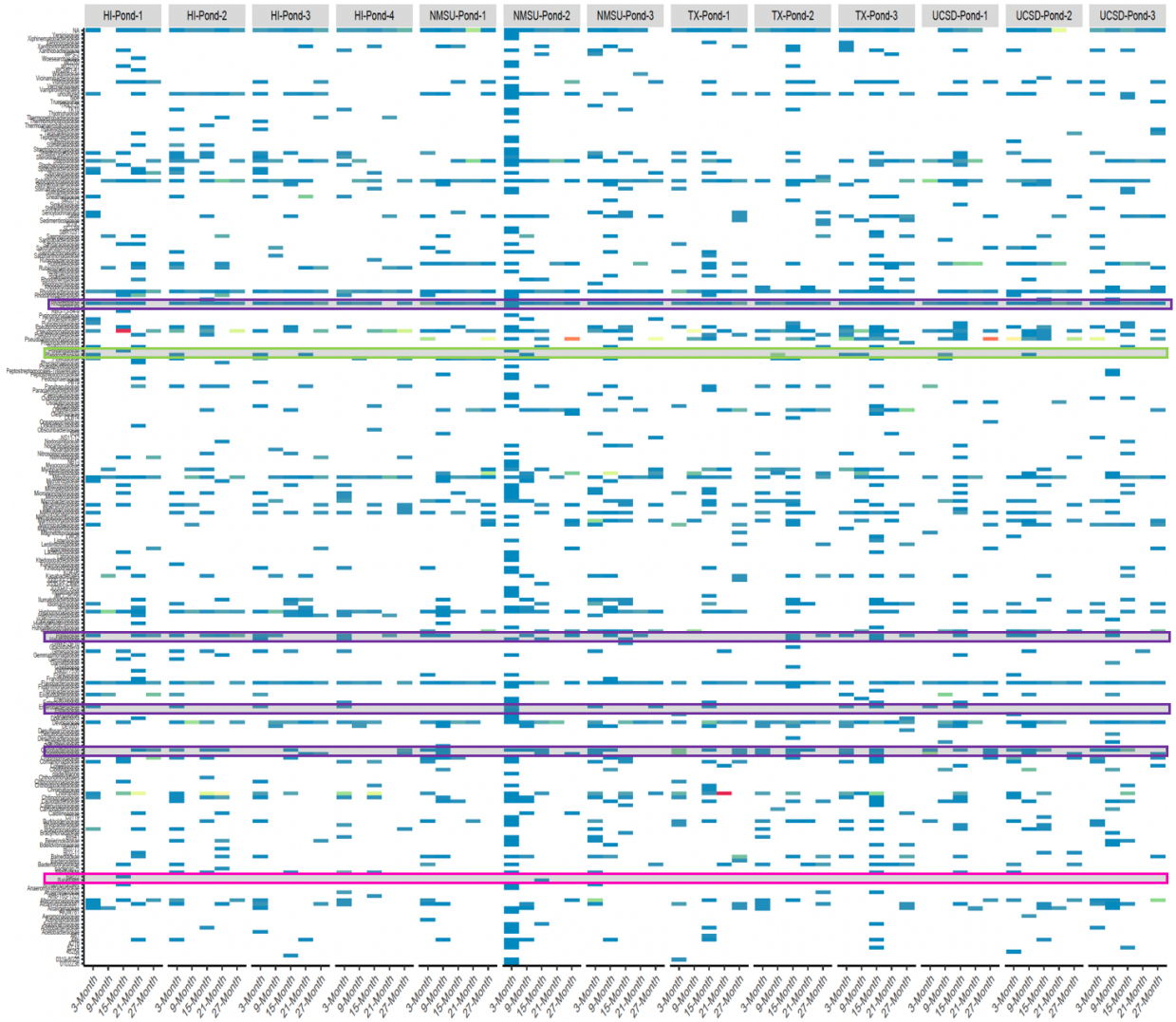

Fig. 3-16. Relative abundance of bacterial families associated with field-maintained cultivars. Hotter colors indicate a greater relative abundance through time.

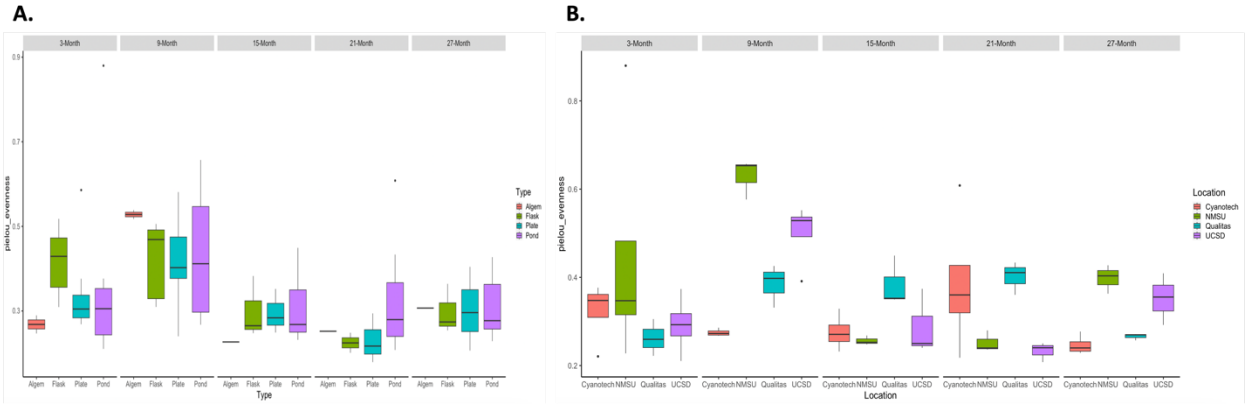

Fig. 3-17. Box plot displaying bacterial species diversity and richness across sites (Pielou). A. **Diversity measured across lab sites split by cultivation through time.** B. **Diversity measured across pond cultivars split by site through time.**

4. Optimization of Pest Management

4.1 Rationale

As long as the algal production industry relies on open, outdoor cultivation systems (Aitken and Antizar-Ladislao, 2012; Kumar et al., 2015; Richardson et al., 2012), algal pests will continue to threaten the productivity and stability of cultures (Carney and Lane, 2014; Day et al., 2017; McBride et al., 2016; Smith and McBride, 2015). Crop protection strategies can be improved with a mechanistic understanding of pests and their life cycles (Ganuza et al., 2016; Lee et al., 2018; Martin, 2002). Pests can be biologically, mechanically, and chemically controlled (Borowitzka, 2005; Mitchell and Richmond, 1987), but effective crop protection relies on the identification and tracking of algal pests in near-real time. The Crop Protection Team at Sapphire Energy implemented a qPCR tool daily to track the predator FD111 in *Nannochloropsis* raceway ponds. Coupled with the use of a laboratory system to test treatment methods, this qPCR tracking allowed 30,000L raceway ponds to be maintained semi-continuously for over two years without crashes. Yet, this implementation required resources that are not always available or feasible at larger cultivation facilities. For example, at their field sites, Qualitas and Cyanotech typically have typically relied on traditional pest-tracking tools like microscopy, which can miss cryptic pests and/or subtleties in life cycles that are important in implementing treatment strategies.

This project component capitalizes on metagenomics to better understand the underlying causes of shifts in field productivity. Metagenomic tools have been used in agriculture and aquaculture to characterize community dynamics, track, and treat pests, and improve cultivation practices (Gupta et al., 2018; Martínez-Porchas and Vargas-Albores, 2017; Nho et al., 2018). Yet, use in algal production systems has lagged behind other disciplines; at present, there are no commercially available metagenomic tools for the algal production industry. This project takes the first step to develop such tools. Briefly, DNA will be extracted from production system samples, sequenced, and assembled into whole genomes and metagenomic fragments to enable taxonomic assignment of each organism present in the pond. By comparing the genomic DNA signatures of productive, stable ponds to that of less productive or stable ponds, we aimed to identify putative pests/pathogens and monitor shifts in the algal population. Custom molecular probes will be developed for organisms of interest, enabling pest tracking in the field.

4.2. Metagenomics to Detect Pests Across Sites

To capture the most comprehensive view of species present within a pond community, we used ProxiMeta, a metagenomic sequencing platform designed by our industry partner Phase Genomics. ProxiMeta is a commercial platform that combines kits and computational services to deconvolute metagenomes by cross-linking genomic DNA in situ followed by sequencing and assembly. Briefly, a Hi-C library was created with the Phase Genomics ProxiMeta Hi-C v4.0 Kit using the manufacturer provided protocol (ProxiMeta Hi-C Kit KT5040). Intact cells from pond samples were crosslinked using a formaldehyde solution, lysed with detergent based lysis buffer, and simultaneously digested using the Sau3AI and MlucI restriction enzymes, and proximity ligated with biotinylated nucleotides to create chimeric molecules composed of

fragments from different regions of genomes that were physically proximal in vivo. Proximity ligated DNA molecules were pulled down with streptavidin beads and processed into an Illumina-compatible sequencing library. At the initiation of this study, we assessed the best practices for practical sample preservation, testing the ideal -80°C-stored, snap-frozen pellets against -20°C 40% glycerol stored and 4°C RNAlater stored samples **(Fig. 4-1)**. After low-pass QC sequencing, we concluded that RNAlater-stored samples produced acceptable yields and library performance to meet the needs of the OSPREY metagenomic survey. This enabled sample collection and storage at site lacking complex laboratory settings.

With a viable storage strategy in place, we sought to test the utility of genome-resolved metagenomics to identify pest species from a mixed community. Using experimental ponds at the NMSU site, we purposefully ceased pest

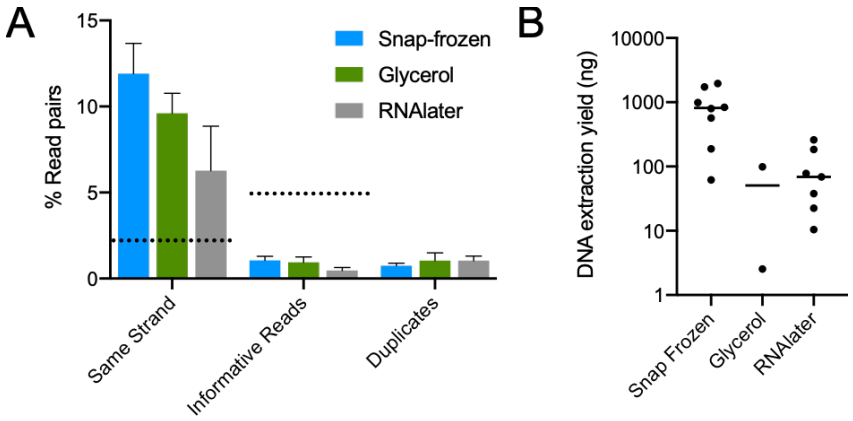

Fig. 4-1. Library performance and DNA extraction yields under varying storage conditions. (A) OSPREY pond samples from NMSU site stored as indicated used to generate ProxiMeta libraries in triplicate and assessed by low pass sequencing were evaluated by hic_qc, Phase Genomics' open-source library assessment tool. All libraries received a 'pass' evaluation. (B) DNA extraction yields from ponds stored as indicated. All generated yields sufficient for shotgun library construction.

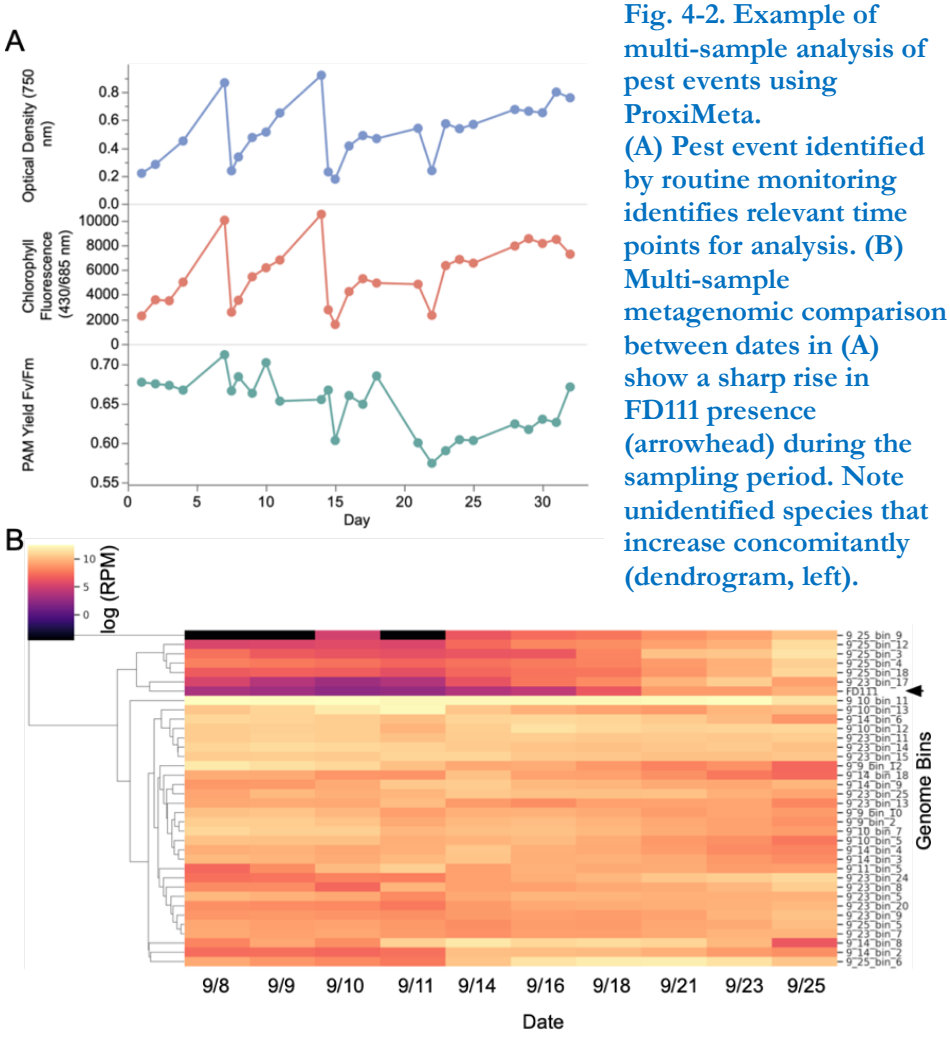

Fig. 4-2. Example of multi-sample analysis of pest events using ProxiMeta. (A) Pest event identified by routine monitoring identifies relevant time points for analysis. (B) Multi-sample metagenomic comparison between dates in (A) show a sharp rise in FD111 presence (arrowhead) during the sampling period. Note unidentified species that increase concomitantly (dendrogram, left).

abatement protocols in a pond while continuing normal pest management protocols in a second control pond. Samples were collected over a ~1 month period, stored, and analyzed by ProxiMeta. Up to this point, ProxiMeta had been used primarily for single timepoint survey studies to identify constituents of complex communities. To address the needs of the OSPREY project, Phase Genomics developed methodologies to analyze time series data and multi-sample comparison. The method devised leverages the high-quality metagenomics bins generated by the ProxiMeta platform for each individual sample, identifying which correspond to each genome across timepoint samples. The most complete bin representing a single taxonomic unit is selected to be the representative genome for the organism for that time series. Shotgun reads from each sample are mapped to the representative genome and the relative abundance of each organism is expressed a mapping reads per million (RPM) sequenced. An example times series from an NMSU pond collected in September 2020 is shown in **Fig. 4-2**. This event was identified by a pronounced decrease in productivity **(Fig 4-2A)** using standard monitoring procedures. In this this time course, there was a clear increase in the abundance of the pest species related to FD111 (arrowhead). The increase in this FD111-like taxon was also accompanied by an increased prevalence with additional genomic bins (grouped together on the dendrogram, left). These previously unidentified species may represent indicator species for pest events, making them candidates for monitoring assays.

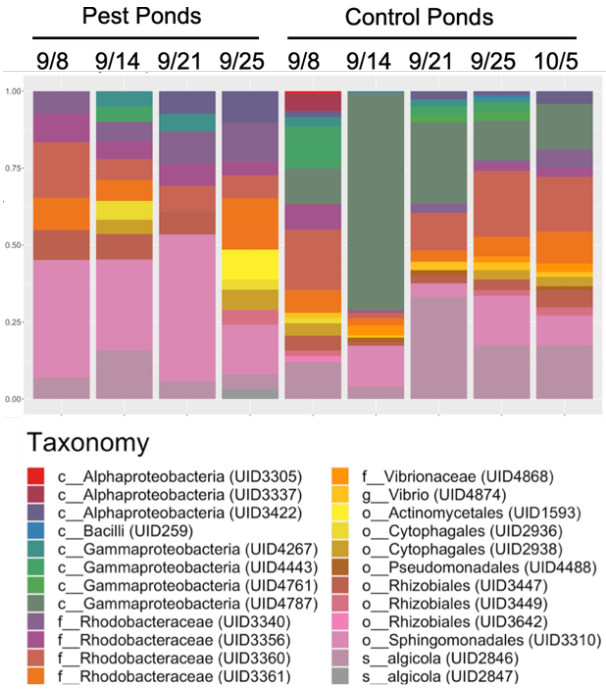

Fig. 4-3. Taxonomic identify of species found in NMSU identified in pest and control ponds. Metagenomic bins taxonomic identity determined using GTDBTK.

Using the same data and matched timepoints from control ponds, we investigated how taxonomically identified species changed over the course of the FD111-like species' infection. We observed that the taxonomy of species present between pest and control pond were highly related and showed dynamic shifts in composition **(Fig. 4-3)**. Broadly speaking, the taxonomic diversity of the control ponds was more stable and showed a greater diversity of detected species than the pest ponds. This motivated additional work, at greater temporal resolution, to survey the composition of pond metagenomes over time. To complete this survey, 16S and 18S sequencing was selected for monitoring. For example, At UCSD, pond health was monitored and tracked for decreases in productivity through time to identify candidate time frames of pest invasion or shifts in microbial dynamics **(Fig. 4-4)**. During this timeframe, 16S and 18S metagenomic analysis was performed on three ponds to characterize microbial diversity shifts before, during, and after the period of low productivity as described previously **(Fig. 4-4)**. We compared the frequency of different species between the low productivity pond (pond 4) to the

other two ponds (ponds 2 and 3). When comparing the most abundant species across time, we identified one genus of bacteria, Flavobacteriaceae *Olleya* that was abundant in the compromised pond 4, during a week of the lowest productivity. However, this genus was also present across all ponds at moderate levels of detection, likely not having a negative impact on the other ponds. We also identified that another bacterium, most similar to Saprospiraceae *Saprospira* sp. CNJ640, was only present in pond 4 during the same period of low productivity **(Fig. 4-4, grey box)**. This family of bacteria has been associated with algacidal and gliding motile activity and is known as a bacterial predator via ixotrophy. While other species were only found in pond 4, we proceeded with this candidate pest for monitoring given its predatory propensity.

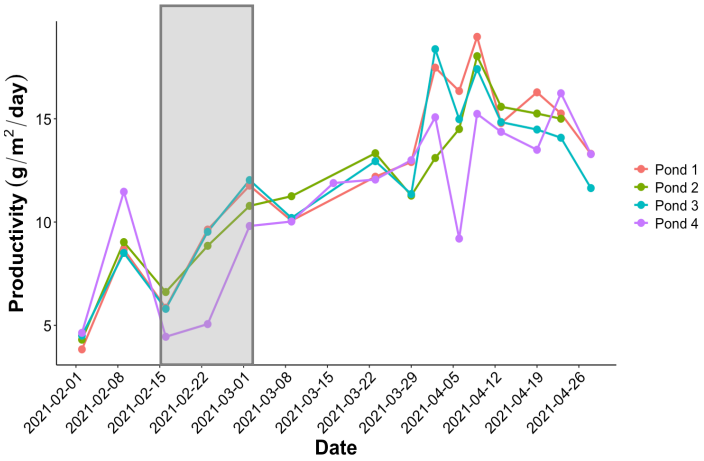

Fig. 4-4. UCSD pond productivity from October 2020 through April 2021. Four ponds were sampled weekly and monitored for periods of low productivity (g/m2/day) pointed out in pond 4 in the greyed region (purple line).

Additional work was conducted adjacent to OSPREY work by Stephanie Getto. Getto explored the metagenomics of treated and untreated ponds at NMSU. At the writing of this report, results from that study have been submitted to NMSU (thesis) and are in preparation for publication. From a practical standpoint, ProxiMeta is poorly suited for this type of analysis because it is burdensome from a resource and cost perspective. ProxiMeta assays were reserved to analyze specific pest events to identify novel pest species and enable qPCR-based pest assay design (see 4.4. Development and Testing of qPCR Tools).

4.3. Comparison of Sick and Healthy Ponds Across Locations

To better understand if observations made in our initial surveys of geographic diversity and pest-pond dynamics were generalizable, we performed ProxiMeta metagenomic deconvolution on a series of pest/low productivity events from NMSU, UCSD, and Cyanotech sites using the multisample comparison methods developed above. Using the collection methods developed at the initiation of the OSPREY project, sites were able to systematically collect and store samples during normal cultivation. We processed samples from periods of low productivity at three sites, including samples preceding decrease in productivity, and a control healthy pond from the same site **(Fig. 4-5)**. Samples were also collected and analyzed for ponds at AzCATI (data not shown). First, this focused study showed that, despite the ponds being within the same geographic region, microbiomes of sick and healthy ponds were distinct, even prior to a noted change in productivity. The composition of organisms in the microbiome remained distinct between healthy and sick ponds that recovered their productivity. These data suggest that there may be biomarkers within a pond that could identify 'at risk' ponds that require either rapid harvest or enhanced intervention to prevent crash. We were unable to directly test this

hypothesis because no OSPREY ponds exhibited crashes during the study period. Second, ProxiMeta was able in this sample set, and the others processed, to provide high completeness genome sequences for candidate pests. This genomic information was successfully used to generate qPCR primer sets to be used to detect pest at field sites. The data generated in this study will be made publicly available for use by researchers for a variety of applications relevant to crop protection.

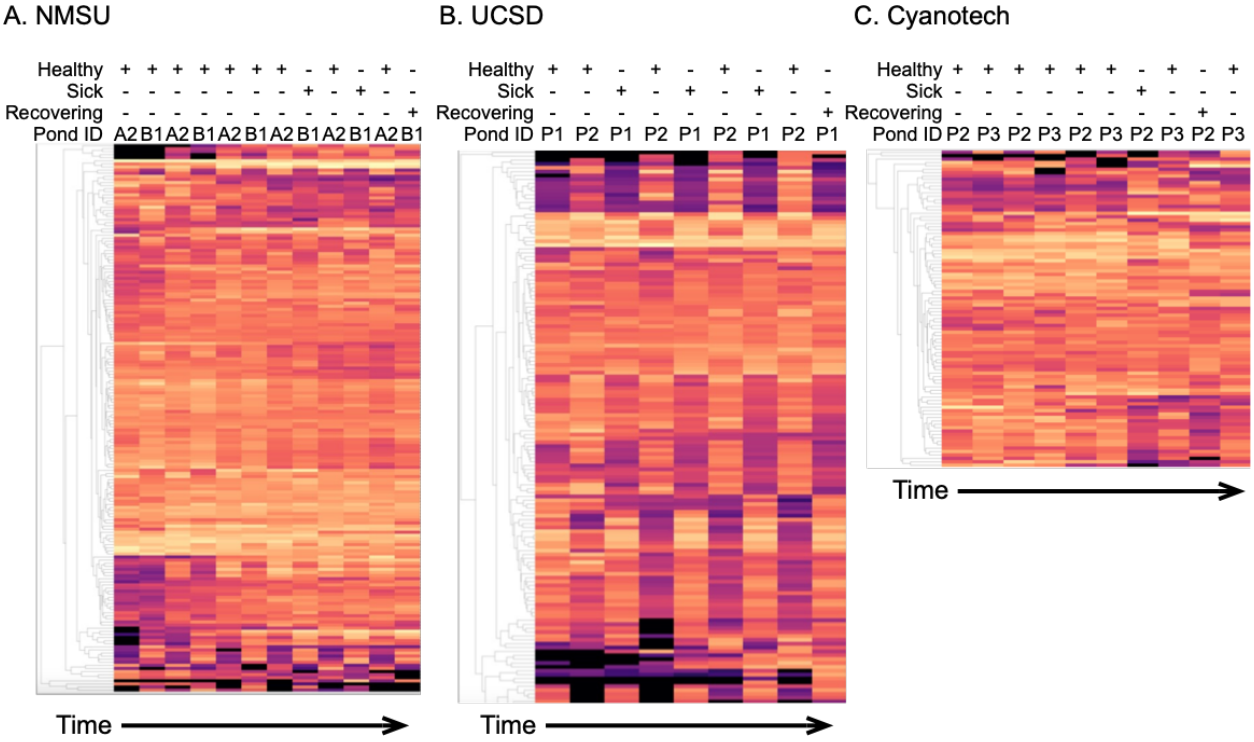

Fig. 4-5. Time series of paired sick and healthy ponds from three of the OSPREY sites. Relative abundance of metagenomic assembled genomes (MAGs) indicated on heatmaps. More abundant genomes indicated by lighter colors while absent genomes indicated by black.

4.4. Development and Testing of qPCR Tools

As a first step in our design and testing of probes, we designed probes to detect a known pest of *N. oceanica* (FD111 bacterium within the order Bdellovibrionales). We compared a variety of low-cost, portable qPCR machines **(Table 4-1)**, chose one for further development, and optimized DNA extraction protocols to detect FD111 in both lab and outdoor field cultures. We assembled genomes within the pond microbiomes during time periods of low productivity, allowing for the design of new primer sets for novel pests at newly established field sites. Merging qPCR, metagenomic analysis and pond health information allowed us to create a framework for field deployable toolkits for regular and rapid monitoring in commercial production systems and provides valuable insight into shifts in microbial dynamics that impact algal health.

Table 4-1. User information about samples processed, cost and size of the compared platforms.

Name	Developer	# of Samples	Cost	Size	Weight	SYBR Green
Open qPCR	Chai	16	Single Channel = $4,999, Double = $6,999	11 x 9.5 x 7.5 inches	9 lbs	✅
Q qPCR	QuantaBio	48	Four Channel = $17,260	5.1 x 5.9 x 5.9 inches	4.5 lbs	✅
PrimePro	Techne	48	$19,290	13.6 x 12.2 x 12.6 inches	30 lbs	✅
UF-150 GENECHECKER	Victoria Scientific	10	$7,348	7.9 x 7.9 x 4.9 inches	7 lbs	✅

Molecular probes and primers were designed to target both *N. oceanica* P7C12 and FD111 by utilizing ProSig PCR primer design software. To test the specificity of the primers, pure lab cultures of *N. oceanica* P7C12 and FD111-infected cultures of *N. oceanica* were grown in flasks to high density and sampled for DNA extraction and qPCR testing. The culture did not completely crash as seen in previous studies but was unhealthy based on visual inspection (chlorosis). After seven days of culturing samples were collected and processed for qPCR analysis. Three replicate qPCR reactions were tested for each target and sample **(Fig. 4-6)**. Average Ct values were calculated for each sample **(Fig. 4-6)**. Primers were specific for each target, shown by the lack of detection for FD111 in the pure *N. oceanica* P7C12 culture. High Ct values represent very low or undetected abundance of the target. The total frequency of *N. oceanica* P7C12 likely decreased in the infected cultures because of the presence of FD111 (indicated by the increase in Ct value for the *N. oceanica* P7C12).

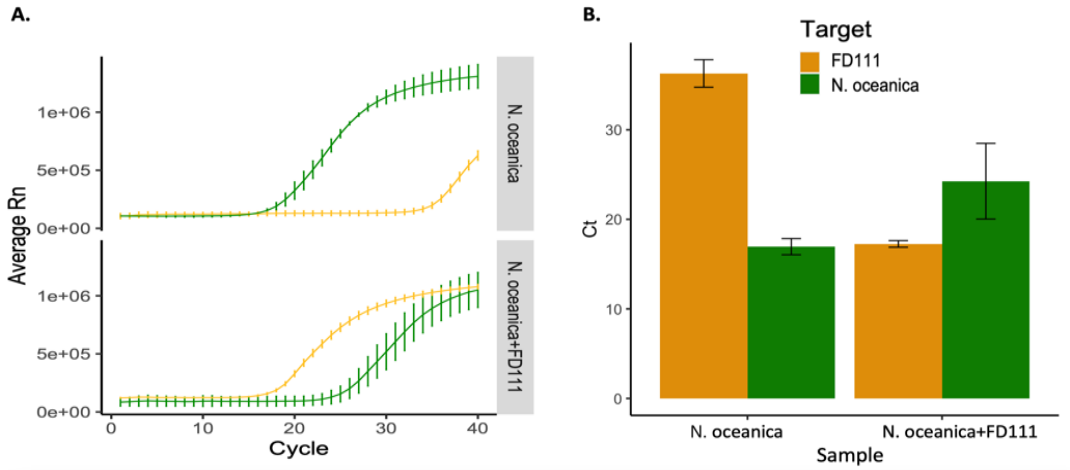

Fig. 4-6. Specificity testing of qPCR primers. A) Average Rn for triplicate qPCR samples colored by target and split by culture. A pure culture of *N. oceanica* P7C12 and a culture infected with FD111 (*N. oceanica* + FD111) were tested for the presence of each target organism. B) Bar graph representing average Ct values for each target detected in each sample. Low Ct values represent high detection of the target.

Beyond FD111, we developed primers for a golden flagellate and *S. saprospira* **(Table 4-2)**. The high-quality assemblies acquired through ProxiMeta allowed us to design different qPCR primer sets targeting different regions of the genome to detect these pests. *S. saprospira* was detected during a period of low productivity at UCSD **(Fig. 4-7)**. We tested two primer *S. saprospira* sets and known control primer sets that targeted *Nannochloropsis* sp. QT001 and FD111 (positive and negative controls) from DNA extracted directly from pond 4 lysate that spanned the low-productivity period to test for the presence of the Saprospiraceae pest using qPCR. We successfully tracked the presence of *S. saprospira* and identified the highest quantity (low Ct value) during the low productivity period but observed that this pest was also present at earlier time points at a lower abundance **(Fig. 4-8)**.

Table 4-2. Primer sets developed during this project.

Oligo Name	Sequence	Description
Nanno_set1_FWD	GGGAGGAAGGGTGTTTCTTT	Nanno_NIR
Nanno_set1_REV	ATGAGGGTGCGGAGATTTATG	Nanno_NIR
Aureispira FWD Set 1	TCATGAGCGTAGCGAACTAATC	Aureispira_Cyanotech
Aureispira REV Set 1	TGGACTTGGGACGAATCTAATG	Aureispira_Cyanotech
Aureispira FWD Set 4	GGCTCTCCTAGCTTCTGAATTT	Aureispira_Cyanotech
Aureispira REV Set 4	TGCGAGGGATGAAGGTTATTT	Aureispira_Cyanotech
FD111_FWD	GGGCAGATTAGCGGAGAAATA	FD111_set1
FD111_FWD	AAAGGGATCCGCCAGTAAAG	FD111_set1
Golden Flagellate Set 11 (F)	CACGAGCCCGACATCTTATG	GF11
Golden Flagellate Set 11 (R)	CGGATCGGAAGTCAGTTGATAC	GF11
Poterioochromonas Set 5 (F)	GGAATAGCAGACAGACACCTTAC	PO5
Poterioochromonas Set 5 (R)	GTGGAGGATGTGTCGATGTTAG	PO5

4.5. Field Deployment at Qualitas Health and Cyanotech

After design and lab testing, probes were deployed at field sites to test efficacy of pest detection in production ponds for site-specific pests at Qualitas Health in Imperial, TX. The designed probes for a golden flagellate and FD111were tested in the field using the field protocols involving simplified DNA extraction method utilizing Edwards buffer followed by qPCR. The results for the tests for the reference NM & Texas production ponds are shown in **Fig. 4-9**. The results were promising in that they picked up on site-specific pests where they were anticipated and showed enough sensitivity to amplify target DNA over background noise. Furthermore, the *Nannochloropsis* probes showed an increasing Ct value with increasing culture sickness, giving an approximate, quantitative measure of culture health, as the higher Ct values were associated with ponds that were visibly sick based on color and appearance and had reduced productivity. Important future work will include time series data and Ct cut-off thresholds that are trigger-points for integrated pest management measures and interventions before the detected pest causes losses of productivity.

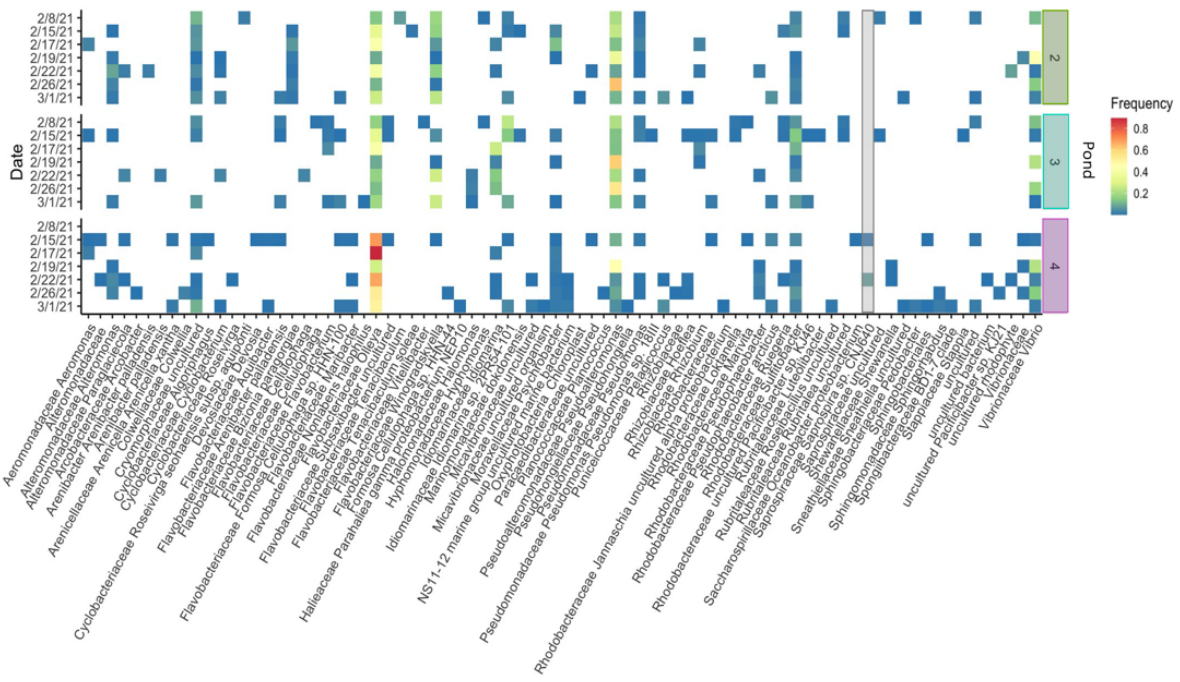

Fig. 4-7. Relative frequency of microbes within each pond spanning the time of low productivity at UCSD. Frequencies were determined though 16S and 18S amplicon sequencing methods. Grey bar represents species that were present in pond 4 during the period of low productivity.

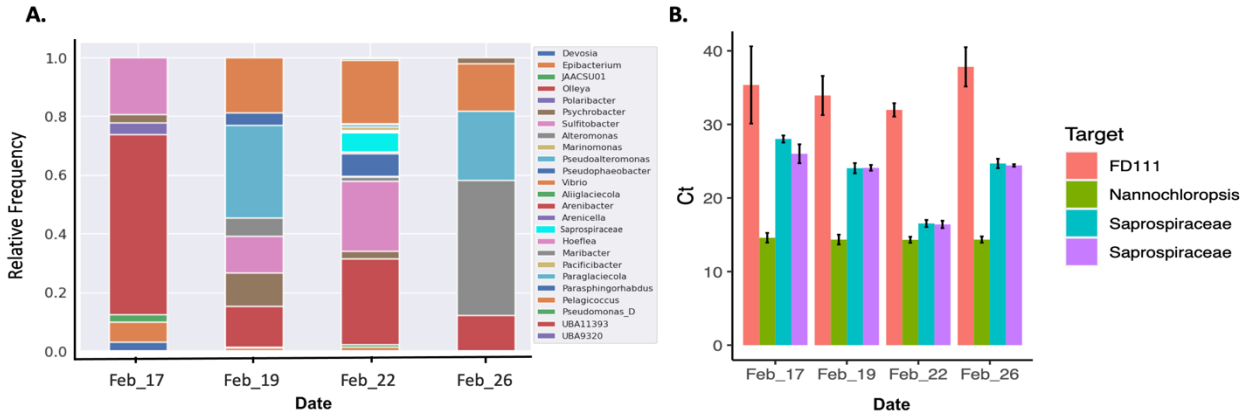

Fig. 4-8. qPCR tracking of Saprospiraceae abundance A.) Stacked bar chart displaying relative frequency of microbes within pond 4 at UCSD spanning the time of low productivity. Frequencies were determined though proxy-meta guided assembly methods. B.) Bar chart displaying average Ct values for qPCR primers targeting a N. oceanica positive control (green bars), a known pest (FD111) that should not be present in these ponds (negative control), and two separate targets within the Saprospiraceae species. Significant difference between both Saprospiraceae probes was between Feb 19th and Feb 22nd (Tukey test p adj<0.001).

Primers were also developed against a strain of *Poterioochromonas*, a well-known pest (both as a grazer and as a weed) of microalgal mass cultures. The strain was isolated from production ponds at Cyanotech Corporation, and it is maintained in Cyanotech's proprietary strain collection. The "golden flagellate" cited above was once thought to be *Poterioochromonas*, which, however, seemed incongruous given the typical salinity of the medium used for

Nannochloropsis outdoor cultivation during this project, and the commonly recognized status of *Poterioochromonas* as a "freshwater" organism. We demonstrated, against expectations, that the cultured *Poterioochromonas* strain was capable of surviving at salinities up to 18 on the practical salinity scale, and, at lower salinities, was a destructive pest of *Nannochloropsis* in laboratory tests. Moreover, we found that the intermediate range, between danger to the crop and safety, was on the order of 4 units on the practical salinity scale. Potentially, therefore, a major rain event at a *Nannochloropsis* production facility could put the crop at risk of *Poterioochromonas* predation. Operationally, *Poterioochromonas* was a very rare component in 18S ribosomal RNA surveys of eukaryotes in the OSPREY ponds. Also, the "golden flagellate" was found to be an unattested species in a lineage of "stramenopile" protists distant from *Poterioochromonas*.

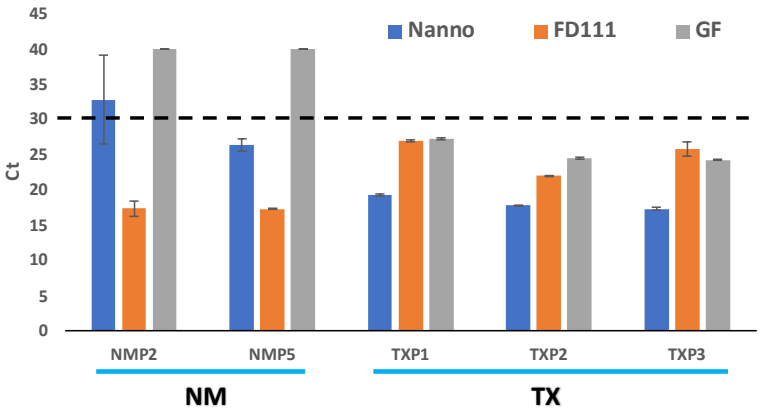

Fig. 4-9. Ct value from qPCR of field deployment at Qualitas in Imperial, TX. Texas ponds and reference NM ponds are tested using field extraction and qPCR protocols and show detection of pests in a site-specific way. The high Ct value of *Nannochloropsis* DNA with *Nannochloropsis* specific primers indicate the poor culture health of NM ponds, with the Texas ponds showing the presence of the pests without yet showing an impact of cultivar health (*Nannochloropsis* Ct value).

Nannochloropsis cultivation ended at Cyanotech before qPCR primers could be tested. However, in a parallel project representing a combination of proprietary and Department of Energy-funded research, a *Poterioochromonas*-like organism appeared in outdoor cultivation of *Chlorella* strains. Primers targeting *Poterioochromonas* were tested against two laboratory strains of *Poterioochromonas* (the original, and a second with slightly differing morphological and culture characteristics), a tubular-bioreactor (PhycoFlow, 600 L) outdoor culture in which the *Poterioochromonas*-like contaminant had not been observed, and a 500 L minipond containing the same *Chlorella* in which the *Poterioochromonas*-like contaminant had been observed. DNA amplification occurred for both cultured *Poterioochromonas* strains and for all three minipond samples, and it did not occur in samples from the tubular bioreactor. No change in the inferred *Poterioochromonas* contamination was observed in the minipond at the three time points sampled (ten, eleven, and fourteen days after the start of the pond run). This finding was consistent with microscopical observations on *Poterioochromonas* cell numbers, and on the expected behavior of the *Poterioochromonas* under the conditions tested (a *Chlorella* strain resistant to *Poterioochromonas* grazing, plus alkaline pH and substantial bicarbonate alkalinity, all of which restrict *Poterioochromonas* growth). The results nevertheless demonstrated the utility of qPCR methodology for pest detection in commercial operations, lessening the dependence on microscopical detection of pests (and the expertise needed to accomplish pest detection in this way).

5. Strain Improvement through Mutagenesis and Adaptive Laboratory Evolution

5.1 Background

Numerous studies have demonstrated the ability of laboratory selection to enhance traits such as productivity, lipid content, temperature range, and pest resistance in algal taxa (Bonnefond et al., 2017; Yi et al., 2015; Yoshida et al., 2003). Of note are non-GM approaches (e.g., mutagenesis, directed evolution) that do not carry regulatory restrictions for field cultivation. Mutagenesis accelerates genomic mutation rates, which can lead to phenotypic changes by altering gene expression and/or protein activities. Rational laboratory selection regimens applied to these libraries can quickly yield novel strains with improved phenotypes (Corcoran et al., 2018). Selection via directed/adaptive evolution can also lead to improvements that are rapidly realized in the laboratory (i.e., in as little as 22 days, but more commonly in 60-100 days (Sun et al., 2018)). With respect to one of our particular traits of interest, pest resistance, mutagenesis in *Synechococcus* uncovered genotypes with resistance to an ameboid predator (Simkovsky et al., 2012). However, often at the transition to the field, improved strains fail. Such failures can occur because selection in a field setting favors new mutants that lead to loss of selected traits or because strain phenotype and performance depend on the environment in which a strain is grown (a gene- environment or 'G x E' interaction (e.g., Cooper et al., 2019; Herrmann et al., 2017)). For instance, Szyjka et al. found that a genetically modified *Scenedesmus* produced a 24-fold increase in C14:0 lipid relative to wildtype when grown in the lab, but only a three-fold improvement when grown in the field (Szyjka et al., 2017). Laboratory pipelines can also lead to fitness reductions resulting from laboratory pipelines. For example, directed evolution under resource rich conditions can paradoxically lead to lower growth potential than selection under conditions where resources are more limited. Collins found that *Chlamydomonas* strains selected for low resource environments (e.g., low CO_2) evolved better carbon concentrating mechanisms and higher growth rates than strains selected under high CO_2 (Collins, 2016). These results suggest that adaptation to low resource environments may result in enhanced growth when strains are moved to a richer medium. This approach (i.e., selection under low growth conditions) has never been experimentally evaluated for biofuel and bioproduct taxa, in part because most lab screening assays attempt to replicate field conditions in the lab.

In this project component, we aimed to increase the performance of our field-adapted *Nannochloropsis sp*. strain by improving (1) year-round productivity and stability through increased tolerance to abiotic and biotic stressors via mutagenesis and selection and (2) biofuel intermediates via alteration of carbon partitioning. We planned to circumvent the challenges that can occur at field transitions by starting with a field-cultivated strain as our baseline strain and testing strains outdoors immediately as improvements are documented.

5.2 Development of Mutant Libraries and Screening of Isolates

In 2020, an initial mutant library was generated at NMSU by exposing cells to ultraviolet (UV) radiation. Preparation of algae cultures for UV mutagenesis was performed as follows. Algal cultures were initially diluted to an optical density (OD) of 0.4 at 750 nm using fresh media.

Approximately 10 ml of this diluted culture was transferred into a 15 mm Petri dish. Subsequently, 4 ml of the culture was carefully removed from each dish. This step was crucial to create a thin micro-layer of the culture spread uniformly across the surface of the Petri dish, facilitated by surface tension. The prepared cultures in the Petri dishes were then subjected to ultraviolet (UV) light exposure. This was carried out using a Hoefer UVC 500 crosslinker, which emits UV light at a wavelength of 254 nm (shortwave). The exposure duration was precisely set to 30 seconds. This specific time frame was chosen based on preliminary experiments that determined a 75-80% mortality rate in the cultures, which was calculated by comparing the relative growth of the treated samples to that of the control cultures.

Immediately following UV exposure, the treated samples were transferred into 50 ml flasks. These flasks were then stored in the dark for a 24-hour period to prevent light induced DNA repair. After this dark incubation period, the samples were moved to incubators set under low-light conditions using shade cloth to facilitate further recovery and prevent photobleaching. This step is critical for the survival and subsequent growth of the UV-treated algal cells, as it provides an optimal environment for the cells to recover and the mutation to be permanently set. The newly created mutant library was subjected to three rounds cultivation under high and low temperatures (i.e., 10 and 36°C), as well as at 25°C, for improved growth during winter (10 °C) and summer (36°C). Following abiotic selection, each culture was plated for single colonies. The fastest growing colonies from each temperature treatment were selected as candidates for further evaluation. This process generated 84 isolates (**Table 5-1)**. All 84 isolates were evaluated for improved growth characteristics compared to the parent culture. Several isolates showed an improvement of 15 to 30% in growth and productivity at elevated and sub-optimal cultivation temperatures. Within the isolates evaluated, several mutants also showed increases in total fatty acids (~15-40% increase) and polyunsaturated fatty acids (~5-50% increase). When

Table 5-1. Summary of mutant libraries created, and number of mutants downselected for field trials.

Strain	Mutagen	# of Isolates screened	Temp (°C)	# of Improved Isolates	# of Isolates With Improved Lipid Content			Selected Isolated for Field Trial	Isolate Characteristics	Fied Trial Date	Field Trial Outcomes
					Total (%)	PUFA (%)	C20:5 (%)				
N. oceanica (P7C4)	UV	36	36	12	10	9	5	2 isolates : isolates: 30	Better survivability	Summer, 2021	Trial failed. Lost P7C4 control cultures due to heavy rain/pond malfunction.
								1 isolate: isolate 5	Better survivability at 36 °C, thick cell	Summer, 2022	Lost the phenotype two weeks after the cultures were brought into the field.
N. oceanica (P7C4)	UV	30	10	10	6	4	4	none			
N. oceanica (P7C4)	UV	18	25	4	2	2	0	none			
N. oceanica (P7C4,P7C12)	UV & EMS	17	Sinusoidal (8°C-15°C)	9	11	10	10	1 isolate: isolate 6	Improved growth rate, increase in PUFAs	Winter, 2022	Phenotype was retained during upscaling of the cultures inside the lab and in the field. Lost the phenotype after the cultures were split for the experiment.

re-evaluated at 25°C, only Mutants 5 and 30 showed reproducible improvement with calculated doubling times of 1.8 and 2 days, representing a >21% and 10% improvement, respectively compared to the control. In sum, Mutant 5 and Mutant 30 outperformed all the other isolates and were advanced to field trials. **(Table 5-1, Fig 5-1)**.

Strain	Doubling Time Days	% Improvement over Control
Mutant 5	1.79	21%
Mutant 30	2.05	10%
Control	2.28	-

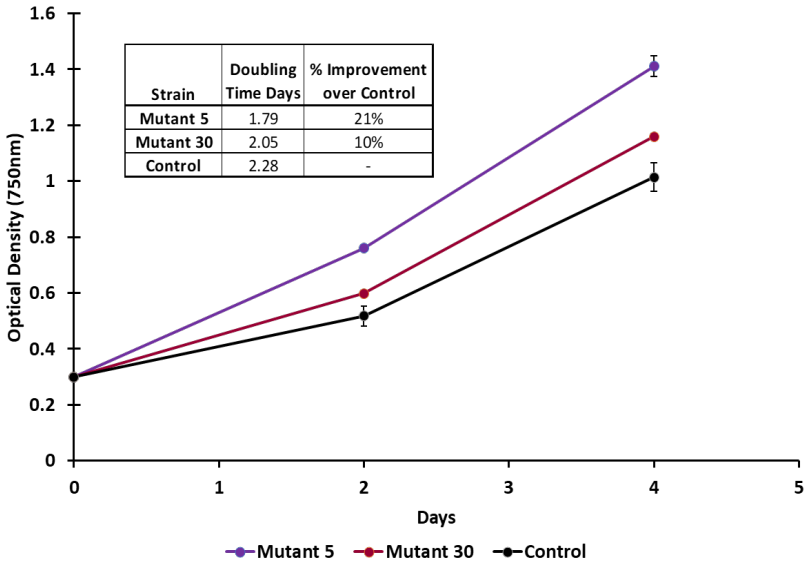

Figure 5-1. Growth parameters of improved strain isolates. Mutants 5 and 30 both outperformed the control strain with significantly improved doubling times when evaluated at 25ºC.

To increase the probability of isolating an improved strain, a mutant library was created by pooling mutagenized cultures treated at LANL with ethyl methanesulfonate (EMS) and cultures treated at NMSU with UV radiation. The resulting pooled culture was scaled and field deployed in March 2022. It was maintained outdoors after initial deployment. In May 2022, the culture was plated and the fastest appearing colonies compared to the control culture were isolated. From this library, 17 isolates were obtained and grown at constant 25ºC and sinusoidal profiles (8-15°C). Among the 17 isolates, nine showed improvement in performance and specific growth rates (~10-25% increase) and >10 mutants showed an increase in total fatty acids and unsaturated fatty acids (~12-45% increase).

Under controlled laboratory settings, Mutant 6 demonstrated a consistently improved growth performance compared to the control culture, particularly under varying temperature regimes. This was evident at the optimal growth temperature of 25°C, a condition that was considered optimal. However, the more remarkable aspect of this mutant's performance was its performance under sinusoidal temperature conditions fluctuating between 8°C and 15°C. This sub-optimal temperature range was linked to performance often resulting in reduced growth rates. Mutant 6's ability to maintain robust growth under these conditions highlighted its enhanced adaptability and cold stress tolerance, making it a standout candidate amongst all strains being evaluated. Another key aspect of Mutant 6's evaluation was its observed stability throughout multiple grow-outs. Stability in this context refers to the mutant's ability to retain its enhanced growth characteristics over successive cultivation cycles. This trait is vital for practical applications, as it suggests that the improvements in growth performance are genetically stable and not merely transient responses to laboratory conditions. Because of Mutant 6's consistent performance over these repeated cycles we concluded this was an indication of its genetic stability and reliability (**Fig. 5-2)**.

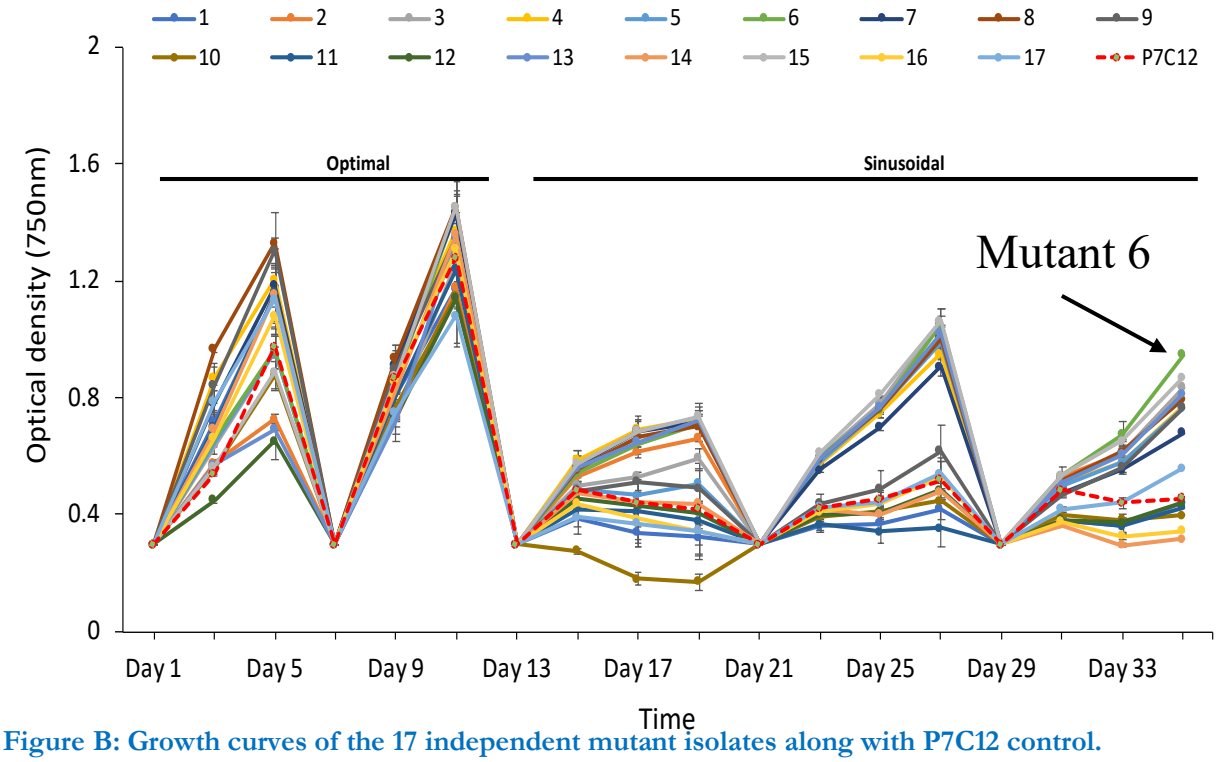

Figure B: Growth curves of the 17 independent mutant isolates along with P7C12 control. Cultures grown at optimal 25°C and sinusoidal temperature profiles(8-15°C) under lab conditions.

Given its performance and demonstrated stability in controlled laboratory settings, Mutant 6 was advanced to outdoor field trials, specifically under cold conditions. This transition from the laboratory to outdoor trials was to assess Mutant 6's applicability in the field, particularly in environments characterized by winter temperatures where lower and large daily temperature fluctuations exist. The outdoor field cold trial aimed to test the mutant's resilience, productivity, and overall adaptability under these conditions. These successive experiments highlight the effectiveness of mutagenesis in a laboratory setting for improving organism traits under various environmental conditions.

5.3 Trait Stacking

To further improve upon identified desirable traits, strategies were developed to include multiple iterations of UV mutagenesis in an attempt to stack multiple desirable traits, such as improved productivity on top of and stable traits such as lipid content. We sought to achieve this through a combination of UV mutagenesis iterations, which induces random DNA mutations. As a mitigation strategy, we used chemical mutagens to manipulate the ploidy levels of the chromosomes. Colchicine and cytochalasin B were chosen as they play a crucial role in destabilizing DNA replication. Colchicine disrupts mitotic spindle formation, leading to polyploid cells that might amplify beneficial traits. Cytochalasin B, on the other hand, inhibits cytokinesis, potentially increasing genetic variation and trait expression. This approach faces challenges like controlling mutation rates, intensive screening processes, and ensuring trait stability. The extensive screening for desirable traits is time-consuming and requires advanced techniques. Moreover, the stability of induced traits across generations, especially in polyploid strains, is a

critical factor. Overall, the combination of UV and chemical mutagenesis was a promising method for enhancing microalgal traits.

To achieve the goal of trait stacking, Mutant isolates 5 and 6 were subjected to a second round of mutagenesis using UV light and chemical agents, specifically colchicine and cytochalasin B (CC). This led to the creation of an additional four mutant libraries referenced as M5UV, M5CC, M6UV, and M5CC from which we isolated 96 distinct single cell cultures. As previously described, we conducted a series of growth experiments evaluating growth performance using our previously established temperature profiles described in section 5.2 on each of these single cell cultures **(Fig. 5-3)**. One isolate, Mutant 20 from the M5CC library, demonstrated superior performance in optimal temperature conditions and showed observable phenotype of increased cell wall intensity under calcofluor-based microscopy **(Fig. 5-4)**. The mutant strain Mutant 20 was subjected to several growth cycles spanning the fall and winter seasons to evaluate its performance relative to control cultures through time. These seasons were chosen deliberately as they present unique environmental challenges in temperature. This approach aimed to assess the resilience and adaptability of Mutant 20 under field conditions that are often characterized by fluctuating environmental parameters. The hypothesis was that if Mutant 20 consistently outperformed the control cultures across these conditions, it would indicate a robust and versatile phenotype, advantageous for field trials.

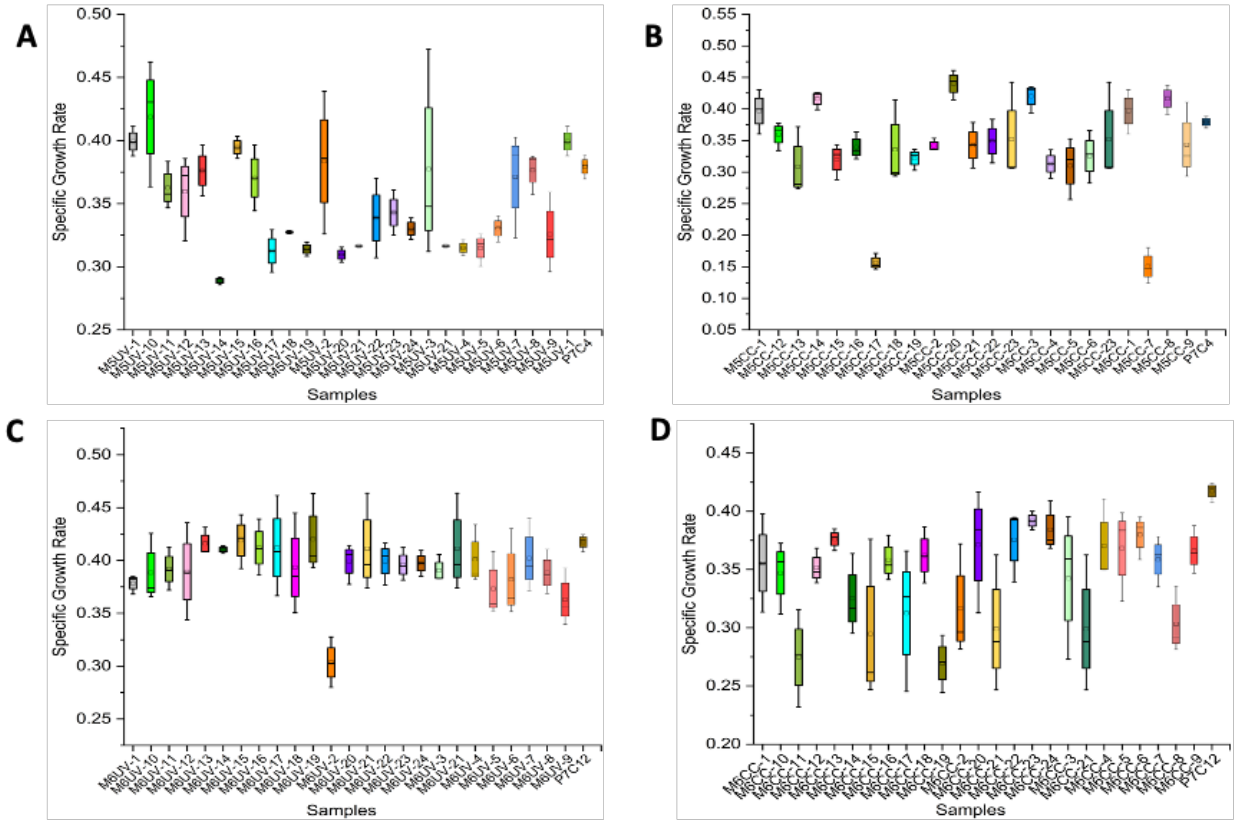

Fig. 5-3. Specific growth rates of 96 trait stacked isolates from the M5UV (A), M5CC (B), M6UV (C) and M6CC (D) libraries.

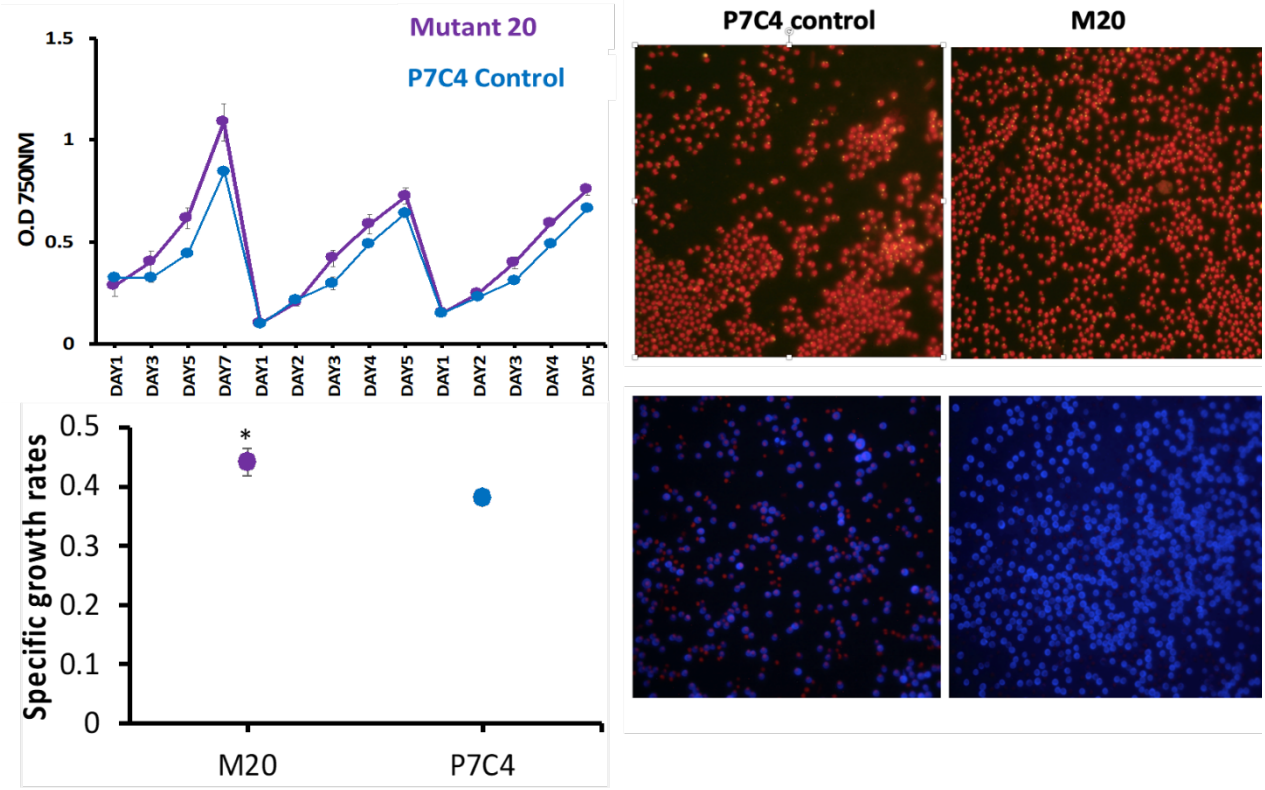

Figure 5-4. A: Optical density and specific growth rates of mutant isolate 20 and P7C4 during three rounds of growth at optimal temperature B: Fluorescent microscopy on the cultures stained with Nile Red (top right) for lipids and stained with calcofluor dye (bottom right) for cell wall intensity.

In parallel, Transmission Electron Microscopy (TEM) was utilized to examine the cell wall thickness of the Mutant 20 strain to identify the source of the increased staining observed **(Fig. 5-4)**. The rationale behind this analysis was to gain insights into the ultrastructure alterations that might have occurred in the cell structure of Mutant 20. Cell walls can be a critical factor that can influence various aspects of a microalgal cell's functionality, including its stress tolerance, nutrient uptake, pest resilience, and overall stability. By comparing the cell wall structure of Mutant 20 with that of the control cultures, the study aimed to establish a correlation between the observed increase in cell wall intensity and possible structural and carbon allocation changes in the mutant strain. We were also interested in understanding how the increased cell wall intensity observed in the Mutant 20 isolate might relate to its overall structural integrity and carbon allocation patterns. Alterations in cell wall composition and thickness could imply changes in the cell's metabolic pathways, potentially leading to enhanced carbon fixation and storage capabilities. Such changes could be a contributing factor to any phenotypic or performance changes observed in Mutant 20, particularly under environmental abiotic stress.

The phenotype of increased calcofluor staining, which was hypothesized to be linked to the changes in the cell wall as observed through TEM analysis **(Fig. 5-5)**. It should be noted that this observation was only made on a single culture and needs to be reproduced. Regardless, the two orthogonal approaches to evaluate the cell wall thickness both suggest there is indeed an stable change.

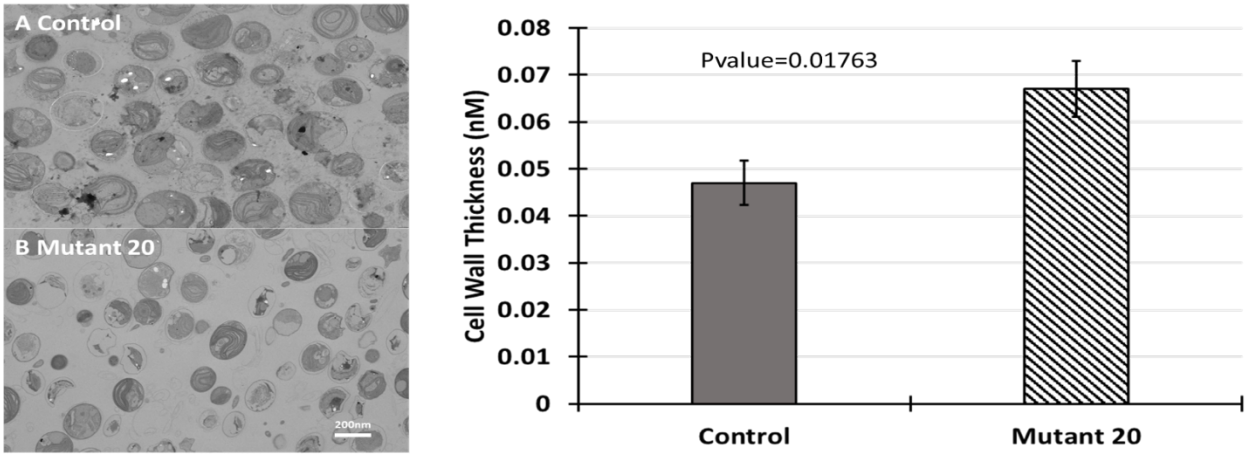

Fig. 5-5. Ultrastructure Analysis of Microalgal Cells. This figure presents an ultrastructural analysis comparing cell wall thickness between control and mutant microalgal cultures. Measurements were taken from a sample size (n=10) for each group, from which the average cell wall thickness and the standard error were determined. While the change in cell wall thickness between control and mutant cultures was significant with a p-value<0.05, the mutant designated as Mutant 20 did show an increase in cell wall thickness.

5.4 Outdoor *In-situ* Mutagenesis

In this component, we aimed to create a comprehensive strategy for UV mutagenesis that could be effectively applied in field conditions. This approach was designed to use natural seasonal selection pressures as the process for enhancing the performance of the strain. One of the key challenges we address is the scalability of this technique, expanding the scope from small-scale applications <1 mL in UV-crosslinkers to larger scales exceeding 100 liters, representing a significant 100,000-fold increase. As mutations arise either through thymidine dimer formation or oxidative break, these occurences lead to insertions and deletions.

Our focus was to identify and evaluate improved microalgal isolates that showed substantial enhancement in the following critical areas such as growth rate, lipid accumulation, and co-product production. To achieve this, we aimed to develop a scalable, efficient, and field-applicable solution for strain enhancement that utilizes natural selection in combination with iterative mutation aka “trait stacking”. To establish a protocol for UV treatment of algal cultures, we used a UV pond clarifier which emitted UV-C light at a dose of 23µW/cm^2 treating algal cultures prepared in 4-liter volumes. In the piloting of the protocol it involved four distinct UV exposure time intervals: 10, 30, 60, and 120 minutes, each tested on a separate 4-liter sample of algal culture **(Fig. 5-6)**. After each 4 liter volume was treated, it was evaluated for growth in comparison to the control which revealed that the 120-minute treatment interval showed the most promising results in terms of mortality on the algal cultures. Based on this finding, the 120-minute exposure time was selected as the optimal treatment duration and used as foundation exposure time to scale the process to a larger volume.

Following the success of the laboratory trials, the 120-minute UV treatment protocol was then applied to the entire outdoor pond. This step was crucial for advancing our mutation

experiments under more natural and variable environmental conditions, thus allowing us to leverage field environmental pressures. Multiple iterations of in-situ UV mutagenesis were conducted in outdoor ponds to optimize the treatment process and its effects on algal cultures. The control pond, serving as a baseline, did not undergo any UV treatments. Meanwhile, two other ponds, UV1 and UV2, were subjected to a series of UV treatments incorporating process improvements.

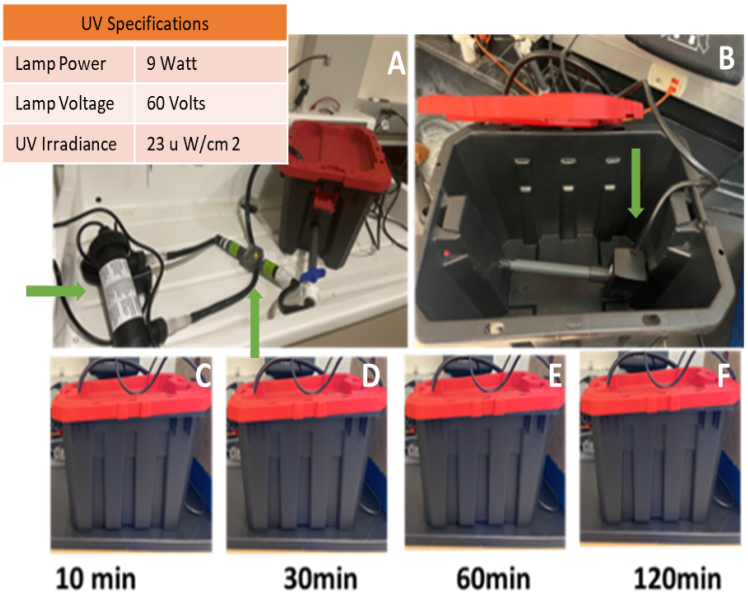

Fig. 5-6. Panels A-F: Initial design concept of "UV Box" for large scale UV mutagenesis. Total Pond UV Specifications (table inlay).

The initial attempt in the UV1 pond involved a continuous 24-hour exposure to UV-C light. Subsequent iterations adjusted both the treatment times and methods, with the objective of achieving a 90% kill rate of the algal culture. The third iteration marked a significant methodological shift: a 15-hour UV treatment was applied to a 10-liter subsample of the pond, and a second UV apparatus was introduced to increase the dosage **(Fig. 5-7)**. During this phase, samples were systematically collected for strain isolation and preservation every third harvest, ensuring a comprehensive evaluation of the mutagenesis effects. The UV2 pond, initially part of the UV1 setup, was later split and subjected to the final iteration, which incorporated an improved method involving additional UV lamps and a reduced culture volume. This strategic adjustment was aimed at intensifying the UV exposure while maintaining manageable culture conditions. The resulting fourth iteration successfully achieved the desired 90% kill rate, demonstrating the effectiveness of the refined approach.

Fig. 5-7. Enhancements in Engineering and Process Execution for In Situ Field Applications. Illustrated are progressive engineering advancements that resulted in an optimized outdoor UV treatment process. Through successive iterations, we achieved an increased kill rate in algal subsamples while concurrently minimizing DNA repair mechanisms activated by light exposure in the field setting.

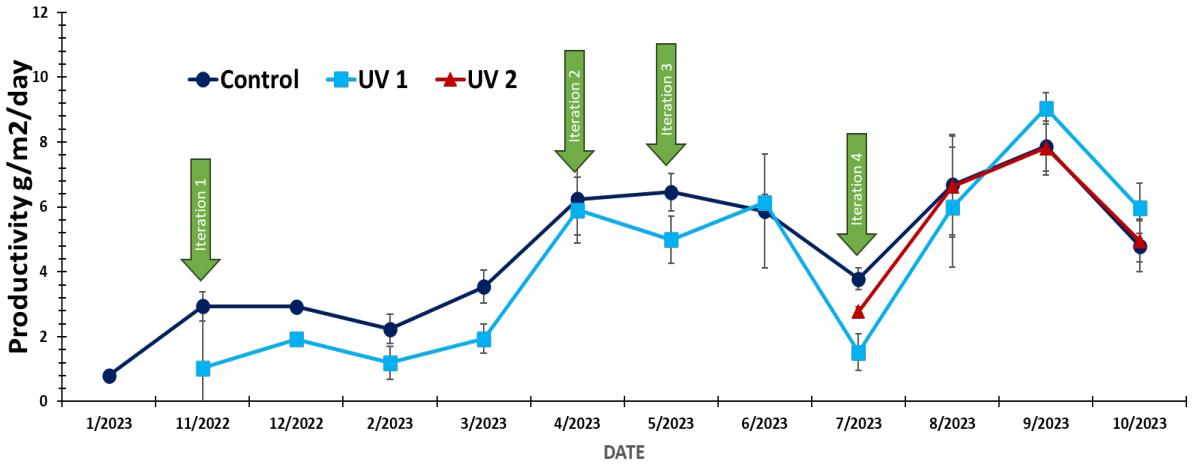

Fig. 5-8. Summary of outdoor in-situ productivity in relation to iterative whole pond mutations. Control pond did not receive any UV treatments, UV1 pond received three successive UV treatments, and UV2 pond was split from UV1 and received the final 4 iteration using an optimized method.

Throughout these iterative treatments, the varying UV exposure times, intensities, and methodologies provided valuable insights into optimizing in-situ UV mutagenesis in outdoor pond settings. When examining the productivity data of the ponds for the entire year, it is observed that there is no significant overall increase in productivity. However, a notable numerical increase in productivity was observed specifically in the UV1 pond in September and October of 2023 **(Fig. 5-8)**.

Strain isolation following the UV-C mutagenesis outdoor experiment indicated a reduced doubling time in many isolates, with about five isolates displaying marked enhancements in growth rates, as depicted in **(Fig. 5-9)**. Interestingly, several isolates exhibited distinct color phenotypes, suggesting alterations in the ratios of photosynthetic pigments. A comet assay, conducted to elucidate the mechanisms underlying the mutagenesis using pond clarifiers, pointed to oxidative DNA breaks as a

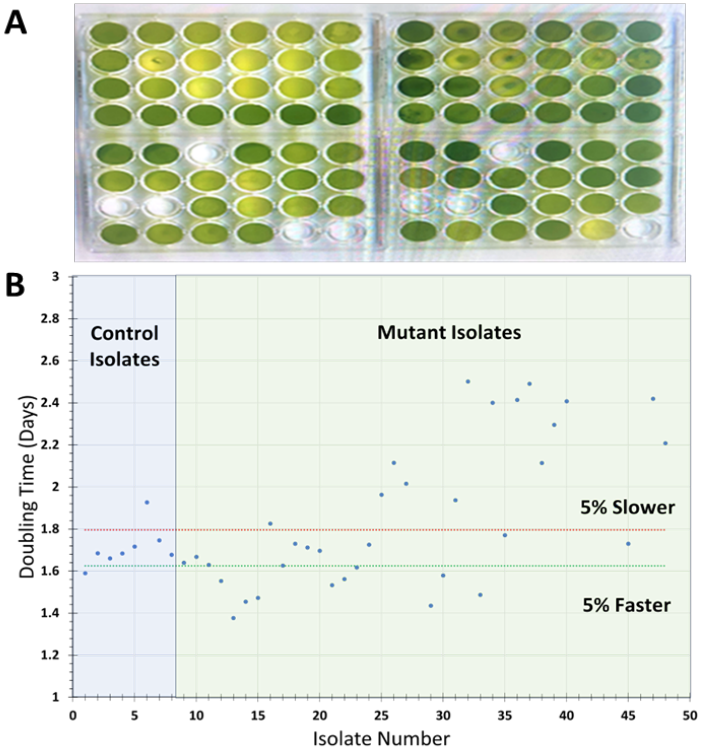

Fig. 5-9 Summary of improved strain phenotype and growth characteristics A) Evaluation of Observed Phenotype B) Calculated Doubling Time of Isolated Colonies. Approximately five individual isolates exhibit improved doubling times.

probable factor. Looking ahead, each isolate will undergo biochemical analysis using dyes and flow cytometer as high throughput screening to identify strains with altered biochemical composition.

5.5. Carbon Partitioning

We aimed to use a laboratory pipeline to increase conversion yield through the manipulation of carbon partitioning in our baseline *Nannochloropsis* field strain. This approach takes advantage of the negative relationship between oxidative stability in fuels derived from glycerol lipid containing feedstocks and unsaturated fatty acid content. That is, we can reduce the cost of liquid transportation fuels by increasing the content of saturated and monosaturated fatty acids. We can also shift polyunsaturated fatty acid (PUFA) remodeling between polar and neutral lipid groups in algal feedstocks to create a higher quality biobase for fuels with increased oxidative stability (neutral lipid pools), while maintaining co-product value in the form of Omega fatty acids found in the polar lipid membrane pools and providing viable biomass for protein and carbohydrate isolation. Environmental perturbation elicits shifts in carbon allocation and lipid production in microalgae (Alboresi et al., 2016; Chen et al., 2017; Guerra et al., 2013; Martin et al., 2014; Tan et al., 2016). TAGs are synthesized either *de novo* through acyl fatty acid assembly to a glycerol backbone, or through fatty acid recycling from existing lipids. Studies suggest that polyunsaturated fatty acid (PUFA) rich polar lipid classes such as phospholipids and galactolipids participate in lipid remodeling in microalgae (Li et al., 2012; Yoon et al., 2012). However, work in *Nannochloropsis sp.* has shown that phospholipids are present at low abundance relative to other lipid classes. *Nannochloropsis* contains, instead, high concentrations of the PUFA rich betaine lipid diacylglycerol tri-methylhomoserine, which likely serves as an analog for phospholipids commonly found in other microalgae. Work in the Holguin lab detected the presence of two predominant monoacylated lipid groups: monoacylglycerol tri-methylhomoserine and monogalactosyl monoacylglycerol during increased TAG synthesis with an elevated PUFA content (Gill et al., 2018; Willette et al., 2018). This result indicated that the diacylated precursors participated in lipid remodeling and TAG synthesis. We aimed to rely on these efforts to increase fatty acid content and remodel the PUFA pools to optimize biomass composition. To achieve this, we focused on two main strategies to enhance fatty acid content and remodel the polyunsaturated fatty acid (PUFA) pools, thereby optimizing biomass composition. The first strategy involved adapting growth conditions by increasing cultivation temperature to 36ºC. This adjustment was based on the hypothesis that higher temperatures would stimulate an increase in PUFA production, helping the cells combat stress associated with elevated levels of reactive oxygen species. By pushing the cells to adapt to heat stress, we expected to see a rise in PUFA synthesis, leading to a higher antioxidant capacity associated with an increase in PUFAs levels.

The second strategy was to explore the effects of extremely reduced cultivation conditions on the selection of mutated population of cells. This approach aimed to improve membrane fluidity and increase PUFA pools, based on the premise that suboptimal environmental conditions would select for cellular adaptations to the cold, leading to a change in lipid profiles. We anticipated that these adaptations would manifest as distinct ultrastructural changes, particularly in the thylakoid membranes rich in PUFAs. Furthermore, we expected an increase in

lipid bodies within the cytosol, resulting in an overall rise in total lipid content per cell mass. This could potentially lead to a decrease in carbohydrate content, as the cells reallocate their carbon resources more towards lipid synthesis.

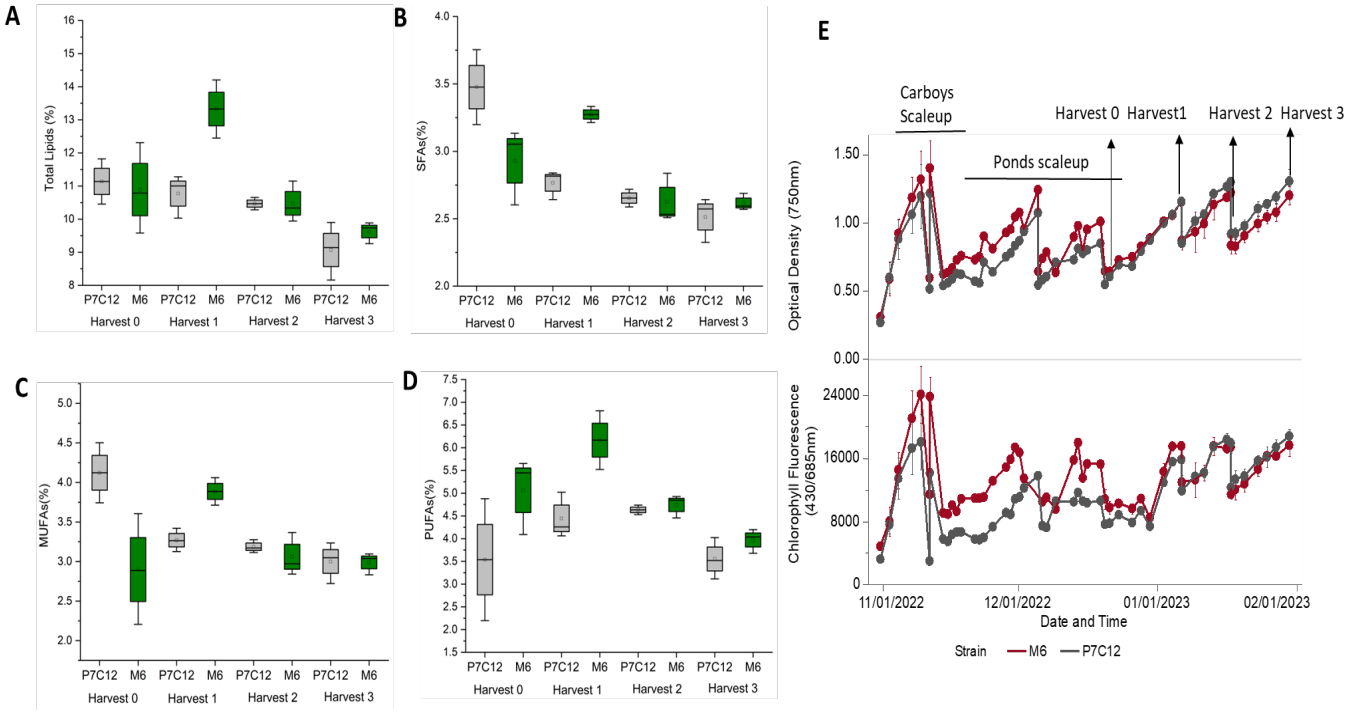

Fig. 5-10. Lipid analysis of the mutant 6 and P7C12 control cultures grown in outdoor field trails at different harvest cycles. A) % Total lipid content B) % Saturated fatty acids (SFAs) C) % monounsaturated fatty acids (MUFAs) D) % Polyunsaturated fatty acids (PUFAs) E) Growth characteristics and harvest points for biochemical analysis.

Our initial research revealed noticeable differences in both the relative and total abundance of fatty acids, along with slight variations in carbohydrate and protein levels, when observed at a laboratory scale. We hypothesized that these differences could be attributed to the relative selection pressure from which the isolate was derived, potentially offering a metabolic advantage in field growth. Indeed, distinct changes were observed in the total fatty acid content and the relative proportions of saturated fatty acids (SFAs), monounsaturated fatty acids (MUFAs), and polyunsaturated fatty acids (PUFAs) in comparison to the control culture (**Fig. 5-10**). However, the magnitude of these variations was not substantial enough to significantly enhance productivity or biomass quality. Though these results suggest the feasibility of employing mutagenesis as a strategy to engineer specific fatty acid profiles, tailored to certain selection pressures throughout this study, it became evident that the selection criteria for the desired outcomes must be carefully formulated. This should be done in conjunction with long term adaptive laboratory evolution practices to effectively develop and optimize these targeted fatty acid profiles and to impact overall carbon allocation, strain performance and translatability to a field setting.

To explore how our mutants may differ from the baseline strain in terms of intercellular carbon allocation, we conducted a detailed TEM ultrastructure analysis on Mutant 20. This inquiry was prompted by previous observations indicating thicker cell walls and a higher degree of calcofluor staining in Mutant 20. The analysis revealed notable differences: the control cells displayed more loosely packed thylakoids and fewer low electron dense regions, likely corresponding to vacuoles, in contrast to the mutant cells, which exhibited tightly stacked thylakoids and an increased presence of plastoglobuli **(Fig. 5-11)**. These morphological distinctions are hypothesized to stem from variations in intracellular carbon allocation, potentially influencing the changes seen in cellular ultrastructure and the observable phenotype of increased cell wall fluorescence. However, it's important to recognize that such observations, particularly regarding thylakoid structure and plastoglobuli abundance, can be dramatically affected by external environmental factors, including temperature and culture density. These elements are critical in determining cellular morphology and function, and therefore must be considered when interpreting our findings. Consequently, to ensure the validity of our conclusions regarding the impact of mutagenesis on carbon partitioning, it is imperative to repeat these ultrastructure studies under a range of controlled environmental conditions replicating our seasonal field conditions. Conducting these experiments repeatedly will enable a more thorough understanding of how genetic modifications from mutagenesis may affect cellular ultrastructure and photosynthetic efficiency.

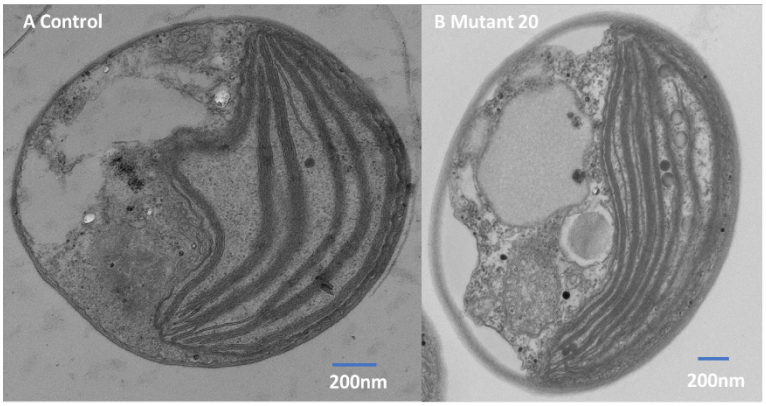

Fig. 5-11. Evaluating Intercellular Carbon Allocation. Ultrastructure analysis was performed parallel growing exponential stage cultures to evaluate any observable differences withing subcellar organelles between the control culture panel A and the mutant culture 20.

To determine the shift in biomass composition we would need to affect the minimum fuel selling price (MFSP), we leveraged our TEA efforts (see section 7). Working in 5% increments, all possible combinations of carbohydrates, proteins, and lipids (on an AFDW basis) were entered into the HTL module to determine the biocrude, aqueous, and gas yield, as well as HTL and upgrading flowrates and energetics. HTL phase yields were determined using a published kinetic model (Sheehan & Savage, 2017) and an additive phase yield model (Leow et al., 2015) with HTL economics modeled using existing studies (Jones et al., 2014). In total, 231 HTL scenarios were modeled with the MFSP determined for each scenario **(Fig. 5-12)**. The additive model from Leow et al. (2015) closed the mass balance more accurately, and the kinetic model from Sheehan & Savage (2017) showed the HTL process favoring lipids, with carbs and proteins producing roughly the same amount of HTL oil. Modeling results produced with the yield fractions from Leow et al. (2015) showed the HTL process favoring lipids and proteins, indicating a larger value add for altering the biomass composition by lowering the carbohydrate

fraction and raising the lipid fraction. The results with the kinetic and additive models showed that if a composition of 40% proteins, 30% lipids, and 30% carbohydrates could be achieved it would reduce the MFSP by 4.7% and 11.9%, respectively.

Our study's findings suggest that translating composition parameters from lab-identified isolates, grown under controlled environmental conditions, to field conditions poses a significant challenge. This difficulty arises due to the substantial impact of metabolic flexibility and adaptation in the field, which often negate the stable phenotypes observed in the laboratory setting.

Composition (Ash Free)	1 (Baseline) Proteins: 40% Lipids: 20% Carbs: 40%	2 (Int. Target) Proteins: 40% Lipids: 25% Carbs: 35%	3 (Milestone) Proteins: 40% Lipids: 30% Carbs: 30%	4 (50% Lipids) Proteins: 40% Lipids: 50% Carbs: 10%	5 (100% Lipids) Proteins: 0% Lipids: 100% Carbs: 0%
Sheehan & Savage (2017) - Kinetic Model	$6.57	$6.41 *(-2.4%)*	$6.26 *(-4.7%)*	$5.74 *(-12.6%)*	$5.42 *(-17.5%)*
Leow et al. (2018) – Additive Model	$5.96	$5.58 *(-6.4%)*	$5.25 *(-11.9%)*	$4.26 *(-28.5%)*	$3.26 *(-45.3%)*

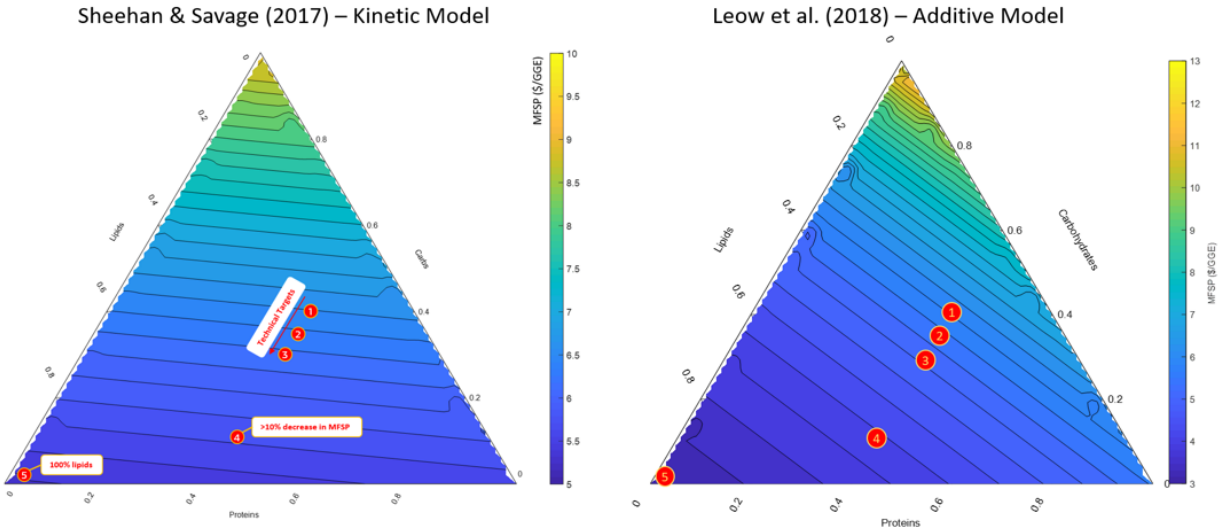

Fig. 5-12. Ternary diagrams showing the minimum fuel selling price (MFSP) as a function of the ash-free composition. Each point on the diagram represents a given composition of carbohydrates, lipids, and proteins adding to unity, and the colors indicate the MFSP. The left plot is based on the kinetic biocrude yield model from Sheehan and Savage (2017) and the right plot is based on the additive phase yield model from Leow et al. (2015).

6. Field Trials with New Strains

Four field trials were conducted to compare the baseline strain to new strains developed throughout the project. Although we aimed to capture new strains from the established field sites, we did not identify isolates with improved productivity, stability, or biomass composition. As such, we focused field trials on strains developed through mutagenesis and selection (see previous section).

All field trials were held at the NMSU Fabian Garcia Research Center (32°16'45.3"N 106°46'19.0"W). Cultures were grown in fiberglass Oswald-style raceways, with a maximum holding volume of 320 L (working volume 260L). Each pond was equipped with a paddlewheel, autofills, and programmed logic controller that controlled CO2 sparging based on pH setpoints. The controller also recorded water temperature, periods of CO2 sparging, and pH in each pond. For each experiment, every treatment and control pond were run in triplicate. Notable differences between experiments were due to practices relevant to the time of year. For example, in the summer, paddle wheels operated continuously, and water was continuously supplied to the ponds via auto-fills to maintain target volume. In the winter, paddle wheels operated from 9am to 7pm, and water auto fills were shut down only allowing ponds to be filled to target volume manually once a day. Winter practices were implemented due to possible freezing events that would damage the ponds. Standard metrics of biomass and health included: optical density at 750nm, chlorophyll fluorescence (430nm excitation, and 685nm emission), Fv/Fm, and AFDW in g/L (collected pre- and post-harvest). Cultures were grown semi-continuously where they were maintained from 0.5 g/L AFDW – 0.8 g/L AFDW. Once cultures reached the 0.8 g/L AFDW, culture was harvested to achieve 0.5 g/L AFDW. The volume of culture removed from the pond was replaced with fresh tap water and media components. Each experiment had three grow outs under field conditions. Pests were managed with chemical treatment, which increased during hotter months. Sample collection occurred Monday through Friday in the summer and three times a week during the winter. Pond parameters of pH, temperature °C, salinity, TDS,

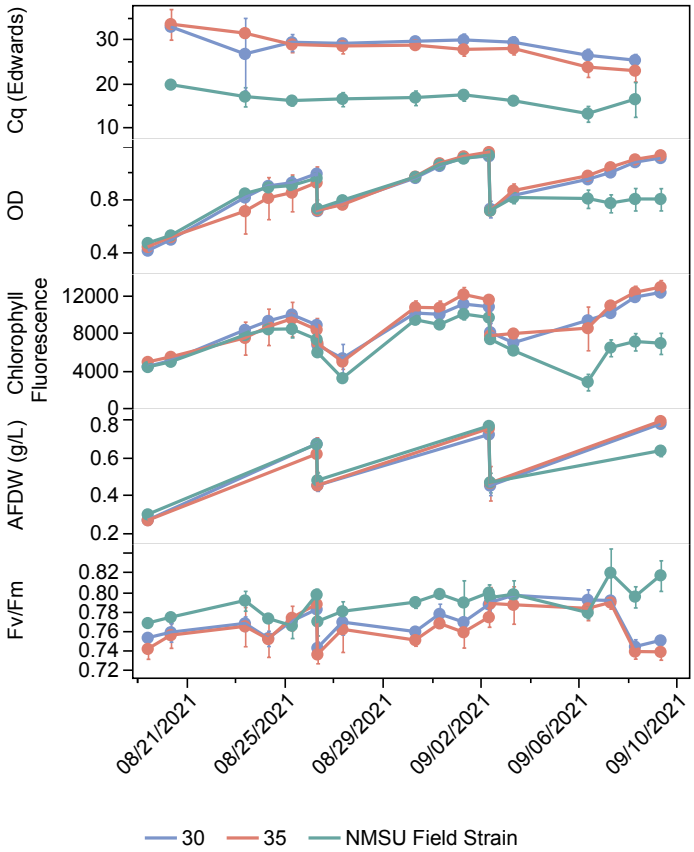

Fig. 6-1. Cq value from qPCR, OD, chlorophyll fluorescence, AFDW and Fv/FM of Mutant 30, Mutant 35 and the NMSU field strain.

and depth were collected on sample days. Culture was collected for biochemical composition on harvest days.

The first trial (experiment NMSU-F-023) focused on UV mutated cultures selected for in a high temperature background of 36°C. This experiment was conducted in the summer of 2021. Two isolates (M30, M35), a control (P7C4), and QT001 (Task 2) field culture were used for this experiment. During the outdoor scaling process, the control culture of P7C4 crashed and there was not enough time to rescale that strain and still run under summer conditions. The decision was made to move forward without a control and only use the two isolates and the pre-existing QT001 ponds as a field treatment. The two mutants performed similarly to the NMSU field strain in the field trial and only showed differences compared to the field culture during the third grow out **(Fig. 6-1)**. In the last grow out, the field strain declined in health, likely due to pest presence. During this trial we tracked the pest FD111 with qPCR primers developed through our efforts described above in section 4. Tracking showed much greater abundance of FD111 in the NMSU field culture **(Fig. 6-1).** Indeed, this culture had been outside for one year and had increased ash and pest presence compared to the isolates, likely resulting in lower OD and chlorophyll fluorescence for the third grow out. Without a proper control, it was difficult to verify growth differences observed in the lab.

The second trial (experiment NMSU-F-028) focused on mutant cultures selected for in a low temperature background of 10°C. This experiment was conducted between December 2021 and January 2022 and lasted only for a single grow out due to the low growth rates of all strains during the winter. Mean air and water temperatures during this period ranged from 0 to 10°C and ice on the ponds was common Two isolates (M1, M5) along with their baseline strain P7C12 (control) were used in this experiment. Isolate M1 grew better initially during pond scaling compared to the control **(Fig. 6-2)**. This strain also had a slightly greater productivity during the experimental period **(Fig. 6-2)**, although this difference was not statistically significant. However, productivities were low overall given the targeting of winter conditions. Even statistically significant gains in the winter are likely not to matter in practice at scales.

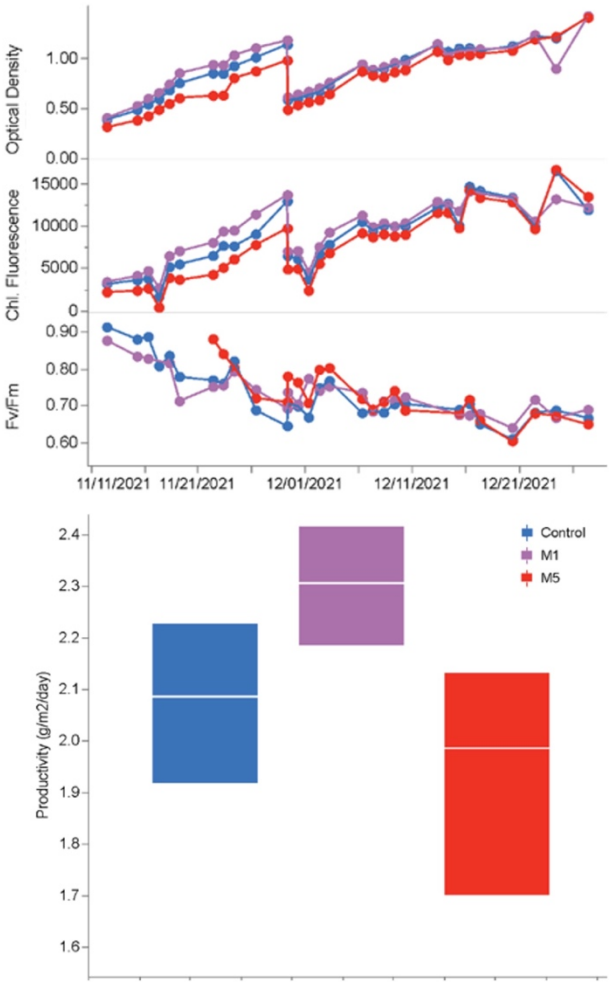

Fig. 6-2. Top: Scaling data in ponds. Bottom: Average productivity in each treatment during the experimental run.

The third trial (Experiment NMSU-F-053) focused on UV mutated cultures selected for in a high temperature background of 36°C. A different isolate (Mutant 5) from that used in the first high temperature field trial was used. This experiment was conducted between August and September 2022. During this period, mean water temperatures started at ~25C and decreased to ~13C through time. There were several rain events during this period, but they did not influence salinity greatly. The scaling process showed significant differences in the health of isolate 5 compared to the control (looking at Fv/Fm), but no other differences were observed **(Fig. 6-3)**. During the field trial, no observable differences were observed between isolate 5 and the control for the three grow outs (data not shown). Discussion about increased growth in isolates due to stressors prompted a fourth grow out with no crop protection to allow pest pressures to increase and cause a natural stressor. During the fourth grow out, all ponds decreased in growth and health but no significant difference between treatments was observed (data not shown).

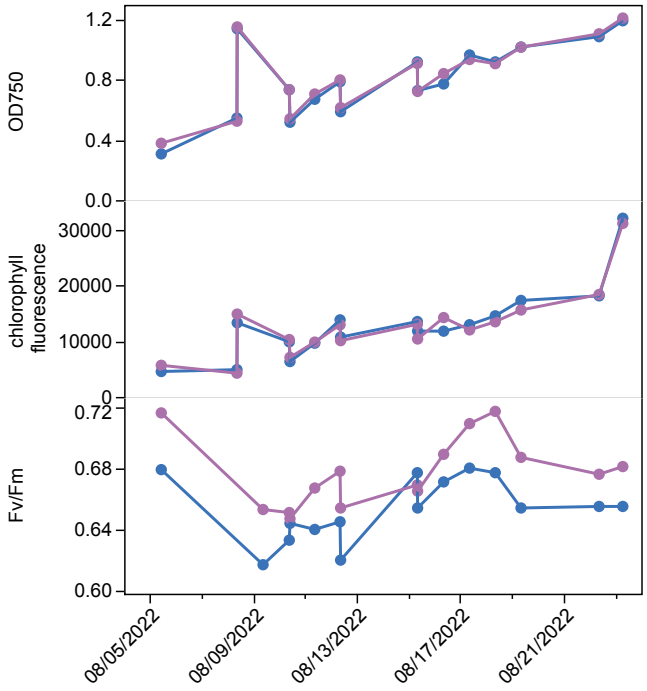

Fig. 6-3. OD, chlorophyll fluorescence and Fv/Fm during scaling of the mutant (purple) and control (blue) strains during the second summer trial.

The last trial (experiment NMSU-F-065) focused on mutated cultures selected for in a low temperature background of 10°C. One isolate (M6) along with its baseline strain of P7C12 (control) was used in this experiment. This experiment was conducted during December 2022 and January 2023. Water temperature was typically less than 5C with multiple freezing events. There were also three rain events during this trial. During the carboy scaling process, there was slightly improved growth in isolate 6 compared to the control **(Fig. 6-4)**. The scaling differences did not continue once the field trial began. M6 showed greater chlorophyll fluorescence during the first grow out, compared to the control, but this effect was transient, and no other differences were noted between treatments (data not shown).

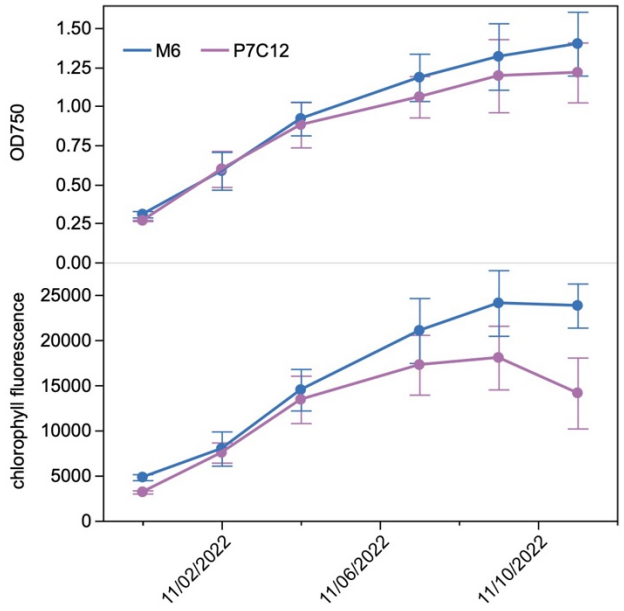

Fig. 6-4. OD and chlorophyll fluorescence during scaling during the second winter trial.

Experiment NMSU-F-091 was scheduled to be the last field trial run to see if there were differences observed in any promising isolates compared to the baseline strain. Although there were differences observed in initial small volume lab experiments, those differences were not repeatable on larger volume lab experiments. This resulted in this field trial being canceled.

7.0 Concurrent Techno-Economic Analysis and Life Cycle Assessment

7.1 Spatiotemporal Growth Modeling

Yearlong simulations (with hourly resolution) were performed at each station in the weather grid (~5,000 locations) and interpolated to produce county-level results illustrated with heat maps. **Fig. 7-1.** shows the annual average productivity for both nutrient deplete and nutrient replete conditions. Nutrient replete cultivation assumes a 20% nutrient excess on top of the stoichiometric nutrient requirements(Davis et al., 2016), while nutrient deplete cultivation uses a time-dependent productivity scaling curve **(Fig. 7-1)** obtained from DISCOVR data for UTEX 393 grown outdoors at AzCATI. Nutrient deplete conditions reduce productivity while triggering lipid accumulation.

7.2 Integrated TEA and LCA Results (HTL)

Several scenarios were used for the simulations to capture the full range of performance of the system. The *SOT Conservative* scenario represents lower productivities, efficiencies, and compositions achieved in recent SOT studies (Gao et al., 2023) while the *SOT Optimistic* scenario represents the combination of the highest productivities, efficiencies, and compositions achieved in SOT studies (Gao et al., 2023). The *Future Optimistic* scenario represents an optimized future configuration with high productivity, high lipids, and low losses in CO_2 and nutrients based on (Davis et al., 2014). Assumptions for critical performance parameters are presented in **Table 7-1.**

The nutrient surplus (% excess nutrients over the stoichiometric requirement), anaerobic storage losses, algae composition (Protein, Carbohydrates, Lipids (FAME), and ash), and recovery of biochar, NH3, and DAP all have direct impacts on both the economic and environmental sustainability of the system. The carbon utilization efficiency, cost of electricity, and cost of CO_2 have significant economic implications but do not impact the GWP or BWF of the system. Results from the modeling simulations include the spatially resolved areal productivity and the associate consumption of energy and materials as well as key sustainability metrics including the MFSP, GWP, and BWF. Values for each individual simulation as well as the mean, quartiles, and outliers of each modeling scenario are shown in **Fig. 7-2**.

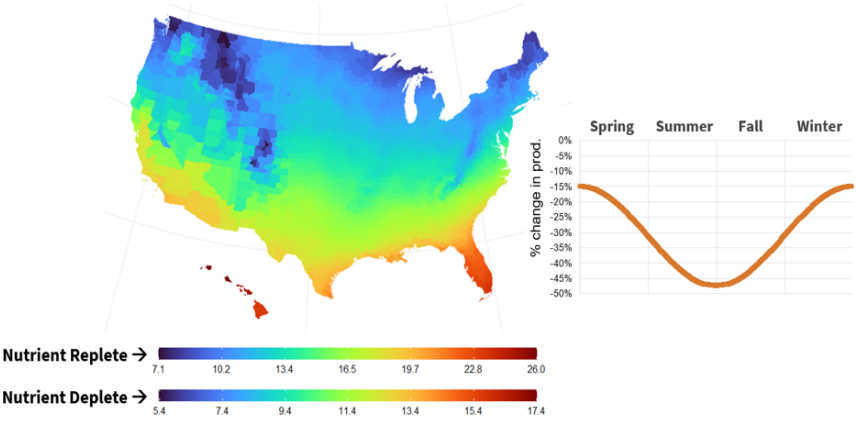

Fig. 7-1. Annual average areal productivity (g AFDW m^{-2} day^{-1}) for the nutrient replete and deplete scenarios [left] and the expected decrease in productivity throughout the year from creating nutrient deplete conditions that trigger lipid accumulation [right].

Table 7-1. Critical Performance Parameters for the Modeled Scenarios

Parameter	Future Optimistic	SOT Optimistic	SOT Conservative	Units
Carbon Utilization Efficiency	0.95	0.80	0.65	% CO_2 in biomass
Nutrient Surplus	0.20	0.20	0.00	% excess nutrients
Proteins	0.09	0.23	0.23	dry wt%
Carbohydrates	0.42	0.38	0.38	dry wt%
Lipids (FAME[1])	0.41	0.16	0.16	dry wt%
Ash	0.02	0.08	0.08	dry wt%
Anaerobic Storage Losses	0.05	0.10	0.15	% dry loss in storage
Biochar Recovery	0.90	0.75	0.60	% of output recovered
NH_3 Recovery (aqueous)	0.90	0.75	0.60	% of output recovered
DAP Recovery (aqueous)	0.90	0.75	0.60	% of output recovered
Cost of Electricity	$0.07	$0.07	$0.07	$/kWh
Cost of CO_2 (from DAC[3])	$50	$125	$325	$/tonne CO_2

[1]FAME: Fatty Acid Methyl Esters (fuel-relevant lipids)
[2]HTL: Hydrothermal Liquefaction
[3]DAC: Direct Air Capture of Atmospheric CO_2

The results in **Fig. 7-2** illustrate significant reductions in the MFSP, GWP, and BWF in response to adjustments to the critical performance parameters summarized in **Table 7-1.** In other words, sustainability can be greatly increased by improving the efficiency of CO_2 delivery and reducing CO_2 costs, achieving a lipid content of > 41%, and recovering 90% of biochar, ammonia, and DAP from the HTL reactor. When moving from the *SOT Conservative* scenario to the *Future Optimistic* scenario (worst case to best case), the MFSP, GWP, and BWF are reduced by 64%, 41%, and 33%, respectively. The results for MFSP, GWP, and BWF were translated to Index Scores following the procedures outlined in the Methods. Index scores < 0.5 were considered failing as they did not satisfy baseline requirements for economic or environmental sustainability. Index scores > 0.75 were considered satisfactory as economic targets are within reach and environmental targets are met or surpassed. Index scores for the main sustainability metrics and scenarios are illustrated in **Fig. 7-3**.

The results in **Fig. 7-3** illustrate the impact of improving system efficiencies on the number of locations in the US that satisfy sustainability targets for future large-scale biorefineries (characterized by an

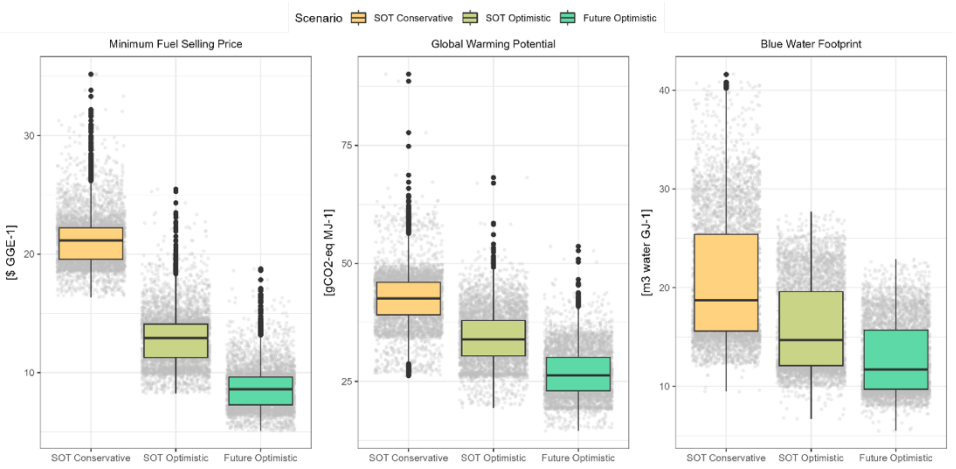

Fig. 7-2. Box plots illustrating the mean, upper and lower quartiles, and outliers for the Minimum Fuel Selling Price [left], Global Warming Potential [middle] and Blue Water Footprint [right] for each modeling scenario. The grey dots show the individual simulation output values for each of the 5,626 locations modeled throughout the US.

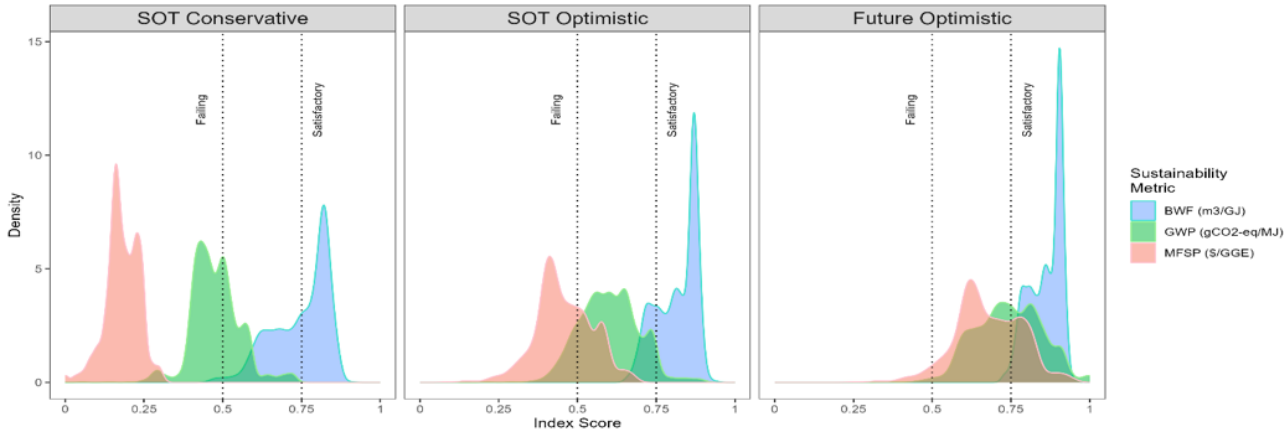

Fig. 7-3. Density plot showing the Index Scores for Minimum Fuel Selling Price (red), Global Warming Potential (green), and Blue Water Footprint (blue) for the SOT Conservative [left], SOT Optimistic [middle], and Future Optimistic [right] scenarios.

Index Score > 0.75). The results in **Fig. 7-3** suggest that every location in the US fails to meet the economic target of < \$10 GGE^{-1}, and most locations fail to satisfy the RFS for renewable diesel when modeled using the assumptions from the *SOT Conservative* scenario. Under *SOT Optimistic* assumptions, most locations satisfy the RFS, but these locations still fail to meet the economic target of a MFSP < \$10 GGE^{-1}. While almost all locations avoid failing (Index Score < 0.5) under the *Future Optimistic* scenario, many locations are still below the satisfactory threshold. Due to high water recycling rates, most locations show a satisfactory BWF for all modeled scenarios, with nearly all locations surpassing the satisfactory threshold under *Future Optimistic* assumptions. The locations in the US that meet baseline sustainability targets of MFSP < \$10, GWP < 45 gCO_2-eq/MJ, and BWF < 20 m3/GJ under the *Future Optimistic, SOT Optimistic, and SOT Conservative* scenarios are shown in **Fig. 7-4.**

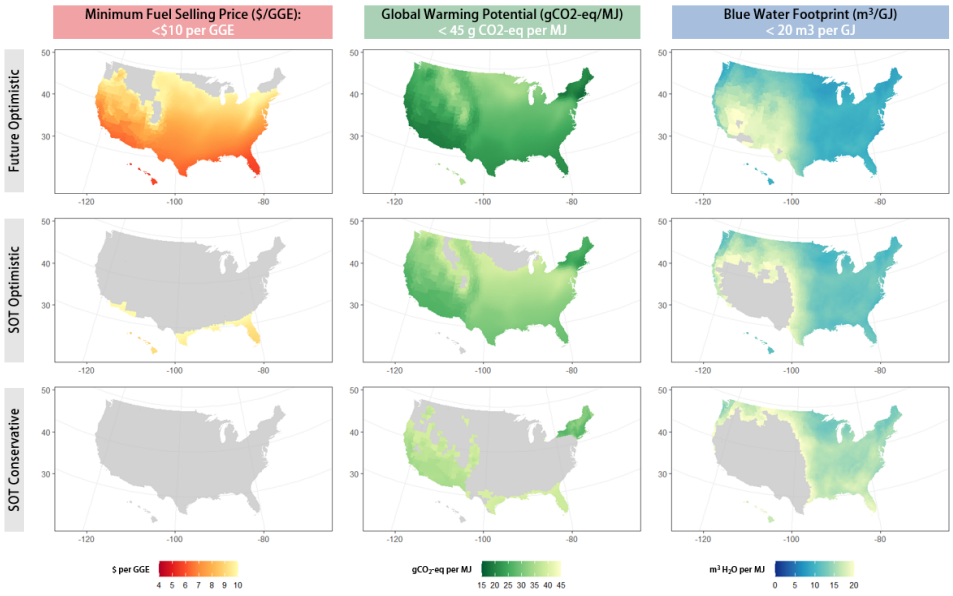

Fig. 7-4. Locations in the US that satisfy sustainability targets for the Minimum Fuel Selling Price (left column), Global Warming Potential (middle column), and Blue Water Footprint (right column). Spatially resolved values for counties that satisfy sustainability targets are shown with the color scales, while counties that fall short of sustainability targets are grey.

7.3. Integrated TEA and LCA Results (Sustainable Aviation Fuel)

In addition to the HTL conversion model, a model was developed to quantify the economic and environmental sustainability of the Hydrotreated Esters and Fatty Acids (HEFA) process to produce sustainable aviation fuel from algae oil extracted through high pressure homogenization and wet hexane extraction. Geographically resolved productivities and associated data (harvesting flowrates, water pumping energy, dewatering energy consumption, anaerobic storage losses, nutrient consumption, CO2 consumption, water consumption, etc.) were integrated with the SAF conversion model and techno-economic analysis (TEA) was used to estimate the minimum jet fuel selling price ($/gallon jet fuel) resulting in a 10% internal rate of return over 30 years of facility operation. Additionally, the LCA model was expanded to include the SAF conversion process to determine the GWP expressed in g CO2-eq/MJ jet fuel. Both metrics were analyzed throughout the US at the county level, with results in **Fig. 7-5.**

Results illustrate an even wider range in costs for the MFSP, ranging from a low of $10.10/gallon SAF to a high of $161.10/gallon SAF. Relative to previous results for renewable diesel through hydrothermal liquefaction, the MFSP from the HEFA pathway is highly sensitive to the lipid content of the algae, spanning an order of magnitude in costs from a 3-fold increase in lipid content between scenarios. Results suggest that SAF from the HEFA pathway only begins to approach feasible costs when lipid content exceeds 40 dry wt% and is still far from DOE targets of $3/gallon. These results highlight the need for an alternative system pathway that recovers more value from the lipid-extracted algae either through high-value co-products or by producing additional SAF by fermenting carbohydrates and upgrading ethanol to jet fuel.

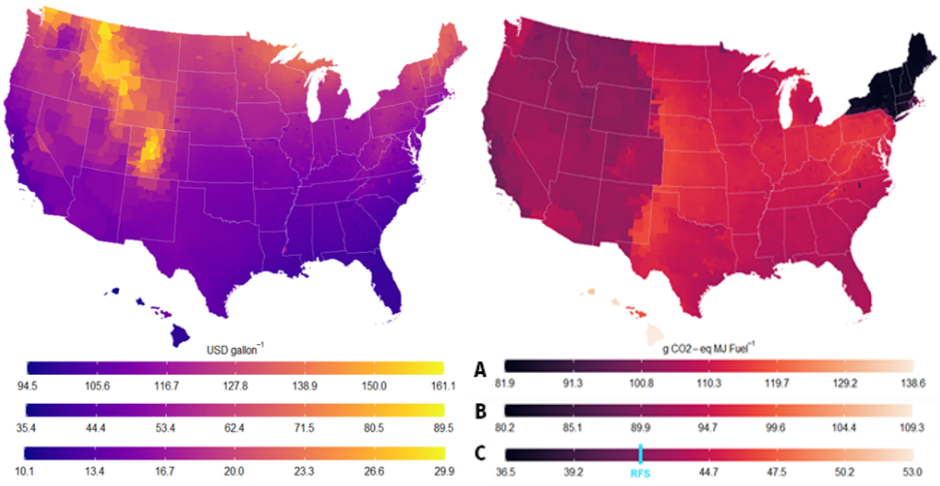

Fig. 7-5 Minimum fuel selling price ($/gallon of jet fuel) [left] and Global Warming Potential (g CO2-eq/MJ Fuel) [right] throughout the contiguous United States for the modeled HEFA pathway. Color scale A corresponds to assumptions used in the "SOT Worst Case" scenario, color scale B is for the "SOT Best Case" scenario and color scale C is for the "Future Best Case" scenario.

8. Institutions and Team Members

New Mexico Consortium (Los Alamos, NM)

Alina Corcoran, Lead PI
Ahlem Jebali, Postdoctoral Researcher
Heather Martinez, Lead Technician
Stephanie Getto, MS Student

Los Alamos National Laboratory (Los Alamos, NM)

Shawn Starkenburg, Group Leader, co-PI
Monica Sanchez, Postdoctoral Researcher
Blake Hovde, Scientist 3
Matthew Green, PhD Student

University of California San Diego (San Diego, CA)

Jonathan Shurin, Professor
Isidora Echenique-Subiabre, Postdoctoral Researcher
Ugbad Farah, PhD Student

New Mexico State University (Las Cruces, NM)

Omar Holguin, Associate Professor
Claudia Galvan, MS Student
Harmanpreet Kaur, PhD Student

Colorado State University (Fort Collins, CO)

Jason Quinn, Associate Professor
Jonah Greene, Research Associate

Cyanotech Corporation (Kailua-Kona, HI)

Charles J. O'Kelly, Director of Applied Research
Julia Gerber, Research Specialist
Marcella Balleza, Research Specialist

Phase Genomics, Inc. (Seattle, WA)

Steven Eacker, Vice President of Research and Development
Ivan Liachko, CEO
Jonas Grove, Senior Computational Biologist

Qualitas Health, Inc. (Imperial, TX)

Jakob O. Nalley, Director of Agronomy

9. Publications

1. Echenique-Subiabre, I., J. Greene, A. Ryan, H. Martinez, M. Balleza, J. Gerber, A. Jebali, S. Getto*, C.J. O'Kelly, S. Mandal, J.C. Quinn, S.R. Starkenburg, A.A. Corcoran, J.B. Shurin. 2023. Local Conditions Override Broad Climatic Gradients in Determining Microalgae Productivity in Open Raceway Ponds. *Algal Research* 103235. https://doi.org/10.1016/j.algal.2023.103235.
2. Sanchez, M.R., E. Denning, T. Biondi, B. Hovde, S. Eacker, S. Getto*, H. Kaur, A. Jebali, I. Echenique-Subiabre, M. Green, J. Gerber, B. Auch, F.O. Holguin, I. Liachko, H. Martinez, M. Balleza, J. Nalley, C.O' Kelly, J.B. Shurin, A.A. Corcoran, S.R. Starkenburg. 2023. Development of a field-deployable qPCR assay for real-time pest monitoring in algal cultivation systems. *Algal Research* 103194. https://doi.org/10.1016/j.algal.2023.103194.
3. Sanchez, M.R., T.C. Biondi, Y.A. Kunde, W. Eng, J.O. Nalley, E. Ganuza, B.T. Hovde, A.A. Corcoran, S.R. Starkenburg. 2022. The genome sequence of algal strain *Nannochloropsis* QH25. *Microbiology Resource Announcements* 1(12):e0092122. https://doi.org/10.1128/mra.00921-22.
4. Jebali, A., M.R. Sanchez, E.R. Hanschen, S.R. Starkenburg, and A.A Corcoran. 2022. Trait drift in microalgae and applications for strain improvement. *Biotechnology Advances* 60: 108034. https://doi.org/10.1016/j.biotechadv.2022.108034

10. Presentations

1. Echenique-Subiabre, I., U. Farah, X. Lin, H. Martinez, A. Jebali, M.R. Sanchez, J. Gerber, M. Balleza, A. Roman C.J. O'Kelly, J. Nalley, S.R. Starkenburg, A.A. Corcoran, J.B. Shurin. Adaptation and plasticity of *Nannochloropsis* to seasonal and geographic climate variation. *Poster Presentation.* Microbial Ecology and Evolution Hub-based Conference. January 2024. San Diego, CA.
2. Getto, S. and A.A. Corcoran. Effects of chemical treatment on the algal microbiome: insight from a metagenomic study. Algae Biomass Summit. October 2023. Madison, WI.
3. Green, M., Sanchez, M.R., Nalley, J., Jebali, A., Starkenburg, S.R. Development of a field-deployable qPCR assay for real-time pest monitoring in algal cultivation systems. Algae Biomass Summit. October 2023. Madison, WI.
4. Kaur, H., Jebali, A., Starkenburg, S.R, Corcoran A.A., Holguin, F.O. Chemical Mutagenesis for Strain Improvement in *Nannochloropsis oceanica:* Towards Higher Lipid Content and Productivity. Algae Biomass Summit. October 2023. Madison, WI.
5. Terrazas, B., Galvan, C., Kaur, H., Holguin, F.O. (2023). UV Mutagenesis as Tool for the Microalgal Strain Improvement. Algae Biomass Summit, October 2023. Madison, WI.
6. Echenique-Subiabre, I, J.M. Greene, A. Ryan, H. Martinez, M. Balleza, J. Gerber, A. Jebali, S. Getto, C.J. O'Kelly, S. Mandal, J.C. Quinn, S.R. Starkenburg, A.A. Corcoran, J.B. Shurin. Site-specific factors override local climatic conditions in determining microalgae productivity in open raceway ponds. *Oral Presentation.* International Conference on Algal Biomass, Biofuels and Bioproduts. June 2023. Kona, HI.
7. Green, M., Sanchez, M.R., Kaur, H., Holguin, F.R., Starkenburg, S.R. Cold adapted *Nannochloropsis oceanica*: Experimental evolution of a microalgae for improved low-temperature growth and year round productivity. International Conference on Algal Biomass, Biofuels & Bioproducts. June, 2023. Kona, HI.
8. Jebali, A. M.R. Sanchez, I. Echenique-Subiabre, H. Martinez, J. Gerber, S. Getto, M. Balleza, J. Nalley, C.J. O'Kelly, F.O. Holguin, J. Shurin, S.R. Starkenburg, A.A. Corcoran. Assessment of phenotype stability in *Nannochloropsis* through time in response to different cultivation practices. International Conference on Algal Biomass, Biofuels and Bioproduts. June 2023. Kona, HI.
9. Sanchez, M. A. Jebali, I. Echenique-Subiabre, E. Denning, M. Balleza, J. Gerber, H. Martinez, F.O. Holguin, J. Nalley, C.J. O'Kelly, J. Shurin, A.A. Corcoran, S.R. Starkenburg. Trait drift in the field and laboratory: Characterizing microbial community composition and genotype shifts through time. International Conference on Algal Biomass, Biofuels and Bioproduts. June 2023. Kona, HI.
10. Kaur, H., M. Sanchez, H. Martinez, M. Neyaz, A. Jebali, S.R. Starkenburg, A.A. Corcoran, F.O. Holguin. Improvement of performance and composition in field adapted *Nannochloropsis oceanica* strain. International Conference on Algal Biomass, Biofuels and Bioproducts. June 2023. Kona, HI.
11. You Mak, K., Sanchez, M., Echenique, I, Farah, U., Shurin, J., Gerber, J., Balleza, M., O'Kelly, C.J., Martinez, H., Jebali, A., Corcoran, A.A., Hovde, B., S.R. Starkenburg. Characterizing microbial communities in long-term algal ponds across sites. Sequencing to Function: Analysis and Application for the Future (SFA²F). *Poster Presentation.* Santa Fe, NM, June 21-

23, 2022.
12. Sanchez, M., A. Jebali, I. Echenique, E. Denning, M. Balleza, J. Nalley, C. O'Kelly, J. Shurin, A.A. Corcoran, S.R. Development of a field-deployable qPCR assay for real-time pest monitoring in algal cultivation systems. Sequencing to Function: Analysis and Application for the Future (SFA²F).. Santa Fe, NM, June 21-23, 2022.
13. Greene, J.M., Balleza, M., Corcoran, A., Echenique, I., Gerber, J., Getto, S., Holguin, O., Jebali, A., Martinez, H., Nalley, J., O'Kelly, C., Starkenburg, S.R., Shurin, J., Quinn, J.C., Hindcasting of algal productivity in open raceway ponds to quantify the impacts of various pest pressures, Algae Biomass Summit, 2022
Greene, J.M., Quiroz, D., Compton, S., Quinn, J.C., Modeling algae cultivation at scale: Productivity, pond reliability, and resource consumption across the United States, ISSST, Pittsburg, PA, 2022
14. Gerber, J.E., M.R. Sanchez, S.R. Starkenburg, and C.J. O'Kelly. Impact of a 'freshwater' chrysomonad flagellate on *Nannochloropsis* at various salinities. Algae Biomass Summit, 2022.
15. Echenique, I. U. Farah, M.R. Sanchez, A. Jebali, H. Kaur, M. Balleza, H. Martinez, J. Nalley, C. O'Kelly, Omar Holguin. A.A. Corcoran, Shawn R. Starkenburg, J. Shurin. Local adaptation of *Nannochloropsis* produces site-specific temperature-growth curves. *Poster Presentation.* Algae Biomass Summit. October 2021. Virtual.
16. Greene, J.M., D. Quiroz, A.A. Corcoran, J. Nalley, J.C. Quinn. Integrating regionally and temporally resolved microalgae growth rate modeling with pond reliability metrics to accurately model the economic and environmental performance of algae cultivation at scale, *Oral Presentation.* Algae Biomass Summit. October 2021. Virtual.
17. Jebali, A., M.R. Sanchez, I. Echenique, M. Balleza, H. Martinez, J. Nalley, C.J. O'Kelly, F.O. Holguin, J. Shurin, S.R. Starkenburg, A.A. Corcoran. Phenotype characterization of field-adapted *Nannochloropsis* for the evaluation of trait drift and evolution in lab and field cultures. *Poster Presentation.* Algae Biomass Summit. October 2021. Virtual.
18. Sanchez, M., A. Jebali, I. Echenique, E. Denning, M. Balleza, J. Nalley, C. O'Kelly, J. Shurin, A.A. Corcoran, S.R. Characterization of trait drift in the field and laboratory: shifts in microbial community composition. *Oral Presentation.* Algae Biomass Summit. October 2021. Virtual.
19. Hovde, B., T. Biondi, S. Eacker, I. Liachko, E. Eenning, S. Starkenburg, A. Corcoran. Managing pests in algal ponds: identification and detection of novel pests using proximity ligation (Hi-C) metagenome assembly. *Oral Presentation.* International Conference on Algal Biomass, Biofuels, and Bioproducts. June 2021. Virtual.
20. Jebali, A.A., F.O. Holguin, I. Echenique, M. Balleza, H. Martinez, J. Nalley, C. O'Kelly, J. Shurin, S.R. Starkenburg, and A.A. Corcoran. Trait drift and evolution of a field-adapted *Nannochloropsis* culture in outdoor raceway ponds. *Poster Presentation.* 75th Annual Phycological Society of America Meeting. July 2021. Virtual.

11. References

Aitken, D. and Antizar-Ladislao, B. (2012) Achieving a green solution: limitations and focus points for sustainable algal fuels. Energies, **5**(5), 1613-1647.

Ayre, J.M., Moheimani, N.R., Borowitzka, M.A. (2017) Growth of microalgae on undiluted anaerobic digestate of piggery effluent with high ammonium concentrations. Algal Research-Biomass Biofuels and Bioproducts, **24**, 218-226.

Berge, T., Daugbjerg, N., Hansen, P.J. (2012) Isolation and cultivation of microalgae select for low growth rate and tolerance to high pH. Harmful Algae, **20**, 101-110.

Borowitzka, M.A. (2005) Culturing microalgae in outdoor ponds. In Algal Culturing Techniques (R. Andersen, ed, Elsevier, Burlington, MA.

Borowitzka, M.A. (2013) Species and Strain Selection. In Algae for Biofuels and Energy (M.A. Borowitzka, ed, Springer, Dordrecht.

Carney, L.T. and Lane, T.W. (2014) Parasites in algae mass culture. Frontiers in Microbiology, **5**, 278.

Cooper, V.S. (2014) The Origins of Specialization: Insights from Bacteria Held 25 Years in Captivity. PLOS Biology, **12**(2), e1001790.

Corcoran, A.A., Saunders, M.A., Hanley, A.P., Lee, P.A., Lopez, S., Ryan, R., Yohn, C.B. (2018) Iterative screening of an evolutionary engineered *Desmodesmus* generates robust field strains with pesticide tolerance. Algal Research, **31**, 443-453.

Cunha, P., Pereira, H., Costa, M., Pereira, J., Silva, J.T., Fernandes, N., Varela, J., Silva, J., Simões, M. (2020) Nannochloropsis oceanica Cultivation in Pilot-Scale Raceway Ponds—From Design to Cultivation. Applied Sciences, **10**(5), 1725.

Day, J.G., Gong, Y.C., Hu, Q. (2017) Microzooplanktonic grazers - A potentially devastating threat to the commercial success of microalgal mass culture. Algal Research-Biomass Biofuels and Bioproducts, **27**, 356-365.

Demott, W.R. and McKinney, E.N. (2015) Use it or lose it? Loss of grazing defenses during laboratory culture of the digestion-resistant green alga Oocystis. Journal of Plankton Research, **37**(2), 399-408.

Dermauw, W., Wybouw, N., Rombauts, S., Menten, B., Vontas, J., Grbic, M., Clark, R.M., Feyereisen, R., Van Leeuwen, T. (2013) A link between host plant adaptation and pesticide resistance in the polyphagous spider mite Tetranychus urticae. Proceedings of the National Academy of Sciences of the United States of America, **110**(2), E113-E122.

Echenique-Subiabre, I., Greene, J.M., Ryan, A., Martinez, H., Balleza, M., Gerber, J., Jebali, A., Getto, S., O'Kelly, C.J., Mandal, S., Quinn, J.C., Starkenburg, S.R., Corcoran, A.A., Shurin, J.B. (2023) Site-specific factors override local climatic conditions in determining microalgae productivity in open raceway ponds. Algal Research, **74**, 103235.

Ganuza, E., Sellers, C.E., Bennett, B.W., Lyons, E.M., Carney, L.T. (2016) A novel treatment protects Chlorella at commercial scale from the predatory bacterium Vampirovibrio chlorellavorus. Frontiers in Microbiology, **7**, 848.

Grobbelaar, J.U. (2012) Microalgae mass culture: the constraints of scaling-up. Journal of Applied Phycology, **24**(3), 315-318.

Gupta, N., Vats, S., Bhargava, P. (2018) Sustainable Agriculture: Role of Metagenomics and Metabolomics in Exploring the Soil Microbiota. In In Silico Approach for Sustainable Agriculture (C. D., K. M., P. R. & K. V., eds), Springer, Singapore.

Hargreaves, J.A. (2003) Pond Mixing (S.R.A. Center, ed.

Henry, R.J. and Nevo, E. (2014) Exploring natural selection to guide breeding for agriculture. Plant Biotechnology Journal, **12**(6), 655-662.

Hien, A.S., Soma, D.D., Hema, O., Bayili, B., Namountougou, M., Gnankine, O., Baldet, T., Diabate, A., Dabire, K.R. (2017) Evidence that agricultural use of pesticides selects pyrethroid resistance within Anopheles gambiae s.l. populations from cotton growing areas in Burkina Faso, West Africa. PLOS ONE, **12**(3), 15.

Hughes, P., Marshall, D., Reid, Y., Parkes, H., Gelber, C. (2007) The costs of using unauthenticated, over-passaged cell lines: how much more data do we need? Biotechniques, **43**(5), 575, 577-578, 581-572 passim.

Ivanova, J., Stoyancheva, G., Pouneva, I. (2014) Lysis of Antarctic algal strains by bacterial pathogen. Antonie Van Leeuwenhoek, **105**(6), 997-1005.

Kumar, K., Mishra, S.K., Shrivastav, A., Park, M.S., Yang, J.-W. (2015) Recent trends in the mass cultivation of algae in raceway ponds. Renewable & Sustainable Energy Reviews, **51**, 875-885.

Lakeman, M.B., von Dassow, P., Cattolico, R.A. (2009) The strain concept in phytoplankton ecology. Harmful Algae, **8**(5), 746-758.

Lee, P.A., Martinez, K.J.L., Letcher, P.M., Corcoran, A.A., Ryan, R.A. (2018) A novel predatory bacterium infecting the eukaryotic alga *Nannochloropsis*. Algal Research-Biomass Biofuels and Bioproducts, **32**, 314-320.

Li, H. and Durbin, R. (2009) Fast and accurate short read alignment with Burrows-Wheeler transform. Bioinformatics, **25**(14), 1754-1760.

Lian, J., Wijffels, R.H., Smidt, H., Sipkema, D. (2018) The effect of the algal microbiome on industrial production of microalgae. Microbial Biotechnology, **11**(5), 806-818.

Liu, P., Kaplan, A., Yuan, B., Hanna, J.H., Lupski, J.R., Reiner, O. (2014) Passage number is a major contributor to genomic structural variations in mouse iPSCs. Stem cells (Dayton, Ohio), **32**(10), 2657-2667.

Mandal, S. and Corcoran, A.A. (2022) A novel approach to build algal consortia for sustainable biomass production. Algal Research, **65**, 102734.

Martin, M. (2002) Predatory prokaryotes: an emerging research opportunity. Journal of Microbiology and Biotechnology, **4**(5), 467-477.

Martínez-Porchas, M. and Vargas-Albores, F. (2017) Microbial metagenomics in aquaculture: a potential tool for a deeper insight into the activity. Reviews in Aquaculture, **9**(1), 42-56.

McBride, R.C., Smith, V.H., Carney, L.T., Lane, T.W. (2016) Crop protection in open ponds. In Microalgal Production for Biomass and High-Value Products (S.P. Slocombe & J.R. Benemann, eds), CRC Press, Boca Raton, FL.

Millán-Oropeza, A. and Fernández-Linares, L. (2017) Biomass and lipid production from Nannochloropsis oculata growth in raceway ponds operated in sequential batch mode under greenhouse conditions. Environmental Science and Pollution Research, **24**(33), 25618-25626.

Mitchell, S.A. and Richmond, A. (1987) The use of rotifers for the maintenance of monoalgal mass cultures of *Spirulina*. Biotechnology and Bioengineering, **30**(2), 164-168.
Mohan, N., Rao, P.H., Boopathy, A.B., Rengasamy, R., Chinnasamy, S. (2021) A sustainable process train for a marine microalga-mediated biomass production and CO2 capture: A pilot-scale cultivation of Nannochloropsis salina in open raceway ponds and harvesting through electropreciflocculation. Renewable Energy, **173**, 263-272.
Mouriaux, F., Zaniolo, K., Bergeron, M.-A., Weidmann, C., De La Fouchardière, A., Fournier, F., Droit, A., Morcos, M.W., Landreville, S., Guérin, S.L. (2016) Effects of Long-term Serial Passaging on the Characteristics and Properties of Cell Lines Derived From Uveal Melanoma Primary Tumors Characteristics of Passaged UM Cells. Investigative Ophthalmology & Visual Science, **57**(13), 5288-5301.
Narala, R.R., Garg, S., Sharma, K.K., Thomas-Hall, S.R., Deme, M., Li, Y., Schenk, P.M. (2016) Comparison of Microalgae Cultivation in Photobioreactor, Open Raceway Pond, and a Two-Stage Hybrid System. Frontiers in Energy Research, **4**.
Nho, S.W., Abdelhamed, H., Paul, D., Park, S., Mauel, M.J., Karsi, A., Lawrence, M.L. (2018) Taxonomic and Functional Metagenomic Profile of Sediment From a Commercial Catfish Pond in Mississippi. Frontiers in Microbiology, **9**(2855).
Oswald, W.J. and Golueke, C.G. (1960) Biological Transformation of Solar Energy. In Advances in Applied Microbiology (W.W. Umbreit, ed, Academic Press: pp 223-262.
Poplin, R., Chang, P.-C., Alexander, D., Schwartz, S., Colthurst, T., Ku, A., Newburger, D., Dijamco, J., Nguyen, N., Afshar, P.T., Gross, S.S., Dorfman, L., McLean, C.Y., DePristo, M.A. (2018) A universal SNP and small-indel variant caller using deep neural networks. Nature Biotechnology, **36**(10), 983-987.
Richardson, J.W., Johnson, M.D., Outlaw, J.L. (2012) Economic comparison of open pond raceways to photo bio-reactors for profitable production of algae for transportation fuels in the Southwest. Algal Research, **1**(1), 93-100.
Sanchez, M.R., Biondi, T.C., Kunde, Y.A., Eng, W., Nalley, J.O., Ganuza, E., Hovde, B.T., Corcoran, A.A., Starkenburg, S.R. (2022) The Genome Sequence of an Algal Strain of Nannochloropsis QH25. Microbiol Resour Announc, **11**(12), e0092122.
Santos, L. and Ramos, F. (2018) Antimicrobial resistance in aquaculture: Current knowledge and alternatives to tackle the problem. International Journal of Antimicrobial Agents, **52**(2), 135-143.
Schröder, R. and Prasse, R. (2013) Do Cultivated Varieties of Native Plants Have the Ability to Outperform Their Wild Relatives? PLOS ONE, **8**(8), e71066.
Sheehan, J., Dunahay, R., Benemann, J., Roessler, P. (1998) A Look Back at the U.S. Department of Energy's Aquatic Species Program—Biodiesel from Algae.
Smith, V.H. and McBride, R.C. (2015) Key ecological challenges in sustainable algal biofuels production. Journal of Plankton Research, **37**(4), 671-682.
Tomasetto, F., Tylianakis, J.M., Reale, M., Wratten, S., Goldson, S.L. (2017) Intensified agriculture favors evolved resistance to biological control. Proceedings of the National Academy of Sciences of the United States of America, **114**(15), 3885-3890.
Van Wychen, S. and Laurens, L.M.L. (2015) Determination of Total Solids and Ash in Algal Biomass Laboratory Analytical Procedure (LAP), National Renewable Energy Laboratory, Golden, CO.

Van Wychen, S. and Laurens, L.M.L. (2016) Determination of Total Solids and Ash in Algal Biomass: Laboratory Analytical Procedure (LAP), United States: pp Medium: ED; Size: 415 KB.

White, R.L. and Ryan, R.A. (2015) Long-term cultivation of algae in open-raceway ponds: lessons from the field. Industrial Biotechnology, **11**(4), 213-220.